Precise predictions for the W boson mass in models beyond the Standard Model

Diplomarbeit

von

Lisa Zeune

geboren in Wuppertal

angefertigt am

II. Physikalischen Institut
der Georg-August-Universität Göttingen

und in der

DESY Theorie Gruppe

2011

Angenommen am: 28. Februar 2011
Referent: Prof. Dr. Arnulf Quadt
Korreferent: Prof. Dr. Georg Weiglein

GEORG-AUGUST-UNIVERSITÄT GÖTTINGEN

II. Physikalisches Institut

Precise predictions for the W boson mass in models beyond the Standard Model

von

Lisa Zeune

Electroweak precision observables, such as the W boson mass, are highly sensitive to quantum effects from the entire particle spectrum of a given model. Therefore they are of utmost importance for testing and constraining physics beyond the Standard Model (SM). The indirect constraints on new physics obtained from precision observables are complementary to the direct searches for new physics carried out at the LHC and elsewhere. In order to fully exploit the improved experimental accuracy expected at the LHC, a precise theoretical prediction for the W boson mass in models beyond the SM is desired. The most precise results for the W boson mass in the SM and the minimal supersymmetric SM (MSSM) with complex parameters are presented, which include all known higher-order corrections of SM- and SUSY-type. The calculation is preformed in a framework that facilitates direct extension to other models beyond the SM.

Post address:
Friedrich-Hund-Platz 1
37077 Göttingen
Germany

II. Physikalisches Institut
Georg-August-Universität Göttingen

February 2011

Contents

Introduction

In an endeavour to find a complete and comprehensive description of nature, elementary particle physicists build theories which identify the basic building blocks of matter and explain the interactions between them. It is fair to say that the major achievement within the field of particle physics of the last century was the development of the Standard Model of electroweak and strong interactions, successfully explaining close to all experimental observations. However, gravity cannot be described within this framework and there are further theoretical and experimental indications that the SM cannot be the all-encompassing theory of nature but must be embedded within a more fundamental theory. Out of a variety of miscellaneous models, supersymmetric (SUSY) models are often considered to be the most natural and appealing extensions of the SM. The widely presumed unification of the electroweak and the strong force at a high energy scale occurs naturally in SUSY models and the new particles predicted in SUSY theories cause a cancellation of the quadratic divergencies in the Higgs sector, thus stabilizing the Higgs mass. The simplest supersymmetric extension of the SM is the Minimal Supersymmetric Standard Model, which approximately doubles the particle content of the SM.

There are in principle two possibilities by which one can probe models beyond the SM such as the MSSM. On one hand one can directly search for the particles predicted by the model. For many years physicist have been looking for SUSY particles at big particle accelerator experiments, especially at LEP and at Tevatron, but so far the search was unsuccessful. Today we are at the brink of discovering new physics. The Large Hadron Collider (LHC) at the European Organization for Nuclear Research (CERN), the world's most powerful accelerator, started running last year, and if SUSY particles exist they are expected to be observed there. The first search for supersymmetry, conducted at the ATLAS and CMS detectors, did not show any significant deviation from the SM, but set new limits on SUSY parameter space [1, 2].

An alternative way to test models is to investigate the virtual effects of the predicted particles on electroweak precision observables, e.g. the masses of the W and the Z boson and the effective electroweak mixing angle. The electroweak precision observables are sensitive to quantum effects from the entire particle spectrum of a model, including particles that are too heavy for direct detection. Therefore they provide a powerful tool by which one can distinguish between different models and derive indirect constraints on the unknown parameters of a model. The strength of this method has been evident since the discovery of the top quark with a measured mass in remarkable agreement with the indirect prediction from electroweak precision observables. Furthermore the precision observables provide a good cross-check, in case SUSY particles will be found in

the following years at LHC, and even if the search remains unsuccessful the electroweak precision observables can help to determine the underlying physics.

We will focus on the prediction of the W boson mass, M_W, in terms of the Z boson mass, the Fermi constant and the fine structure constant, which can be derived from the decay of the muon. This relation constitutes one of the most important quantities of a given model, since it is highly sensitive to quantum effects from all other particles in the model.

The current experimental value of the W boson mass is 80.399 ± 0.023 GeV [3] (natural units will be used throughout this thesis) and the current accuracy of 0.03% is expected to improve further at LHC. It is reasonable to expect a reduction of the error down to 15 MeV. In order to utilize the precise experimental determination of the W boson mass and benefit from electroweak precision tests, a precise theoretical prediction for M_W is essential, which can be achieved by calculating higher orders in perturbation theory, corresponding to loop corrections to muon decay.

Within the SM the calculation of the W boson mass is quite sophisticated. The full one-loop [4, 5] and two-loop [6–17], as well as the leading three-loop [18–22] and four-loop [23, 24] corrections are also known. In addition a convenient fitting formula for M_W containing all numerically relevant contributions has been developed which approximates the result for M_W to better than 0.5 MeV for a SM Higgs mass between 10 GeV and 1 TeV [25]. A comparable accuracy would also be desirable for SUSY models, but so far the calculation is less advanced: In the MSSM the one-loop result [26–29] and leading two-loop corrections have been calculated [30–33]. Recently also in the Next To Minimal Supersymmetric Standard Model (NMSSM), the one-loop calculation [34, 35] and leading two-loop contributions [35] have been worked out.

In this thesis, we present the first step on the way towards a higher level of theoretical accuracy for the electroweak precision observables beyond the SM. A full one-loop calculation of the W boson mass in the SM and in the MSSM with complex parameters is performed for the most general set of parameters without any restrictions on the SUSY parameter space and taking the full phase dependence in the SUSY sectors into account. Previous results have been checked and confirmed. Our one-loop result is combined with all known higher order corrections, of SM and SUSY type, and consequently we obtain the most precise prediction for the W boson mass in the MSSM. All one-loop and higher order contributions are implemented in *Mathematica* which makes our result very flexible with respect to modifications and extensions. This framework and the structure of our calculation allow an easy extension to further models, like the NMSSM, models with four fermion generations, the inert doublet model and many more, with the great advantage of enabling a consistent comparison between them.

The thesis is organized as follows: In the next chapter a theoretical introduction to the SM of particle physics is given, followed by an introduction to its minimal extension, the MSSM, in chapter 2, focusing on its extended particle sector. Chapter 3 gives the basic concepts of regularization and renormalization needed for loop calculations. Technical details of our calculation, such as the programs used, are described in chapter 4. As already alluded to, the main topic of this thesis is the theoretical determination

of W boson mass in the SM and the MSSM. Therefore this calculation is extensively discussed in chapters 5, 6 and 7. In chapter 8 we show the numerical evaluation of our results, before summarizing and concluding in chapter 9.

1. The Standard Model

1.1. Gauge groups and particle content

The Standard Model of particle physics [36–38] is a theory formulated (in its current version) in the 1970s, which describes all elementary particles and their interactions, apart from gravity, which have experimentally been discovered so far. It is a quantum field theory that exhibits translation invariance and Lorentz invariance, two global symmetries following from special relativity. Further the SM is also locally gauge invariant under the gauge group $SU(3) \otimes SU(2) \otimes U(1)$. It is split into two parts, the quantum theory of electroweak interactions and Quantum Chromo Dynamics (QCD), of which the former one is based on $SU(2) \otimes U(1)$ and the latter one on the $SU(3)$ group. QCD will only briefly be discussed here, for a review see Ref. [39].

The particles of the SM are classified into fermionic (half-integer spin) and bosonic (integer spin) particles. Fermions account for the matter of the universe, a consequence of the Pauli exclusion principle [40], and bosons carry the forces between them. A special role among the bosons is played by the Higgs boson, the only SM particle that has not been observed yet. Particles of the SM obtain masses by coupling to the Higgs field. The different sectors of the SM will be outlined in the next section. We follow predominantly Refs. [41, 42].

1.1.1. Gauge sector

There are four fundamental interactions in nature, out of which three are described within the SM: the electromagnetic interaction between charged particles, the weak interaction that causes radioactive β-decay and the strong interaction which binds protons and neutrons together. The fourth interaction, most apparent in everyday life, is gravity. To this day, there is no possibility to describe gravity in a renormalizable (further explanation in section 3.2) quantum field theory, such as the SM. Quantum gravity effects are expected to be seen at energy scales of $M_{\text{Planck}} = 10^{19}$ GeV, far beyond the energy scales reachable in collider experiments. Its implications for particle physics is therefore very limited and gravity is not further explored here.

Each of the tree SM forces has an associated coupling constant, which determines the strength of the interaction, and is mediated by a (spin 1) gauge boson. The gauge bosons are not put in the SM 'by hand' but they result from requiring local gauge invariance. Table 1.1 lists the gauge fields of the SM gauge group, with their particular couplings. The gauge fields belonging to the color group $SU(3)_C$ are the eight gluons g^a $(a = 1...8)$ and g_s is the strong coupling constant. The three fields W^a $(a = 1, 2, 3)$

belong to the weak isospin group $SU(2)_I$, and the B field to the weak hypercharge group $U(1)_Y$; their couplings are denoted g and g'. The generators of the isospin group are denoted I^a and the generator of the weak hypercharge Y. I_3 is the third component of the weak isospin operator and $Q = I_3 + \frac{Y}{2}$ is the electric charge operator.

The Lagrangian of the Yang-Mills gauge sector is

$$\mathcal{L}_{YM} = -\frac{1}{4}\left(\partial_\mu W^a_\nu - \partial_\nu W^a_\mu + g\varepsilon^{abc} W^b_\mu W^c_\nu\right)^2 - \frac{1}{4}\left(\partial_\mu B_\nu - \partial_\nu B_\mu\right)^2 \ , \tag{1.1}$$

where ε^{abc} is the totally antisymmetric tensor in three dimensions, and $a, b, c \in \{1, 2, 3\}$. In this work the Einstein summation convention is used throughout. The physical gauge boson states do not directly correspond to the electroweak gauge fields of Table 1.1 but are mixtures of those. The observed fields are the charged W bosons

$$W^\pm = \frac{1}{\sqrt{2}}(W^1 \mp \mathrm{i}W^2), \tag{1.2}$$

the neutral Z boson and the photon A

$$\begin{pmatrix} Z \\ A \end{pmatrix} = \begin{pmatrix} c_W & s_W \\ -s_W & c_W \end{pmatrix} \begin{pmatrix} W^3 \\ B \end{pmatrix}. \tag{1.3}$$

Here s_W and c_W are the sine and cosine of the weak mixing angle, which at tree level are given by

$$s_W := \sin\Theta_W = \frac{g'}{\sqrt{g'^2 + g^2}} \quad , \quad c_W := \cos\Theta_W = \frac{g}{\sqrt{g'^2 + g^2}}. \tag{1.4}$$

The photon is the carrier of the electromagnetic force, and all charged particles are subject to the electromagnetic interaction. The weak force is carried by the charged gauge bosons $W^\pm$ and the neutral gauge boson Z. The neutral interaction involves all (left- and right-handed) fermions, while $W^\pm$ couples only to left-handed fermions.

Gauge group	Gauge fields	Coupling
$SU(2)_I$	W^a $(a = 1..3)$	g
$U(1)_Y$	B	g'
$SU(3)_C$	Gluons g^a $(a = 1...8)$	g_s

Table 1.1.: SM gauge fields and couplings.

1.1.2. Higgs sector

It can be shown that it is impossible to write down gauge-invariant explicit mass terms for gauge fields. However, massive gauge bosons, with masses

$$M_W = 80.399 \text{ GeV} \quad , \quad M_Z = 91.1875 \text{ GeV} \tag{1.5}$$

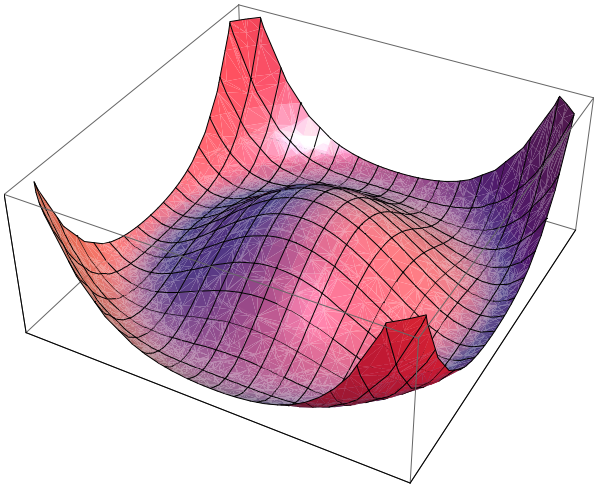

Figure 1.1.: Generic shape of the Higgs potential.

(from Ref. [3] and the LEP electroweak working group [43, 44]) have been observed, so the $SU(2)_I \otimes U(1)_Y$ gauge symmetry must be broken. The breaking is accomplished by the Higgs mechanism, which is furthermore also responsible for the generation of fermion masses. In this framework, gauge boson masses are obtained by adding another term

$$\mathcal{L}_{Higgs} = (D_\mu \phi)^\dagger (D^\mu \phi) - V(|\phi^2|) \tag{1.6}$$

to the Lagrangian. The Higgs field is a complex scalar $SU(2)$ doublet,

$$\phi = \begin{pmatrix} \phi^+ \\ \phi_0 \end{pmatrix} , \tag{1.7}$$

and D_μ the covariant derivative

$$D_\mu = \partial_\mu - \mathrm{i}gI^a W_\mu^a - i\frac{g'}{2} Y B_\mu \, . \tag{1.8}$$

Requiring gauge invariance and renormalizability, the potential can be written as

$$V(|\phi|^2) = -\mu^2 |\phi|^2 + \frac{\lambda}{4} |\phi|^4 \, , \tag{1.9}$$

where λ must be positive, so that the energy is bounded from below. For $\mu^2 > 0$, the shape of the graph of this potential looks like a Mexican hat and is minimized on a circle with non-vanishing radius. This is demonstrated in Figure 1.1. Its minimal value is at

$$|\phi|^2 = \frac{2\mu^2}{\lambda} \equiv \frac{v^2}{2}, \tag{1.10}$$

where v is the (non-zero) vacuum expectation value. After choosing one specific minimum (out of all possible states on the circle)

$$\langle \phi \rangle = \begin{pmatrix} 0 \\ \frac{v}{\sqrt{2}} \end{pmatrix} , \tag{1.11}$$

this ground state does not reflect the symmetry of the potential anymore. This feature is termed spontaneous symmetry breaking. The full scalar doublet can then be written as an expansion around the ground state

$$\phi = \begin{pmatrix} \phi^+ \\ \frac{1}{\sqrt{2}}(v + H + i\chi) \end{pmatrix} \tag{1.12}$$

where ϕ^+ and χ are the unphysical degrees of freedom, called Goldstone bosons, that give the longitudinal part of the gauge bosons. The Goldstone bosons can be eliminated by choosing a special gauge (the concept of gauge fixing will be explained in section 1.1.4). The gauge in which the Goldstone fields vanish, is called unitary gauge. H is the only physical field - the Higgs boson with a mass of

$$m_H = \sqrt{2}\mu. \tag{1.13}$$

In the later sections, when we talk about the SM and the MSSM simultaneously, we will denote the SM Higgs boson as h_{SM}, instead of H, to avoid confusions.

The masses of the physical particles can be extracted most easily in unitary gauge. Therefore (1.12) with $\phi^+ = \chi = 0$ and (1.8) are inserted into the Lagrangian (1.6). From the first term of (1.6) one finds terms where v couples to the W^a and B fields and thus generates the gauge boson masses

$$M_W = c_W M_Z = \frac{1}{2}\, g\, v\ . \tag{1.14}$$

1.1.3. Fermion sector

The fermions in the SM are divided into leptons and quarks. Leptons exist as free particles, while quarks are always bound inside hadrons, such as protons and neutrons. All fermions are listed in Table 1.2 with their corresponding quantum numbers. The fermions can be divided into three generations, which have the same quantum numbers and differ only by the mass of the particles. The number three is not given by the theory but we know from experimental results that there must be at least three fermion generations and not more than three light neutrinos. The left-handed fermions build weak isospin doublets

$$L_j^L = \begin{pmatrix} \nu_j^L \\ l_j^L \end{pmatrix} \quad , \quad Q_j^L = \begin{pmatrix} u_j^L \\ d_j^L \end{pmatrix}, \tag{1.15}$$

which implies that a (left-handed) fermion with quantum number $I_3 = +1/2$ can interact weakly with a W boson and a (left-handed) fermion with quantum number $I_3 = -1/2$. The right-handed fermions build weak isospin singlets

$$l_j^R \quad , \quad u_j^R \quad , \quad d_j^R\ . \tag{1.16}$$

In (1.15) and (1.16), j indicates the generation index, ν a neutrino, l a charged lepton, u an up-type quark and d a down-type quark. There are no right-handed neutrinos in the SM.

An explicit Dirac-type fermion mass term in the Lagrangian would not preserve gauge invariance. Fermion masses are generated by so called Yukawa couplings of the Higgs field to the fermion fields. The Lagrangian of the fermionic sector is

$$\begin{aligned}\mathcal{L}_F = &\sum_i \left(\bar{L}_i^L \mathrm{i}\gamma^\mu D_\mu L_i^L + \bar{Q}_i^L \mathrm{i}\gamma^\mu D_\mu Q_i^L\right) \\ &+ \sum_i \left(\bar{l}_i^R \mathrm{i}\gamma^\mu D_\mu l_i^R + \bar{u}_i^R \mathrm{i}\gamma^\mu D_\mu u_i^R + \bar{d}_i^R \mathrm{i}\gamma^\mu D_\mu d_i^R\right) \\ &- \sum_{ij} \left(\bar{L}_i^L G_{ij}^l l_j^R \phi + \bar{Q}_i^L G_{ij}^u u_j^R \tilde{\phi} + \bar{Q}_i^L G_{ij}^d d_j^R \phi + h.c.\right)\end{aligned} \tag{1.17}$$

where $\tilde{\phi} = \mathrm{i}\sigma_2\phi^*$ is the charge conjugated Higgs field and G^l, G^u and G^d are the Yukawa coupling matrices. The sums run over the three generations. The γ-matrices are defined by

$$\{\gamma_\mu, \gamma_\nu\} = 2g_{\mu\nu} \ , \tag{1.18}$$

where $g_{\mu\nu}$ denotes the Minkowski metric. Without right-handed neutrinos, no neutrino Yukawa terms are possible and they remain massless in the SM.* The mass eigenstates of the quarks do not correspond to their weak interaction eigenstates. The relation of the weak interaction quark eigenstates to the mass eigenstates is

$$\begin{aligned}{q'}_i^L &= U_{ik}^{q,L} q_k^L \\ {q'}_i^R &= U_{ik}^{q,R} q_k^R\end{aligned} \tag{1.19}$$

with masses

$$m_{q',i} = U_{ik}^{q,L} G_{km}^q U_{mi}^{q,R\dagger} \frac{v}{\sqrt{2}}. \tag{1.20}$$

where $q \in \{u, d\}$. The product

$$V_{ij} = U_{ik}^{u,L} U_{kj}^{d,L\dagger} \tag{1.21}$$

is referred to as quark mixing matrix or Cabibbo-Kobayashi-Maskawa (CKM) matrix. A complex phase in the quark mixing matrix gives the only source of CP-violation in the SM. We neglect quark mixing throughout this work. Then V_{ij} is a unit matrix.

1.1.4. Gauge fixing, ghost sector

The electroweak field theory is defined by the Lagrangian

$$\mathcal{L}_{EWSM} = \mathcal{L}_{YM} + \mathcal{L}_{Higgs} + \mathcal{L}_F \ . \tag{1.22}$$

*But neutrino masses have been observed, which shows that the SM in its current form cannot be the full theory but is probably embedded in a more fundamental, so far unknown theory. More indications for physics beyond the SM are given in section 2.1

	1.	2.	3.	I_3	Y	Q
Leptons	$\begin{pmatrix} \nu_e \\ e \end{pmatrix}_L$	$\begin{pmatrix} \nu_\mu \\ \mu \end{pmatrix}_L$	$\begin{pmatrix} \nu_\tau \\ \tau \end{pmatrix}_L$	1/2	-1	0
				-1/2	-1	-1
	e_R	μ_R	τ_R	0	-2	-1
Quarks	$\begin{pmatrix} u \\ d \end{pmatrix}_L$	$\begin{pmatrix} c \\ s \end{pmatrix}_L$	$\begin{pmatrix} t \\ b \end{pmatrix}_L$	1/2	1/3	2/3
				-1/2	1/3	-1/3
	u_R	c_R	t_R	0	4/3	2/3
	d_R	s_R	b_R	0	-2/3	-1/3

Table 1.2.: All SM fermions with associated quantum numbers. I_3 is the third component of the of the weak isospin, Y the weak hypercharge and $Q = I_3 + Y/2$ the electric charge.

For the incorporation of quantum effects, the SM needs to be quantized.

The propagators are the Green functions of the free field equations, which can be derived from Feynman path integrals [45, 46]. But naively applying the path integral formalism to non-abelian gauge theories yields mathematical inconsistencies. This is described in detail in Ref. [42]. For the quantization of the SM this problem, which is due to the gauge invariance of the Lagrangian, must be solved.

This requires the insertion of additional, gauge fixing, terms in the Lagrangian. Using the renormalizable 't Hooft gauge, in which the propagators behave like $1/k^2$ for large momentum k, the gauge fixing term is

$$\mathcal{L}_{fix} = -\frac{1}{2}\left[(F^A)^2 + (F^Z)^2 + 2F^{W^+}F^{W^-}\right] , \tag{1.23}$$

with

$$\begin{aligned} F^{W^\pm} &= (\xi_1^W)^{-\frac{1}{2}}\partial^\mu W_\mu^\pm \mp \mathrm{i}M_W(\xi_2^W)^{\frac{1}{2}}\phi^\pm \\ F^Z &= (\xi_1^Z)^{-\frac{1}{2}}\partial^\mu Z_\mu - M_Z(\xi_2^Z)^{\frac{1}{2}}\chi \\ F^A &= (\xi_1^A)^{-\frac{1}{2}}\partial^\mu A_\mu \ . \end{aligned} \tag{1.24}$$

Here $\xi_1^W, \xi_2^W, \xi_1^Z, \xi_2^Z$ and ξ_1^A are the five gauge parameters. Mixing terms between gauge boson fields and Goldstone fields arise from electroweak symmetry breaking. If $\xi_2^W = \xi_1^W$ and $\xi_2^Z = \xi_1^Z$ is chosen, these mixing terms are absent, since they are canceled by the terms $\mathrm{i}M_W(\xi_2^W)^{\frac{1}{2}}\phi^\pm$ and $M_Z(\xi_2^Z)^{\frac{1}{2}}\chi$.

In these equations non-physical contributions appear, which can be canceled by introducing so called Faddeev-Popov ghost $u^\alpha(x)$ and antighost $\bar{u}^\alpha(x)$ fields ($\alpha = W^\pm, A, Z$). Ghosts are unphysical mathematical entities, which do not correspond to 'real' external particles and only appear as virtual particles in Feynman diagrams. The additional Faddeev-Popov term we get in the Lagrangian is

$$\mathcal{L}_{FP} = \sum_{\alpha,\beta=W^\pm,A,Z} \bar{u}^\alpha(x)\frac{\delta F^\alpha}{\delta\theta^\beta(x)}u^\beta(x). \tag{1.25}$$

where the θ^α are infinitesimal gauge transformations. From the variations of the involved fields $A, Z, W^\pm, \phi^+$ and χ under the infinitesimal gauge transformations, the variations of the gauge fixing operators $\frac{\delta F^\alpha}{\delta \theta^\beta}$ can be determined. The resulting formulas can be found in Ref. [42]. Including these additional terms $\mathcal{L}_{fix}$ and $\mathcal{L}_{FP}$, the full Lagrangian of the electroweak SM can be written as

$$\mathcal{L}_{GSW} = \mathcal{L}_{EWSM} + \mathcal{L}_{fix} + \mathcal{L}_{FP} \,, \tag{1.26}$$

where GSW stands for Glashow-Salam-Weinberg Model. The parameters ξ_i^α can be chosen freely, however in the end the S-matrix element must be independent of the gauge fixing. In this work the particularly simple Feynman-'t Hooft gauge is chosen, where all ξ_i^α are set equal 1. In the Feynman-'t Hooft gauge each ghost field acquires the same mass as its associated gauge boson field.

In a scattering process, the probability for an incoming state $|i\rangle$ to transform into an outgoing state $|f\rangle$ is related to the absolute square of the scattering matrix (S-matrix) element $\langle f|S|i\rangle$. The relation between the S-matrix and the matrix element $\mathcal{M}$ is given by

$$\langle f|S|i\rangle = \langle f|i\rangle + \mathrm{i}(2\pi)^4 \delta^{(4)}\left(p_i - p_f\right) \mathcal{M} \,, \tag{1.27}$$

and the four momenta are on the mass shell, so $p^0_{i/f} = E_{i/f}$ where $E_{i/f}$ denotes the energy of the incoming/outgoing particles.

In quantum field theories, where the coupling g is small, the matrix element $\mathcal{M}$ (and therewith observables $O \propto |\mathcal{M}|^2$) can be calculated perturbatively, i.e. $\mathcal{M}$ can be expressed as a power series in g and for small enough g higher orders can be truncated. The series can be illustrated by Feynman diagrams with increasing number of loops and vertices. In renormalizable theories only 3-point and 4-point interaction vertices are allowed.

2. The Minimal Supersymmetric Standard Model

2.1. Motivation

Though the SM is a very successful theory that describes nearly all experimental results so far with high precision, there are a few open questions that cannot be answered within the SM. The MSSM is the minimal supersymmetric extension of the SM which addresses some of the problems and open questions. In this section we list the most important shortcomings of the SM and briefly sketch possible solutions.

One important remaining issue in the SM is the hierarchy problem: The mass of the Higgs boson is not given in the SM, but the highest possible value for m_H is about 1 TeV, since otherwise unitarity would be violated in certain scattering processes, and the SM would become inconsistent. Electroweak precision observables favour a much lower value of $m_H \approx 100$ GeV, whereas the lower mass limit from experimental searches is 114.4 GeV [47]. As we mentioned before, the SM does not include gravity, therefore it fails at least at $M_{\text{Planck}} = 10^{19}$ GeV, where quantum gravitational effects become important. This implies that the SM must be the effective limit of a more fundamental theory, so it can only be valid up to a cutoff scale Λ, at which new physics appear. The Higgs mass can be calculated as

$$m_H^2 = m_{H,0}^2 + \Delta m_H^2 \ , \tag{2.1}$$

where $m_{H,0}^2$ is the bare mass that appears in the Lagrangian and Δm_H^2 contains the higher order corrections. Calculating one-loop corrections from a fermion loop to the Higgs mass and cutting off the integrals at Λ yields

$$\Delta m_H^2 = \frac{\lambda^2}{8\pi^2}\Lambda^2 + ... \ , \tag{2.2}$$

where λ is the coupling of the fermion to the Higgs field, which is ≈ 1 for heavy quarks. The ellipsis denote terms proportional to m_f^2 that grow at most logarithmically with Λ. This means that for $\Lambda = M_{\text{Planck}}$ the corrections to the Higgs mass are of the size $\Delta m_H^2 \approx 10^{38}$ GeV^2. But we know that that $m_H \lesssim 1$ TeV, so $m_H^2 \lesssim 10^6$ GeV^2, which means that immense cancellation between $m_{H,0}^2$ and Δm_H^2 is necessary (extreme 'fine-tuning'). This seems very unnatural and is known as the hierarchy problem.

In SUSY all fermions have superpartners which give additional corrections to the Higgs mass

$$\Delta m_H^2 = \frac{\lambda_S^2}{8\pi^2}\Lambda^2 + \dots . \tag{2.3}$$

With $\lambda_S^2 = -\lambda^2$ the quadratic divergencies cancel and the Higgs mass is stable. In unbroken supersymmetry the superpartners have the same mass as the fermions, then the Higgs mass corrections cancel completely. But as we will argue in the next section, supersymmetry must be a broken, which implies that the masses of the superpartners differ from the mass of the SM particles: $m_{\tilde{f}}^2 = m_f^2 + \Delta^2$. This is not a problem, as long as the relation between the couplings remains unchanged. Small logarithmic corrections to the Higgs masses is acceptable. As long as the splitting between the masses of the SM and the SUSY particles is not too large, SUSY provides an appealing solution of the hierarchy problem.

So far there is no consistent quantum field theory describing all interactions including gravitation, but the algebra of general relativity, the framework in which gravity is described, is part of the local SUSY algebra, witch gives a natural connection between these two theories and makes the supersymmetry based approaches to describe gravitation particularly promising.

Another striking quality of SUSY is that the unification of the couplings of the three forces at a high energy scale, which is not possible in the SM, appears naturally in electroweak scale SUSY, even though it was not specially constructed for that purpose. Theories in which the three interactions merge are called Grand Unified Theories (GUTs).

Finally we want to mention two more astrophysical observations, that indicate that the SM cannot be the complete theory, but must be embedded in a more fundamental theory, like the MSSM. This first observation is the baryon asymmetry in the universe. This discrepancy cannot be explained by just the CP-violation from the CKM phase in the SM alone and indicates, that further sources of CP-violation must exist. Secondly it is required by cosmological measurements that 23% of the total energy in the universe is in the form of cold dark matter. If elementary particles make up for dark matter they can at most interact weakly with other particles and they have to be stable over cosmological timescales. The SM does not provide any such candidate for dark matter, while in the MSSM the lightest SUSY particle can be be a suitable candidate.

2.2. Theory

A supersymmetric transformation Q acting on a fermionic state gives a bosonic state and vice versa. The spin 1/2 fermions get spin 0 superpartners called sfermions. Left and right handed fermions have different superpartners, resulting in two up-type squarks $\tilde{u}_{L,R}$, two down-type squarks $\tilde{d}_{L,R}$, two sleptons $\tilde{l}_{L,R}$ and a sneutrino $\tilde{\nu}$ for each of the three generations. The gauge bosons are assigned fermionic superpartners called

gauginos, composed of a wino $\tilde{W^{\pm}}$, a zino $\tilde{Z}$, a photino $\tilde{\gamma}$ and a gluino $\tilde{g}$. Instead of one Higgs doublet, as in the SM, the MSSM has two Higgs doublets, involving five physical Higgs bosons. The fermionic superpartners of the Higgs bosons are the Higgsinos $\tilde{H}$. Each particle and its superpartner have identical quantum numbers except for the spin. This implies that, in an unbroken supersymmetric model, particles and antiparticles have degenerate masses.

But since no superparticles have been observed experimentally yet, supersymmetry, if existing, cannot be an exact symmetry and must be spontaneously broken. The breaking is described by explicitly adding terms, called soft breaking terms, to the Lagrangian density. Not to reintroduce quadratic divergencies and therewith the hierarchy problem, the relation between the dimensionless couplings λ and λ_S must be maintained, which is the meaning of the term 'soft'.

Lepton and baryon number conservation have experimentally been probed precisely and have been confirmed. Whereas in the SM these symmetries result directly from the theory requirements, in supersymmetric models lepton and baryon number can be violated, which would lead to an unstable proton. This problem can be solved by requiring that every coupling in the MSSM preserves R parity

$$R = (-1)^{3B+L+2S} = \begin{cases} +1 & \text{for SM particles} \\ -1 & \text{for SUSY particles} \end{cases} \tag{2.4}$$

where B is the Baryon number (quarks have baryon number $+\frac{1}{3}$, the antiquarks have baryon number $-\frac{1}{3}$), L the Lepton number (leptons have lepton number $+1$), the antileptons have lepton number -1) and S is the spin. The conservation of R parity implies that supersymmetric particles can only be produced in pairs and that the lightest supersymmetric particle (LSP) is stable.

2.3. Particle content of the MSSM

In this section the particle sectors of the MSSM, that do not exist in the SM or differ from it, are described. The conventions and notations are introduced and formulas needed for the work in this thesis are presented.

2.3.1. Sfermion sector

In the MSSM Lagrangian the masses of the sfermions, $\tilde{f}$, superpartners of quarks and leptons, are described by the mass term

$$\mathcal{L}_{m_{\tilde{f}}} = -\frac{1}{2} \left(\tilde{f}_L^{\dagger}, \tilde{f}_R^{\dagger} \right) M_{\tilde{f}} \begin{pmatrix} \tilde{f}_L \\ \tilde{f}_R \end{pmatrix}. \tag{2.5}$$

$M_{\tilde{f}}$ is the sfermion mass matrix

$$M_{\tilde{f}} = \begin{pmatrix} M_L^2 + m_f^2 & m_f X_f^* \\ m_f X_f & M_R^2 + m_f^2 \end{pmatrix} \tag{2.6}$$

with

$$\begin{aligned} M_L^2 &= M_{\tilde{f}_L}^2 + M_Z^2 \cos 2\beta (I_3^f - Q_f s_W^2) \\ M_R^2 &= M_{\tilde{f}_R}^2 + M_Z^2 \cos 2\beta Q_f s_W^2 \\ X_f &= A_f - \mu^* \{\cot\beta, \tan\beta\} \ , \end{aligned} \tag{2.7}$$

where in the last line $\cot\beta$ refers to up-type fermions and $\tan\beta$ to down-type fermions. $M_{\tilde{f}_L}$ and $M_{\tilde{f}_R}$ denote the soft SUSY breaking parameters. For right-handed fermions the soft SUSY breaking parameters can be chosen independently for leptons, up-type quarks and down-type quarks, whereas for left-handed fermions SU(2) gauge invariance requires the soft SUSY breaking parameters for up- and down-type quarks to be equal. Our calculation is done for the general case of five independent soft SUSY breaking parameters, however in the numerical evaluation only scenarios in which all $M_{\tilde{f}_L}$ and $M_{\tilde{f}_R}$ are set equal to M_{SUSY} are considered. We are looking at the MSSM with complex parameters, in the following often referred to as complex MSSM or cMSSM. In this extended model, the sfermion sector can have N_f+1 complex phases $A_f = |A_f| \exp i\phi_{A_f}$ and $\mu = |\mu| \exp i\phi_\mu$, where N_f is the number of fermions.

The mass eigenstates of the sfermions arise from the left- and right-handed states $\tilde{f}_L$ and $\tilde{f}_R$ via a rotation by an angle $\theta_{\tilde{f}}$

$$\begin{pmatrix} \tilde{f'}_1 \\ \tilde{f'}_2 \end{pmatrix} = \begin{pmatrix} \cos\theta_{\tilde{f}} & \sin\theta_{\tilde{f}} \\ -\sin\theta_{\tilde{f}} & \cos\theta_{\tilde{f}} \end{pmatrix} \begin{pmatrix} \tilde{f}_L \\ \tilde{f}_R \end{pmatrix} .$$

In our convention $\tilde{f}_1$ is always lighter than $\tilde{f}_2$. If $m_{\tilde{f'}_1} < m_{\tilde{f'}_2}$ we set $\tilde{f}_1 = \tilde{f'}_1$ and $\tilde{f}_2 = \tilde{f'}_2$, otherwise

$$\begin{pmatrix} \tilde{f}_1 \\ \tilde{f}_2 \end{pmatrix} = \begin{pmatrix} 0 & 1 \\ 1 & 0 \end{pmatrix} \begin{pmatrix} \tilde{f'}_1 \\ \tilde{f'}_2 \end{pmatrix} .$$

In terms of the sfermion masses $m_{\tilde{f}'_1}$ and $m_{\tilde{f}'_2}$ and the mixing angle $\theta_{\tilde{f}}$ the mass matrix (2.6) can also be written as

$$M_{\tilde{f}} = \begin{pmatrix} \cos^2\theta_{\tilde{f}} m^2_{\tilde{f}'_1} + \sin^2\theta_{\tilde{f}} m^2_{\tilde{f}'_2} & \sin\theta_{\tilde{f}}\cos\theta_{\tilde{f}}(m^2_{\tilde{f}'_1} - m^2_{\tilde{f}'_2}) \\ \sin\theta_{\tilde{f}}\cos\theta_{\tilde{f}}(m^2_{\tilde{f}'_1} - m^2_{\tilde{f}'_2}) & \sin^2\theta_{\tilde{f}} m^2_{\tilde{f}'_1} + \cos^2\theta_{\tilde{f}} m^2_{\tilde{f}'_2} \end{pmatrix} . \tag{2.8}$$

By comparison of the two descriptions one obtains expressions for the sfermion masses and mixing angles.

The off-diagonal entries of $M_{\tilde{f}}$, see (2.6), are proportional to the mass of the associated fermion. Therefore the effect of sfermion mixing is exiguous, apart from the stop and (for large $\tan\beta$) the sbottom sector. If mixing is neglected $\cos\theta_{\tilde{f}} = 1$ and $m_{\tilde{f'}_{1,2}} = m_{\tilde{f}_{L,R}}$. Our analytic results allow free choices of all A_f, while in the numerical analysis, we choose $A_f = A_t$ for all sfermions.

2.3.2. Higgs sector

Unlike the Higgs sector of the SM, the Higgs sector of the MSSM cannot be of the minimal type, but needs two Higgs doublets to give masses to up-type and down-type fermions. The two Higgs doublets in the complex MSSM, with opposite hypercharge $-Y_{H_1} = Y_{H_2} = 1$, are

$$H_1 = \begin{pmatrix} v_1 + \frac{1}{\sqrt{2}}(\phi_1^0 + \mathrm{i}\chi_1^0) \\ -\phi_1^- \end{pmatrix} \qquad H_2 = e^{\mathrm{i}\xi} \begin{pmatrix} \phi_2^+ \\ v_2 + \frac{1}{\sqrt{2}}(\phi_2^0 + \mathrm{i}\chi_2^0) \end{pmatrix} , \tag{2.9}$$

where v_1 and v_2 are the vacuum expectation values of the two doublets. The Higgs potential of the MSSM, the supersymmetric analogue to (1.10), is

$$\begin{aligned} V = {} & m_1^2 H_1 \bar{H}_1 + m_2 H_2 \bar{H}_2 - m_{12}^2(\epsilon_{ab} H_1^a H_2^b + \text{h.c.}) \\ & + \frac{g^2 + g'^2}{8}(H_1\bar{H}_1 - H_2\bar{H}_2)^2 + \frac{g^2}{2}|H_1\bar{H}_2|^2 , \end{aligned} \tag{2.10}$$

where $m_{1,2}^2 = \tilde{m}_{1,2}^2 + |\mu|^2$ are the mass parameters and $\tilde{m}_{1,2}^2$ and m_{12} the soft breaking parameters, of which m_{12} can be complex but its phase can be rotated away. ϵ_{ab} is the two-dimensional antisymmetric tensor and g and g' the gauge couplings given in Table 1.1.

In order to fulfill the minimum condition of the Higgs potential, the complex phase ξ has to vanish at tree-level. First we will discuss the tree level case, where we have no CP violation. There are eight degrees of freedom, from which five physical Higgs and 3 unphysical Goldstone bosons (which become the longitudinal mode of the Z^0 and $W^\pm$ bosons) originate. The fields ϕ_1^0 and ϕ_2^0 mix and form the CP-even mass eigenstates H and h. The neutral CP-odd state A and the neutral Goldstone boson G are obtained from the mixing of the states χ_1^0 and χ_2^0. The mixing of $\phi_1^\pm$ and $\phi_2^\pm$ (ϕ_1^+ is defined as $(\phi_1^-)^*$ and ϕ_2^- as $(\phi_2^+)^*$) described by the same angle gives the charged Higgs $H^\pm$ and the charged Goldstone bosons $G^\pm$:

$$\begin{aligned} \begin{pmatrix} H \\ h \end{pmatrix} &= \begin{pmatrix} \cos\alpha & \sin\alpha \\ -\sin\alpha & \cos\alpha \end{pmatrix} \begin{pmatrix} \phi_1^0 \\ \phi_2^0 \end{pmatrix} \\ \begin{pmatrix} G \\ A \end{pmatrix} &= \begin{pmatrix} \cos\beta & \sin\beta \\ -\sin\beta & \cos\beta \end{pmatrix} \begin{pmatrix} \chi_1^0 \\ \chi_2^0 \end{pmatrix} \\ \begin{pmatrix} G^\pm \\ H^\pm \end{pmatrix} &= \begin{pmatrix} \cos\beta & \sin\beta \\ -\sin\beta & \cos\beta \end{pmatrix} \begin{pmatrix} \phi_1^\pm \\ \phi_2^\pm \end{pmatrix} . \end{aligned} \tag{2.11}$$

The angles α and β are defined as

$$\tan\beta = \frac{v_2}{v_1} \quad , \quad \tan 2\alpha = \frac{m_A^2 + m_Z^2}{m_A^2 - m_Z^2} \tan 2\beta . \tag{2.12}$$

Corresponding to the SM case (2.13) the generated gauge boson masses are

$$M_W = c_W M_Z = \frac{1}{2} g \sqrt{v_1^2 + v_2^2}. \tag{2.13}$$

Expressing the Higgs doublets in terms of the mass eigenvalues and using that v_1 and v_2 minimize the potential, one finds the tree-level mass relations

$$\begin{aligned} m_A^2 &= \frac{2m_{12}^2}{\sin 2\beta} \\ m_{H,h}^2 &= \frac{1}{2}\left(m_A^2 + M_Z^2 \pm \sqrt{(m_A^2 + M_Z^2)^2 - 4M_Z^2 m_A^2 \cos^2 2\beta}\right) \\ m_{H^\pm}^2 &= m_A^2 + M_{W^\pm}^2 \,. \end{aligned} \tag{2.14}$$

At tree level the MSSM Higgs sector is fully described by two new parameters, often chosen as m_A and $\tan\beta$.

Higher order corrections to the Higgs masses can be sizable and must be included. Particularly important are the one- and two-loop contributions from the $t/\tilde{t}$ sector. Beyond tree-level CP-violating effects appear in the cMSSM. When loops are included, the Higgs sector depends also on other SUSY parameters, some of which can be complex (A_f and μ), inducing a mixing between h, H and A. In that case usually $m_{H^\pm}$ instead of m_A is taken as input value. The Higgs masses in the cMSSM, including one- and two-loop corrections, are calculated in *FeynHiggs* [48] (see section 4.2). For a detailed discussion on the loop corrections in the Higgs sector of the cMSSM we refer to Ref. [49].

2.3.3. Chargino sector

The fermionic superpartners $\tilde{W}^\pm$, $\tilde{Z}$, $\tilde{A}$ and $\tilde{H}$ of the SM gauge bosons and the Higgs fields are not mass eigenstates. The charged Higgsinos and gauginos mix into charginos $\tilde{\chi}_{1,2}^\pm$, whose mass matrix is given by

$$X = \begin{pmatrix} M_2 & \sqrt{2}M_W \sin\beta \\ \sqrt{2}M_W \cos\beta & \mu \end{pmatrix} , \tag{2.15}$$

with the soft breaking parameter M_2. Using a singular value decomposition, the mass matrix can be diagonalized with two unitary matrices U and V

$$U^* X V^\dagger = \begin{pmatrix} m_{\tilde{\chi}_1^+} & 0 \\ 0 & m_{\tilde{\chi}_2^+} \end{pmatrix} \tag{2.16}$$

and one finds the eigenvalues

$$m_{\tilde{\chi}_{1,2}^+}^2 = \frac{M_2^2 + |\mu|^2 + 2M_W^2}{2} \mp \sqrt{\left(\frac{M_2^2 + |\mu|^2 + 2M_W^2}{2}\right)^2 - \left|M_W^2 \sin 2\beta - \mu M_2\right|^2} \,. \tag{2.17}$$

2.3.4. Neutralino sector

Neutralinos, $\tilde{\chi}_i^0$ ($i \in \{1,2,3,4\}$), are fermions which evolve from the mixing of the neutral Higgsinos, the Zino and the Photino (similar to the SM the latter two are composed of Bino and Wino) via the matrix

$$Y = \begin{pmatrix} M_1 & 0 & -M_Z s_W \cos\beta & M_Z s_W \sin\beta \\ 0 & M_2 & M_Z c_W \cos\beta & -M_Z c_W \sin\beta \\ -M_Z s_W \cos\beta & M_Z c_W \cos\beta & 0 & -\mu \\ M_Z s_W \sin\beta & -M_Z c_W \sin\beta & -\mu & 0 \end{pmatrix}. \tag{2.18}$$

The neutralino masses are obtained by a diagonalization of the mass matrix with a unitary transformation matrix N

$$N^* Y N^\dagger = \begin{pmatrix} m_{\tilde{\chi}_1^0} & 0 & 0 & 0 \\ 0 & m_{\tilde{\chi}_2^0} & 0 & 0 \\ 0 & 0 & m_{\tilde{\chi}_3^0} & 0 \\ 0 & 0 & 0 & m_{\tilde{\chi}_4^0} \end{pmatrix}. \tag{2.19}$$

In our calculation the computation of the eigenvalues of a complex 4×4 matrix is done in *FeynHiggs* (see section 4.2).

In the chargino and neutralino sector M_1 and M_2 can (in addition to μ) be complex. However, there are only two physical phases and one of the phases, usually M_2, can be rotated away.

2.3.5. Gluinos

Gluinos are the spin 1/2 superpartners of the gluons. Gluons exist in eight color states. Correspondingly there are also eight gluinos that all get the same Majorana mass

$$m_{\tilde{g}} = |M_3|. \tag{2.20}$$

In the cMSSM M_3 can be complex, $M_3 = |M_3| e^{\mathrm{i}\phi_{M_3}}$.

3. Regularization and renormalization

3.1. Regularization

For the perturbative evaluation of a quantum field theory, loops have to be included. The loop diagrams contributing to a propagator are combined into a quantity called the self-energy Σ,

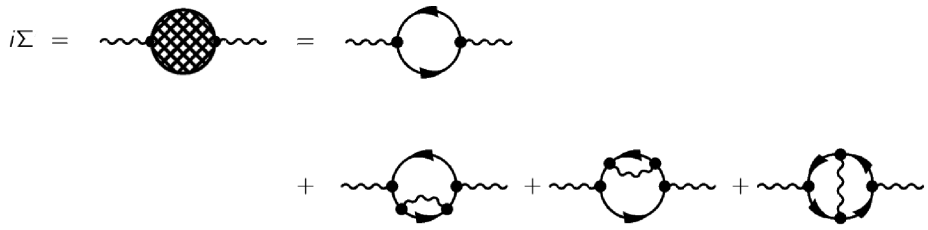

(3.1)

which is the sum of all one-particle irreducible loop diagrams. Irreducible means that the diagram cannot be cut into two (non-trivial) parts by cutting a single line. The full propagator, D, can then be calculated by summing over all diagrams with an increasing number of self-energy corrections to the tree-level propagator D^0

$$\begin{aligned} \mathrm{i}D &= \mathrm{i}D^0 + \mathrm{i}D^0(\mathrm{i}\Sigma)\mathrm{i}D^0 + \mathrm{i}D^0(\mathrm{i}\Sigma)\mathrm{i}D^0(\mathrm{i}\Sigma)\mathrm{i}D^0 + ... \\ &= \mathrm{i}D^0\left(1 - \Sigma D^0 + (\Sigma D^0)^2 - ...\right) \\ &= \mathrm{i}D^0 \sum_{n=1}^{\infty} \left(-\Sigma D^0\right)^n = \mathrm{i}D^0 \frac{1}{1+\Sigma D^0} \end{aligned} \tag{3.2}$$

with the result

$$(D)^{-1} = (D^0)^{-1} + \Sigma\ . \tag{3.3}$$

The self-energy of a gauge boson can be written as

$$\Sigma_{\mu\nu}\left(p^2\right) = \left(-g_{\mu\nu} + \frac{p_\mu p_\nu}{p^2}\right)\Sigma_T\left(p^2\right) - \frac{p_\mu p_\nu}{p^2}\Sigma_L\left(p^2\right) \tag{3.4}$$

where $\Sigma_T(p^2)$ is the transverse part and $\Sigma_L(p^2)$ the longitudinal part of the gauge boson self-energy.

The fermion self-energy can be split into a vector, an axial vector, a scalar and a pseudoscalar part

$$\Sigma(p) = \not{p}\Sigma_V\left(p^2\right) + \not{p}\gamma^5\Sigma_A\left(p^2\right) + m_f\Sigma_S\left(p^2\right) + m_f\gamma^5\Sigma_P\left(p^2\right) \tag{3.5}$$

with $\gamma_5 = \mathrm{i}\gamma^0\gamma^1\gamma^2\gamma^3 \propto \epsilon^{\mu\nu\rho\sigma}\gamma_\mu\gamma_\nu\gamma_\rho\gamma_\sigma$, or alternatively into left and right handed parts

$$\begin{aligned}\Sigma(p) =& \frac{1}{2}\not{p}\left(1-\gamma^5\right)\Sigma_L\left(p^2\right) + \frac{1}{2}\not{p}\left(1+\gamma^5\right)\Sigma_R\left(p^2\right) \\ &+ \frac{1}{2}m_f\left(1-\gamma^5\right)\Sigma_{L'}\left(p^2\right) + \frac{1}{2}m_f\left(1+\gamma^5\right)\Sigma_{R'}\left(p^2\right)\end{aligned} \tag{3.6}$$

with

$$\begin{aligned}\Sigma_R\left(p^2\right) &= \Sigma_V\left(p^2\right) + \Sigma_A\left(p^2\right) \\ \Sigma_L\left(p^2\right) &= \Sigma_V\left(p^2\right) - \Sigma_A\left(p^2\right)\ ,\end{aligned} \tag{3.7}$$

and

$$\begin{aligned}\Sigma_{R'}\left(p^2\right) &= \Sigma_S\left(p^2\right) + \Sigma_P\left(p^2\right) \\ \Sigma_{L'}\left(p^2\right) &= \Sigma_S\left(p^2\right) - \Sigma_P\left(p^2\right)\ .\end{aligned} \tag{3.8}$$

To calculate the loop diagrams an integration over all four-momentum of the off-shell particle in the loop must be performed, which generally yields UV-divergencies. To get finite results the concepts of regularization and renormalization are needed. Regularization introduces a new parameter δ, in a way that the original theory is retrieved for $\delta \to \delta_0$. The loop integral is finite for $\delta \neq \delta_0$, but has a pole at $\delta = \delta_0$. Only after renormalization (see section 3.2) the limit $\delta \to \delta_0$ can be taken and finite results (Green functions) in terms of renormalized parameters are obtained. There are several different regularization schemes which do not necessarily yield the same result for a specific loop diagram, but the results for physical observables must always be independent of the regularization scheme. If a regularization scheme that breaks the symmetry of the theory is chosen, this needs to be corrected by symmetry-restoring terms. The three different regularization schemes used in our work will be introduced in the next sections.

3.1.1. Dimensional Regularization

Dimensional Regularization (DR) [50] is a regularization method introduced by t'Hooft and Veltman (1972) which features an elegant convenient formalism for simple loop calculations. In DR the definition of momenta and Lorentz covariants is extended from 4 to $D = 4 - \epsilon$ dimensions. Identities of metric tensors and Dirac matrices in D dimensions are listed in appendix B.1.

A difficulty arises in chiral theories, since γ_5 is a four-dimensional object with no natural continuation to D dimensions. Ref. [51] introduces a naive scheme with an anticommuting γ_5 in all dimensions that can be used for one-loop calculations.

With the extension of space-time dimensions also the integrals have to be calculated in $D = 4 - \epsilon$ instead of 4 dimensions and the crucial point of DR is that the integrals that are UV-divergent in 4 dimensions are convergent for $\epsilon \neq 0$

$$\int \frac{\mathrm{d}^4 q}{(2\pi^4)} \to \mu^{4-D} \int \frac{\mathrm{d}^D q}{(2\pi)^D}. \tag{3.9}$$

An arbitrary energy scale μ is introduced here to keep the couplings dimensionless. At one-loop order any of these loop integrals can be decomposed into scalar one-loop integrals, that do not contain any Lorentz index in the numerator. The scalar integrals we used are derived and listed in appendix B.2. In the result, one finds terms proportional to $\frac{1}{\epsilon}$, terms independent of ϵ and terms proportional to ϵ. By appropriate renormalization, the terms with $\frac{1}{\epsilon}$ can be subtracted and then the limit $\epsilon \to 0$ can be taken.

3.1.2. Dimensional Reduction and Constrained Differential Renormalization

Dimensional Regularization is known to give problems in supersymmetric models since an action which is supersymmetric in 4 dimensions does not have to remain supersymmetric in $D \neq 4$ dimensions [52].

For loop calculations in supersymmetric theories Dimensional Reduction [53, 54] (DRED), a modified version of DR, is commonly used, in which supersymmetric identities have been verified up to the two-loop level [54, 55]. In DRED the integration momenta are D dimensional as in DR, while the Dirac algebra is kept four dimensional. This method has successfully been used for many calculations in supersymmetric theories.

For the calculation of diagrams containing SUSY particles we use Constrained Differential Renormalization (CDR) [56], an alternative method for the calculation of loop integrals in 4 dimensions, which preserves supersymmetry and gauge invariance at one-loop level. In CDR the Feynman diagrams are reduced to a sum of (divergent) basic functions and their derivatives. The renormalized diagram is described by the same sum but with renormalized basic functions. CDR works in coordinate space, but using Fourier transformation it is possible to convert the basic functions into momentum space, where they correspond to the tensor integrals of DR. This allows us to express our results for SUSY diagrams, calculated in CDR, in the same way as our SM results, meaning in terms of the standard one-loop integrals in appendix B.2.

In fact it has been shown that CDR is equivalent to Dimensional Reduction at one-loop level [57].

3.1.3. Pauli-Villars regularization

For one particular diagram that we will discuss below the calculation in D dimensions is problematic and the Pauli-Villars Regularization is used instead. In this method an additional propagator of a fictitious heavy photon is introduced which is subtracted from the original photon propagator

$$\frac{1}{k^2} \to \frac{1}{k^2} - \frac{1}{k^2 - \Lambda^2}. \tag{3.10}$$

Λ is the introduced mass regulator. After this replacement, the former divergent integrals can then be calculated in 4 dimensions and the original theory is regained for $\Lambda \to \infty$.

3.2. Renormalization

Theories, like the SM or the MSSM, involve several free parameters that have to be determined by experiments. At tree level the relation between these parameters and the experimental quantities is often intuitive, but including radiative corrections alters this relation and changes the physical interpretation of the parameters in the Lagrangian density ('bare' parameters). A redefinition (or renormalization) of the parameters is then required.

The concept of renormalization (using the counter term approach) is the following: The bare parameters are expressed in terms of renormalized parameters and renormalization constants (= counter terms), where the renormalization constants contain the divergencies and the renormalized parameters are finite. The counter terms are fixed by renormalization conditions. Different renormalization conditions can be chosen, the ones we use are given in the next section. The renormalized parameters can be related to physical, measurable quantities and are fixed by experiments. In renormalizable theories the divergencies have to cancel in relations between physical quantities. t' Hooft showed that all nonabelian gauge theories with spontaneous symmetry breaking, as the SM, are renormalizable [58].

For our work only the renormalization of the electroweak SM is needed, since we calculate only one-loop corrections and the considered tree-level diagram contains only SM particles. Therefore we will limit our discussion of renormalization in the following to this part of the theory. Also the renormalization of the gauge-fixing sector and the renormalization of tadpoles is not shown here, since they only contribute in higher orders. For a comprehensive review of the renormalization of the SM, we refer to Ref. [42]. Neglecting quark mixing the parameters of the electroweak SM can be chosen as the gauge boson masses M_W and M_Z, the Higgs mass M_H, the fermion masses m_f, and the electric charge e, which is defined by

$$e = \frac{gg'}{\sqrt{g^2 + g'^2}} \,. \tag{3.11}$$

3.2.1. On-shell renormalization

The renormalization of a theory is not unique and different approaches can be used. It is fixed by a renormalization scheme, which gives the renormalization conditions. The most prominent ones are the minimal subtraction MS (and the modified MS, short $\overline{MS}$) scheme, where only the UV-divergence is absorbed in the renormalization constant, and the on-shell scheme. The on-shell scheme has the advantage, that all parameters have a direct physical meaning and can be determined directly in experiments, which makes it suitable for many applications. The on-shell renormalization scheme is used for this work and presented in this section.

Following the steps described in the previous section, the bare parameters are replaced by renormalized parameters and renormalization constants. The renormalized parameters are finite, while the UV divergencies are contained in the renormalization constants. The renormalized parameters and renormalization constants of the electroweak SM are defined by

$$\begin{aligned} e_0 &= Z_e e = (1+\delta Z_e)e \\ M^2_{W,0} &= M^2_W + \delta M^2_W \\ M^2_{Z,0} &= M^2_Z + \delta M^2_Z \\ M^2_{H,0} &= M^2_H + \delta M^2_H \\ m_{f,0} &= m_f + \delta m_f \ , \end{aligned} \tag{3.12}$$

where the bare parameters are denoted by the index 0. With these renormalization constants the S-matrix elements are finite.

In order to get finite Green functions, it is useful to define renormalized fields

$$\begin{aligned} W^\pm_0 &= Z^{1/2}_W W^\pm = (1+\frac{1}{2}\delta Z_W)W^\pm \\ \begin{pmatrix} Z_0 \\ A_0 \end{pmatrix} &= \begin{pmatrix} Z^{1/2}_{ZZ} & Z^{1/2}_{ZA} \\ Z^{1/2}_{AZ} & Z^{1/2}_{AA} \end{pmatrix} \begin{pmatrix} Z \\ A \end{pmatrix} = \begin{pmatrix} 1+\frac{1}{2}\delta Z_{ZZ} & \frac{1}{2}\delta Z_{ZA} \\ \frac{1}{2}\delta Z_{AZ} & 1+\frac{1}{2}\delta Z_{AA} \end{pmatrix} \begin{pmatrix} Z \\ A \end{pmatrix} \\ H_0 &= Z^{1/2}_H H = (1+\frac{1}{2}\delta Z_H)H \\ f^L_{i,0} &= Z^{1/2,f,L}_{ij} f^L_j = (\delta_{ij}+\frac{1}{2}\delta Z^{f,L}_{ij})f^L_j \\ f^R_{i,0} &= Z^{1/2,f,R}_{ij} f^R_j = (\delta_{ij}+\frac{1}{2}\delta Z^{f,R}_{ij})f^R_j. \end{aligned} \tag{3.13}$$

Using the relations between bare and renormalized parameters and fields, given in (3.12) and (3.13), the Lagrangian can be split into two parts

$$\mathcal{L}_0 = \mathcal{L} + \delta\mathcal{L}. \tag{3.14}$$

The Lagrangian $\mathcal{L}$ looks like the bare Lagrangian $\mathcal{L}_0$ but with renormalized parameters, and $\delta\mathcal{L}$ contains the counter terms. From this Lagrangian we get an extended set of Feynman rules, consisting of the 'original' Feynman rules with renormalized parameters and additionally new Feynman rules for the counter terms.

We fix the renormalization constants by the on-shell renormalization conditions, demanding that the renormalized mass parameters are equal to the real parts of the propagator poles, that the residues of the renormalized propagators are equal to 1 and that e is the elementary charge from Thomson-scattering, resulting in vanishing loop contributions to the eeA vertex on-shell and for zero momentum transfer. From these conditions the renormalization constants are calculated. At one loop level one finds for the mass and field renormalization constants: (for a more detailed derivation see Ref. [42])

$$\begin{aligned}
\delta M_W^2 &= \mathrm{Re}\,\Sigma_T^W(M_W^2)\\
\delta Z_W &= -\mathrm{Re}\,\frac{\partial\Sigma_T^W(k^2)}{\partial k^2}|_{k^2=M_W^2}\\
\delta M_Z^2 &= \mathrm{Re}\,\Sigma_T^{ZZ}(M_Z^2)\\
\delta Z_{ZZ} &= -\mathrm{Re}\frac{\partial\Sigma_T^{ZZ}(k^2)}{\partial k^2}|_{k^2=M_Z^2}\\
\delta Z_{AZ} &= -2\mathrm{Re}\,\frac{\Sigma_T^{AZ}(M_Z^2)}{M_Z^2}\\
\delta Z_{ZA} &= 2\frac{\Sigma_T^{AZ}(0)}{M_Z^2}\\
\delta Z_{AA} &= -\Pi^{AA}(0)\\
\delta M_H^2 &= \mathrm{Re}\,\Sigma^H(M_H^2)\\
\delta Z_H &= -\mathrm{Re}\,\frac{\partial\Sigma^H(k^2)}{\partial k^2}|_{k^2=M_H^2}\\
\delta m_f &= \frac{m_f}{2}\mathrm{Re}\,\left(\Sigma_L^f(m_f^2)+\Sigma_R^f(m_f^2)+2\Sigma_S^f({m_f}^2)\right)\\
\delta Z^{f,L} &= -\mathrm{Re}\,\Sigma_L^f(m_f^2) - m_f^2\frac{\partial}{\partial p^2}\mathrm{Re}\,\left[\Sigma_L^f(p^2)+\Sigma_R^f(p^2)+2\Sigma_S^f(p^2)\right]|_{p^2=m_f^2}\\
\delta Z^{f,R} &= -\mathrm{Re}\,\Sigma_R^f(m_f^2) - m_f^2\frac{\partial}{\partial p^2}\mathrm{Re}\,\left[\Sigma_L^f(p^2)+\Sigma_R^f(p^2)+2\Sigma_R^f(p^2)\right]|_{p^2=m_f^2}\,.
\end{aligned} \tag{3.15}$$

Here Π is defined as

$$\Pi^{AA}(k^2) = \frac{\Sigma_T^{AA}(k^2)}{k^2}, \tag{3.16}$$

so

$$\Pi^{AA}(0) = \frac{\partial\Sigma_T^{AA}(k^2)}{\partial k^2}|_{k^2=0}, \tag{3.17}$$

since $\Sigma_T^{AA}(0) = 0$.

The on-shell renormalization condition for the electric charge gives the renormalization constant

$$\delta Z_e = -\frac{1}{2}\delta Z_{AA} - \frac{s_W}{c_W}\frac{1}{2}\delta Z_{ZA} = \frac{1}{2}\frac{\partial \Sigma_T^{AA}(k^2)}{\partial k^2}|_{k^2=0} - \frac{s_W}{c_W}\frac{\Sigma_T^{AZ}(0)}{M_Z^2} \,. \tag{3.18}$$

Sine and cosine of the weak mixing angle are not independent parameters in the on-shell renormalization scheme. Their counter terms

$$s_{W,0} = s_W + \delta s_W \quad , \quad c_{W,0} = c_W + \delta c_W \tag{3.19}$$

are fixed by the weak gauge boson mass counter terms. Since they are frequently used, we list their counter terms here as well:

$$\begin{aligned} \frac{\delta c_W}{c_W} &= \frac{1}{2}\left(\frac{\delta M_W^2}{M_W^2} - \frac{\delta M_Z^2}{M_Z^2}\right) = \frac{1}{2}\mathrm{Re}\left(\frac{\Sigma_T^W(M_W^2)}{M_W^2} - \frac{\Sigma_T^{ZZ}(M_Z^2)}{M_Z^2}\right) \\ \frac{\delta s_W}{s_W} &= -\frac{c_W^2}{s_W^2}\frac{\delta c_W}{c_W} = -\frac{1}{2}\frac{c_W^2}{s_W^2}\mathrm{Re}\left(\frac{\Sigma_T^W(M_W^2)}{M_W^2} - \frac{\Sigma_T^{ZZ}(M_Z^2)}{M_Z^2}\right) . \end{aligned} \tag{3.20}$$

4. Technical aspects of the calculations

4.1. FeynArts, FormCalc and LoopTools

For the determination of the W boson mass many Feynman diagrams have to be calculated. In the SM the one-loop calculation could still be done by hand with a reasonable effort. However, the proliferation of contributing diagrams makes the same rather cumbersome in the MSSM. Therefore the calculations in this thesis for both the SM and the MSSM are done by using the *Mathematica* based programs *FeynArts*[*] [59] and *FormCalc*[†] [57]. *FeynArts* generates the amplitudes of the Feynman diagrams, which are then calculated using *FormCalc*. It returns the results in a way that is applicable for further numerical evaluation. *FormCalc* has a *Mathematica* user interface but internally the actual computation is mainly done in *FORM* [60]. Our approach to the calculation, using these programs, is presented in the following.

First the diagrams are produced in two steps by *FeynArts*:

1. To begin with the number of incoming and outgoing particles and the loop order of the desired diagrams are defined. Then *FeynArts* creates all possible topologies, meaning sets of lines (propagators) and connection points (vertices). The set of topologies can be adjusted to a special purpose by demanding certain shapes (triangle, box etc) or manually excluding the undesired topologies.

2. In the next step the incoming and outgoing fields are inserted into the topologies. Restrictions on the intermediate particles can be imposed to obtain only the diagrams that should be computed. For this step *FeynArts* needs a model file, which specifies the particles and interactions in a certain model. We used the *FeynArts* model files for the SM and the MSSM. *FeynArts* distinguishes between three levels of fields: generic fields (e.g. fermions), class fields (e.g. leptons) or particle fields (e.g. electron). Making use of this concept highly simplifies the generation of all desired diagrams.

Once the diagrams have been created, *FeynArts* applies the Feynman rules to produce the actual amplitudes. The amplitude output has a complicated structure, which provides the basis for further computation in *FormCalc*.

[*] Version FeynArts 3.5
[†] Version FormCalc 6

Before *FormCalc* calculates the amplitude, the regularization scheme must be defined. DR is used for SM diagrams and CDR for diagrams containing SUSY particles. In addition we specify that fermion chains should be returned in Dirac notation. *FormCalc* then contracts the indices, evaluates the fermion traces, simplifies open fermion chains using the Dirac equation and finally performs the reduction of the tensor integrals (for an explanation of tensor integrals see appendix B). More details about our calculation are presented in sections 6 and 7. In the numerical analysis of our results, we use *LoopTools*[‡] [57] for the evaluation of the one-loop tensor integrals.

At this point we want to mention one peculiarity that must be considered when working in both models, SM and MSSM, with *FeynArts*. For historical reasons, the covariant derivative is defined differently in the two model files. In the SM model file the covariant derivative is defined as in (1.8), but the first minus sign is replaced by a plus sign in the MSSM model file. As a consequences, s_W has to be replaced by $-s_W$ in the Feynman rules and an additional minus sign must be added for every Higgs field in a coupling. We adopt this convention, so that all formulas in this work are consistent with *FeynArts* results.

4.2. FeynHiggs

All masses and mixing matrices in the SUSY sector are calculated in *FeynHiggs*[§] [48], a FORTRAN code for the calculation of the Higgs masses and other parameters and observables in the complex MSSM. For the calculation of the Higgs masses the full one-loop result and leading two-loop corrections are taken into account.

The diagonalization of the neutralino mass matrix is done in *FeynHiggs* via the Takagi factorization, a diagonalization method for complex symmetric matrices based on the Jacobi algorithm [61].

[‡]Version LoopTools 2.5
[§]Version FeynHiggs 2.7.0

5. Determination of the W-boson mass

5.1. Muon decay

Muons decay via the weak interaction almost exclusively into $e\bar{\nu}_e\nu_\mu$. The decay was originally described in the Fermi model, which is an effective theory that evolves from the SM in the limit of small momentum transfer. It is non-renormalizable and violates the unitarity of the S-matrix at higher orders. Within the Fermi model the muon decay is described by a local four-coupling of the four fermions, as depicted in Figure 5.1. The tree-level matrix element for this decay is

$$\mathcal{M}_{\text{Fermi}} = \frac{4G_\mu}{\sqrt{2}} \left(\bar{u}_{\nu_\mu}\gamma_\lambda\omega_- u_\mu\right)\left(\bar{u}_e\gamma^\lambda\omega_- v_{\nu_e}\right) \ , \tag{5.1}$$

where G_μ is the Fermi constant and $\omega_\pm = (1 \pm \gamma_5)/2$ the projection operators. The value of G_μ is not given in the Fermi model but can be obtained from the muon decay width.

The differential width of this decay can be calculated from the matrix element via

$$\mathrm{d}\Gamma_\mu^{\text{Fermi}} = \frac{1}{2m_\mu}|\mathcal{M}_{\text{Fermi}}|^2(2\pi)^4\delta^{(4)}(p_\mu - p_{\nu_\mu} - p_e - p_{\nu_e}) \prod_{f=\nu_\mu,\nu_e,e} \frac{\mathrm{d}^3\mathbf{p}_f}{(2\pi)^3}\frac{1}{2E_f} \tag{5.2}$$

where $p = (E, \mathbf{p})$ denotes the four-momentum of the particles. Calculating $\mathrm{d}\Gamma$ and integrating over the phase space, one finds the tree-level decay width

$$\Gamma_\mu^{\text{Fermi}} = \frac{G_\mu^2 m_\mu^5}{192\pi^3} F\left(\frac{m_e^2}{m_\mu^2}\right) \ , \tag{5.3}$$

with

$$F(x) = 1 - 8 + 8x^3 - x^4 - 12x^2\ln x. \tag{5.4}$$

When QED radiative corrections are factored into the decay width, (5.3) gets modified. $\Gamma_\mu^{\text{Fermi}}$ can then be written as

$$\Gamma_\mu^{\text{Fermi}} = \frac{G_\mu^2 m_\mu^5}{192\pi^3} F\left(\frac{m_e^2}{m_\mu^2}\right)(1 + \Delta q) \ , \tag{5.5}$$

where the added term Δq contains the electromagnetic corrections to the four-fermion contact vertex. The exact first order corrections to Δq [62–64] and the second order

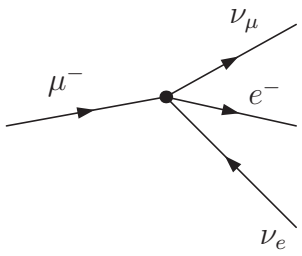

Figure 5.1.: Muon decay in the Fermi model. Tree level diagram with four-fermion vertex.

corrections in the limit $m_e \to 0$ [65–67] have been known for some time, and the second order result has recently been extended to the case of finite m_e [68].

The Fermi constant, G_μ, is defined by (5.5) and therefore incorporates the QED corrections. Thus, with the precisely calculated Δq and the alike precise measurement of the muon life time, G_μ is determined with high accuracy. In this work we use the currently most precise value [69]

$$G_\mu = 1.1663788(7) \times 10^{-5}\ \text{GeV}^{-2}. \tag{5.6}$$

Nowadays the Fermi model is known to be inconsistent and the muon decay is described in the electroweak SM. At lowest order the matrix element, called Born matrix element, for the muon decay in the SM via a W-boson exchange (shown in Figure 5.2) is

$$\begin{aligned} \mathcal{M}_{\text{Born}} &= \left(\bar{u}_{\nu_\mu} \frac{\mathrm{i}e}{\sqrt{2}s_W} \gamma_\lambda \omega_- u_\mu\right) \frac{1}{q^2 - M_W^2} \left(\bar{u}_e \frac{\mathrm{i}e}{\sqrt{2}s_W} \gamma^\lambda \omega_- v_{\nu_e}\right) \\ &\approx \frac{e^2}{2s_W^2 M_W^2} \left(\bar{u}_{\nu_\mu} \gamma_\lambda \omega_- u_\mu\right) \left(\bar{u}_e \gamma^\lambda \omega_- v_{\nu_e}\right) \ , \end{aligned} \tag{5.7}$$

where the second line of (5.7) results from neglecting the momentum transfer q^2 and hence the masses and momenta of the external particles. To legitimate this approximation, one expands the full result for small q^2 and finds that already the first term is very small ($\approx 10^{-6}$). This factor is put into Δq and therefore already included in the value of G_μ, even though it is numerically insignificant. There is another contributing tree-level diagrams in the SM with an exchange of an unphysical Goldstone boson. But the Goldstone fermion coupling is proportional to the fermion mass, so this diagram is also negligible.

As the electroweak SM reproduces the Fermi model for vanishing momentum transfer, the second line of (5.7) has to coincide with (5.1) and a comparison yields

$$\frac{G_\mu}{\sqrt{2}} = \frac{e^2}{8s_W^2 M_W^2} = \frac{\pi}{2} \frac{\alpha M_Z^2}{M_W^2 (M_Z^2 - M_W^2)}. \tag{5.8}$$

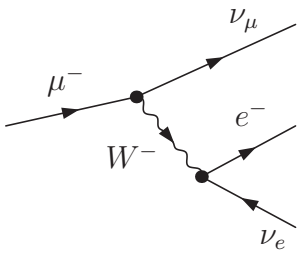

Figure 5.2.: Muon decay in the electroweak SM. Tree level diagram with W boson exchange.

This equation provides a tree-level relation between the W boson mass and the SM quantities M_Z, G_μ and the electroweak coupling $\alpha = e^2/4\pi$, which are all known with a very high precision of better than 0.05 per thousand.

5.2. Definition of Δr

Aside from the already considered QED corrections, there are further loop contributions that alter the relation between M_W and other parameters of the SM (or other models under consideration). We will study the effect of the additional loop diagrams, where diagrams with Higgs-fermion interactions are omitted for light fermions, since the Higgs fermion coupling is proportional to the small fermion mass.

After splitting off the Δq part, all other radiative corrections can be reduced to a term proportional to the Born matrix element, if masses and momenta of the external fermions are neglected. Each of these loop diagrams can be written in the form

$$\mathcal{M}_{\text{Loop,i}} \propto \left(\bar{u}_{\nu_\mu}\Gamma^1_\lambda u_\mu\right)\left(\bar{u}_e\Gamma^\lambda_2 v_{\nu_e}\right) \ , \tag{5.9}$$

where Γ^1 and Γ^2 can be expressed in the orthonormal Dirac basis as

$$\Gamma_\mu = a_\mu\omega_- + b_\mu\omega_+ + c_{\mu\nu}\gamma^\nu\omega_- + d_{\mu\nu}\gamma^\nu\omega_+ + e_{\mu\nu\rho}\sigma^{\nu\rho} \ , \tag{5.10}$$

where $\sigma^{\nu\rho}$ is defined as $\sigma^{\nu\rho} = \mathrm{i}/2[\gamma^\nu, \gamma^\rho]$. For massless fermions the helicity (spin component in momentum direction) is conserved and equivalent to chirality. Since the W boson only couples to left-handed particles, all couplings have to be left-handed, which means that b_μ, $d_{\mu\nu}$ and $e_{\mu\nu\rho}$ are equal to zero. Additionally the term $a_\mu\omega_-$ has to vanish, since if the momenta are neglected, the coefficients a_μ and $c_{\mu\nu}$ can only depend on masses, coupling constants and the metric $g^{\mu\nu}$, and it is impossible to form a vector by combining scalars and tensors. Only the terms proportional to $\gamma^\nu\omega_-$ survive and the matrix element of the loop diagram can be written as a proportionality factor Δr_i times the Born matrix element

$$\mathcal{M}_{\text{Loop,i}} = \Delta r_i \ \mathcal{M}_{\text{Born}} \ . \tag{5.11}$$

Taking into account all non-QED loop contributions, the relation in (5.9) gets a correction factor $(1 + \Delta r)$

$$\frac{G_\mu}{\sqrt{2}} = \frac{e^2}{8 s_W^2 M_W^2} (1 + \Delta r) \tag{5.12}$$

where Δr represents the sum of all contributing loop diagrams. By rearranging formula (5.12), the W boson mass can be calculated via

$$M_W^2 = M_Z^2 \left(\frac{1}{2} + \sqrt{\frac{1}{4} - \frac{\alpha\pi}{\sqrt{2} G_\mu M_Z^2} (1 + \Delta r)} \right). \tag{5.13}$$

In different models, different particles can occur as virtual particles in the loop contributions to the muon decay. Therefore the quantity Δr depends on the specific model parameters and (5.13) provides a model dependent prediction for the W boson mass. The comparison of the theoretical M_W prediction with the current experimental result for the W boson mass can be used either to test a model, or to constrain the model parameters. The second opportunity is particularly important in the SM where it can be used to set bounds on the Higgs mass.

Of course, Δr also depends on M_W itself, so practically M_W is calculated iteratively, using (5.13). In most cases this procedure converges quickly and only a few iterations are needed.

5.3. Current status of the Δr calculation

The calculation of Δr in the SM is more advanced than in the MSSM and any other model. Not only the complete one-loop [4,5] and two-loop [6–17] results are known, but even leading three-loop [18–22] and four-loop [23,24] corrections have been obtained. In the MSSM the one-loop result has been worked out completely [26–29], and additionally some leading two-loop contributions [30–33] have been calculated.

We performed a new independent one-loop calculation in the SM and in the MSSM with complex parameters, for a general set of MSSM parameters. SUSY-GUT relations between the parameters are not assumed in the first place. Flavor violation, in the SM and the MSSM, is not included in our calculation, but we plan to extend our result also to models with a non-minimal flavor structure, where generation mixing is possible. Furthermore we incorporated all known higher order corrections, of SM and SUSY type, into our Δr formula and gain the most precise prediction for the W boson mass in the MSSM. The details of our calculation will be presented next.

5.4. Δr formula at one-loop order

The one-loop radiative corrections consist of the W boson self-energy, vertex and box diagrams and the related counter terms (CT)

$$\begin{aligned}\Delta r \;&=\; \text{W Self-energy} + \text{W Self-energy CT} + \text{Vertex} + \text{Vertex CT} + \text{Box} \\ &= \frac{\Sigma_T^{WW}(0)}{M_W^2} + \left(-\delta Z_W - \frac{\delta M_W^2}{M_W^2}\right) + \text{Vertex} \\ &+ \left(2\delta Z_e - 2\frac{\delta s_W}{s_W} + \delta Z_W + \frac{1}{2}\left(\delta Z^{\mu} + \delta Z^{e} + \delta Z^{\nu_\mu} + \delta Z^{\nu_e}\right)\right) + \text{Box}\,.\end{aligned} \tag{5.14}$$

Since the W boson appears only as a virtual particle, its field renormalization constant δZ_W drops out in the Δr formula. The self-energy of the W boson $\Sigma^{WW}(p^2)$ has to be calculated at $p^2 = 0$, as we are neglecting the momentum transfer. From (3.4) it can be seen that the two terms with p^2 in the denominator must cancel in the limit $p^2 \to 0$ in order to retain a non divergent result for Σ^{WW}, so

$$\Sigma_T\left(p^2=0\right) = \Sigma_L\left(p^2=0\right) \quad \text{and} \quad \Sigma_{\mu\nu}\left(p^2=0\right) = -g_{\mu\nu}\Sigma_T\left(p^2=0\right). \tag{5.15}$$

The box diagrams are themselves finite, whereas the self-energy and vertex diagrams are UV divergent, and their counter terms must be included to obtain a physical result. For the determination of the counter terms the renormalization constants for the W boson mass, the electric charge, the weak mixing angle and the fermion fields are needed, which are given in (3.15)-(3.19). Inserting the (on-shell) renormalization constants (the fermion field renormalization constants simplify to $\delta Z_L^f = -\mathrm{Re}\Sigma_L^f(0)$ when the fermion masses are neglected) we find

$$\begin{aligned}\Delta r =& \frac{\Sigma_T^{WW}(0) - \mathrm{Re}\left(\Sigma_T^{WW}(M_W^2)\right)}{M_W^2} + \Pi^{AA}(0) - \frac{c_W^2}{s_W^2}\,\mathrm{Re}\left[\frac{\Sigma_T^{ZZ}(M_Z^2)}{M_Z^2} - \frac{\Sigma_T^{WW}(M_W^2)}{M_W^2}\right] \\ &- 2\frac{s_W}{c_W}\frac{\Sigma_T^{AZ}(0)}{M_Z^2} + \text{Vertex} + \text{Box} - \frac{1}{2}\mathrm{Re}\left(\Sigma_L^{e}(0) + \Sigma_L^{\mu}(0) + \Sigma_L^{\nu_e}(0) + \Sigma_L^{\nu_\mu}(0)\right).\end{aligned} \tag{5.16}$$

This formula only holds for Δr in the SM. Considering the MSSM, the sign of s_W has to be changed, due to the different definition of the covariant derivative, as explained in section 4.1. A modification of this formula for the MSSM will be given in section 7.1.

6. Calculation of Δr in the SM

6.1. One-loop contributions

To obtain the first order result for Δr in the SM, the self-energy, vertex and box diagrams in (5.16) need to be calculated at one-loop level. In doing so, the QED corrections to the Fermi model have to be subtracted, according to the definition of G_μ. For all SM one-loop diagrams, except for one box diagram that we will discuss separately, the calculation is performed using DR.

In the following sections, the different types of SM one-loop diagrams will be shown, the calculations will be described and, if possible, analytic results will be given.

6.1.1. Gauge boson self-energies

Apart from the treatment of the vacuum polarization Π^{AA} (see below) the calculation of the gauge boson self-energies is straightforward. The contributions to the gauge boson self-energies can be divided into diagrams with fermions in the loop (Figure 6.1), diagrams with gauge bosons, Higgs and Goldstone bosons in the loop (Figure 6.2) and into diagrams with ghost loops (Figure 6.3). The full contribution of fermion loops to the gauge boson self-energies in Δr is finite by itself, while the latter two contributions only become finite together with the vertex and fermion self-energy contributions, discussed in the next sections. Analytic results for Σ_T^{WW}, Σ_T^{ZZ} and Σ_T^{AZ} are lengthy and will not be given here.

The term $\Pi^{AA}(0)$ arising from the charge renormalization needs special regard for

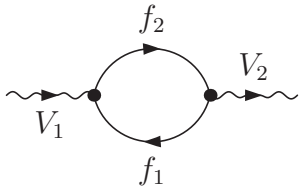

Figure 6.1.: Generic SM one-loop gauge boson self-energy diagram with a fermion loop; V_1, $V_2 = \gamma$, Z, $W^\pm$ and f_1, $f_2 = \nu$, l, u, d.

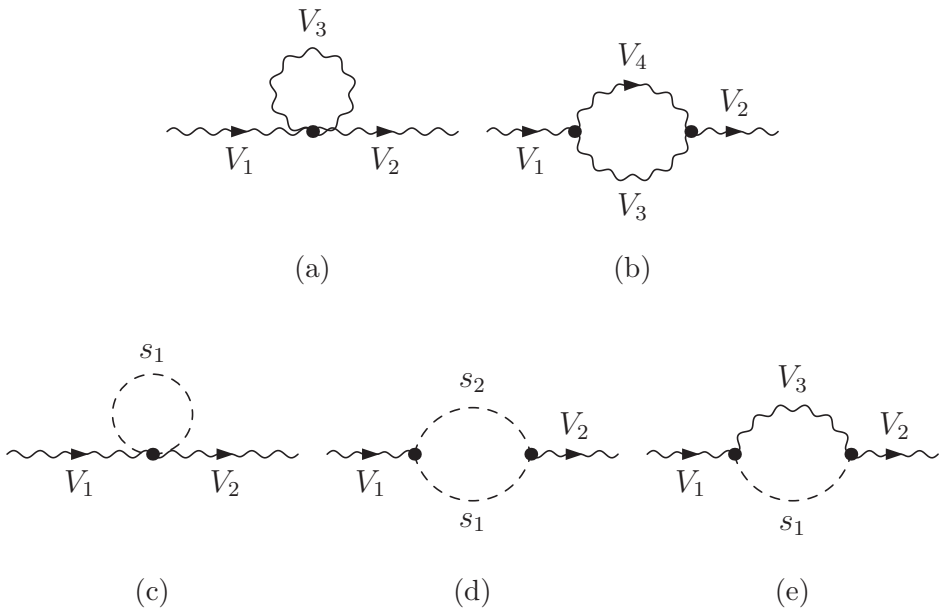

Figure 6.2.: Generic one-loop gauge boson self-energy diagrams with gauge bosons, Higgs and Goldstone bosons in the loop.
SM: V_1, V_2, V_3, $V_4 = \gamma$, Z, $W^\pm$ and s_1, $s_2 = h_{\mathrm{SM}}$, $\phi^\pm$, χ.
MSSM: V_1, V_2, V_3, $V_4 = \gamma$, Z, $W^\pm$ and s_1, $s_2 = h$, H, A, $H^\pm$, G,$G^\pm$.

loops with light fermions. To treat this part separately we split Π^{AA} into three parts

$$\Pi^{AA}(0) = \Pi^{AA}_{\text{top quark}}(0) + \Pi^{AA}_{\text{bosons}}(0) + \Pi^{AA}_{\text{light fermions}}(0)\,. \tag{6.1}$$

The function Π was defined in (3.16) and (3.17), and the parts $\Pi^{AA}_{\text{top quark}}(0)$ and $\Pi^{AA}_{\text{bosons}}(0)$ can be obtained directly by calculating $(\partial\Sigma^{AA}_T(k^2)/\partial k^2)|_{k^2=0}$. More difficult is the term for the light fermions, because the calculation of

$$\Pi^{AA}_{\text{light fermions}}(0) = \frac{\partial\Sigma^{AA}_T(k^2)}{\partial k^2}|_{k^2=0,m_f\to 0}$$

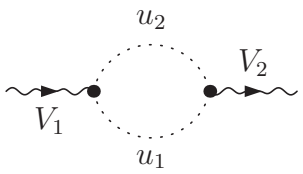

(d)

Figure 6.3.: Generic SM one-loop gauge boson self-energy diagram with a ghost loop.
V_1, $V_2 = \gamma$, Z, $W^\pm$ and u_1, $u_2 = u^{W^\pm}$, u^Z, u^A.

yields terms proportional to $\log(\mu^2/m_f^2)$ (the energy scale μ was introduced in (3.9)), that diverge for vanishing fermion masses.

To solve this problem $\Pi^{AA}_{\text{light fermions}}$ is expanded in the following way

$$\begin{aligned}\Pi^{AA}_{\text{light fermions}}(0) &= \Pi^{AA}_{\text{light fermions}}(0) - \text{Re}\,\Pi^{AA}_{\text{light fermions}}\left(M_Z^2\right) + \text{Re}\,\Pi^{AA}_{\text{light fermions}}\left(M_Z^2\right) \\ &\equiv \Delta\alpha + \text{Re}\,\Pi^{AA}_{\text{light fermions}}\left(M_Z^2\right).\end{aligned} \tag{6.2}$$

The term $\text{Re}\,\Pi^{AA}_{\text{light fermions}}(M_Z^2)$ can be calculated straightforward by neglecting the light fermion masses. The UV-finite quantity

$$\begin{aligned}\Delta\alpha &= \Pi^{AA}_{\text{light fermions}}(0) - \text{Re}\,\Pi^{AA}_{\text{light fermions}}\left(M_Z^2\right) \\ &= \Pi^{AA}_{\text{light fermions}}(0) - \text{Re}\,\frac{\Sigma^{AA}_{T\ \text{light fermions}}(M_Z^2)}{M_Z^2},\end{aligned} \tag{6.3}$$

describes the running of the electromagnetic coupling from $q^2 = 0$, where light fermion masses set the scale, to the electroweak scale $q^2 = M_Z^2$. $\Delta\alpha$ can directly be calculated for the light leptons. The one-loop result can be expressed in the easy form

$$\Delta\alpha_{\text{leptons}} = \frac{\alpha}{3\pi}\sum_{l=e,\mu,\tau}\left(\log\frac{M_Z^2}{m_l^2} - \frac{5}{3}\right), \tag{6.4}$$

and the three-loop calculation of Ref. [70] gives

$$\Delta\alpha_{\text{leptons}} = 0.0314976. \tag{6.5}$$

The hadronic contribution cannot be calculated the same way, since the masses of the light quarks are not known with sufficient accuracy. This makes a theoretical determination impossible, and the hadronic contribution must instead be determined from experimental measurements. $\Delta\alpha$ is related to the measurable quantity

$$R(s) = \frac{\sigma(e^+e^- \to \gamma^* \to \text{hadrons})}{\sigma(e^+e^- \to \gamma^* \to \mu^+\mu^-)} \tag{6.6}$$

via the dispersion relation [71]

$$\Delta\alpha_{\text{hadrons}} = -\frac{\alpha}{3\pi}M_Z^2\text{Re}\left[\int_{4m_\pi^2}^{\infty} ds\frac{R(s)}{s(s - M_Z^2 - i\epsilon)}\right], \tag{6.7}$$

which has been used in Ref. [72] to calculate the currently most accurate value for the hadronic contribution

$$\Delta\alpha_{\text{hadrons}} = (274.9 \pm 1.0) \times 10^{-4}\,. \tag{6.8}$$

including new data from KLOE [73] and the available multi-hadron data from BABAR [74–81]. Adding the leptonic and hadronic contributions, the final value for $\Delta\alpha$ is

$$\Delta\alpha = 0.0590 \pm 0.0001. \tag{6.9}$$

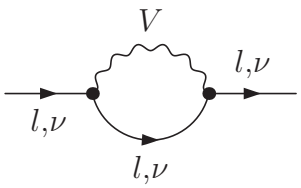

Figure 6.4.: Generic SM one-loop fermion self-energy diagram; $V = Z, W^{\pm}$.

6.1.2. Fermion self-energies

The fermion self-energies contain contributions with photon exchange loops, which are already included in the QED corrections to the Fermi model and therefore have to be subtracted. With only this subtraction the result for Δr is not finite anymore. But, as we will show in section 6.1.4, there is another box diagram with photon exchange that has to be subtracted for the same reason. The two appearing UV divergencies cancel to give a finite final result for Δr without QED corrections. A generic fermion self-energy diagram is sketched in Figure 6.4.

For the calculation of Δr the left-handed parts of the fermion self-energies are needed (see (5.16)). These are obtained using (3.5) and (3.8), where the vector and axial-vector parts can be projected out of the full $\Sigma^f(p)$ by the traces

$$\begin{aligned} \mathrm{Tr}(\not{p}\Sigma(p^2)) &= p^2 D\Sigma_V(p^2) \\ \mathrm{Tr}(\not{p}\gamma^5\Sigma(p^2)) &= -p^2 D\Sigma_A(p^2). \end{aligned} \tag{6.10}$$

In Feynman-'t Hooft gauge, the result (calculated in DR) for the fermion-self energy part in Δr is

$$\begin{aligned} -\frac{1}{2}\mathrm{Re}\left(\Sigma_L^e(0) + \Sigma_L^\mu(0) + \Sigma_L^{\nu_e}(0) + \Sigma_L^{\nu_\mu}(0)\right) = \\ \frac{\alpha}{4\pi}\frac{1}{4s_W^2}\left(\frac{6c_W^4+3}{c_W^2} - 4\frac{A_0(M_W^2)}{M_W^2} - \left(\frac{4c_W^4-4c_W^2+2}{c_W^2}\right)\frac{A_0(M_Z^2)}{M_Z^2}\right), \end{aligned} \tag{6.11}$$

where A_0 is the scalar one-loop one-point integral, defined in appendix B.2.

6.1.3. Vertex diagrams

Besides the self-energies, there are vertex and box diagrams contributing to the Δr one-loop result in the SM, the former shown in Figure 6.5. The same vertex corrections exist also for the other, $We\bar{\nu}_e$, vertex, and since the external fermion masses have been neglected the contributions of the two vertex corrections are equal. All diagrams have

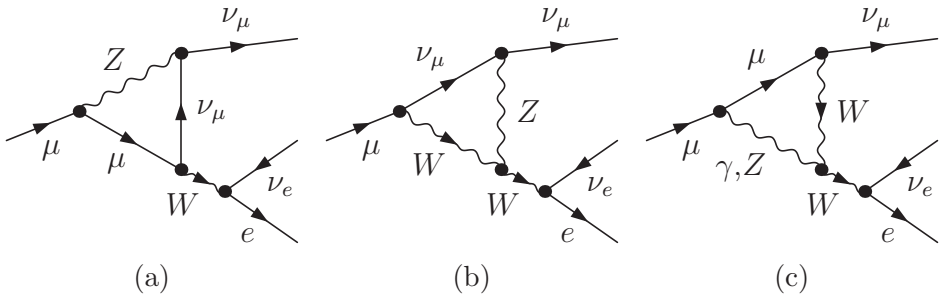

Figure 6.5.: Vertex diagrams in the SM.

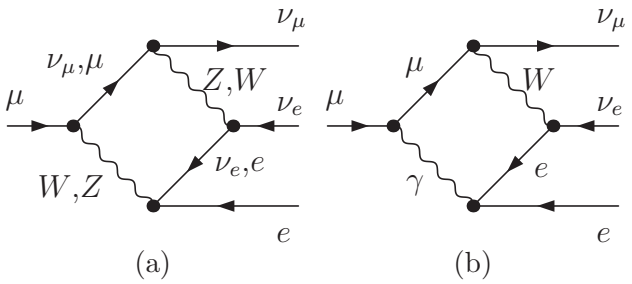

Figure 6.6.: Box diagrams in the SM.

been calculated in DR, and the result for the Δr contribution from the SM vertices can be expressed in the compact form (in Feynman-'t Hooft gauge)

$$\begin{aligned}\text{Vertex} = \frac{\alpha}{4\pi}\frac{1}{4s_W^2}\Bigg(2 - 3\frac{M_Z^2}{M_W^2} + \frac{24(2M_W^2 - M_Z^2)}{M_W^2 - M_Z^2}\frac{A_0(M_W^2)}{M_W^2} \\ + \frac{2}{s_W^2}\left(\frac{14M_W^4 - 3M_W^2M_Z^2 + M_Z^4}{M_W^2 M_Z^2}\right)\frac{A_0(M_Z^2)}{M_Z^2}\Bigg)\,.\end{aligned} \tag{6.12}$$

6.1.4. Box diagrams

The box diagrams contributing to muon decay in the SM are depicted in Figure 6.6. We start the discussion of box diagrams with the box diagrams including a neutral weak current (Figure 6.6(a)), since the one diagram with a QED correction (Figure 6.6(b)) is particularly difficult and has to be discussed separately. Each box diagram is finite by itself and can be calculated in four dimensions. The spinor structure can be converted to that one of the Born matrix element using the Chisholm identity

$$\gamma_\mu\gamma_\nu\gamma_\rho = -\mathrm{i}\epsilon_{\mu\nu\rho\sigma}\gamma^\sigma\gamma_5 + g_{\mu\nu}\gamma_\rho + g_{\nu\rho}\gamma_\mu - g_{\mu\rho}\gamma_\nu,$$

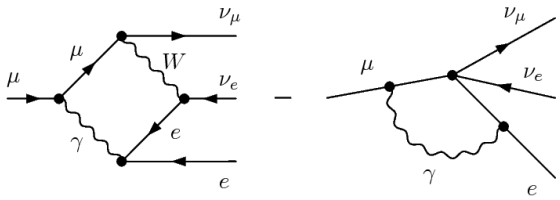

Figure 6.7.: Difference of the SM box diagram with photon exchange and the diagram in the Fermi model with photon exchange.

where $\epsilon_{\mu\nu\rho\sigma}$ is the four-dimensional Levi-Civita tensor. In Feynman-'t Hooft gauge, the result for all box diagrams, apart from the QED one, is

$$\mathrm{Box}_{(a)} = \frac{\alpha}{4\pi}\frac{1}{4s_W^2}\frac{10 - 20s_W^2 + 4s_W^4}{s_W^2}\left(\frac{A_0(M_W^2)}{M_W^2} - \frac{A_0(M_Z^2)}{M_Z^2}\right). \tag{6.13}$$

This expression is finite, and the scalar integrals A_0 have been introduced only to make it easier to combine this result with the other terms in Δr. The inserted divergencies cancel, since the UV divergent part of $A_0(M^2)$ is proportional to M^2.

The QED corrections to muon decay in the effective theory already contain a 'box-diagram' with photon exchange, but the topologies differ. This diagram is included in the definition of G_μ and has to be subtracted, therefore the QED SM box diagram minus the QED 'box' diagram in the Fermi model is needed for Δr. The difference is shown in Figure 6.7. While the SM box diagram is IR-divergent but UV-finite, the 'box' diagram of the Fermi model is both IR- and UV-divergent, which makes the calculation somewhat tricky. If one uses DR, the Chisholm identity, which holds only in four dimensions (as it is given above), cannot be applied. The original analysis of this calculation is given in Refs. [4, 5]. We follow Ref. [82] and calculate the diagram of the effective theory using Pauli-Villars Regularization. In the difference term the IR-divergencies cancel each other, which can be achieved easiest using Pauli-Villars Regularization also for the box diagram of the SM. Doing so, we find the result for the difference term

$$\mathrm{Box}_{(b)} = \frac{\alpha}{4\pi}\ln\frac{M_W^2}{\Lambda^2},$$

where Λ is the Pauli-Villars regulator, introduced in section 3.1.3. In order to put this result into the rest of the calculation, performed in dimensional regularization, we proceed as follows: From the difference term we subtract the photonic part of the fermion field renormalization (also calculated with Pauli-Villars Regularization), so that the result is UV-finite and does not contain the regulator anymore. Then we add the same contribution again, this time calculated in DR, and obtain

$$\mathrm{Box}_{(b)} = \frac{\alpha}{4\pi}\left(\frac{3}{2} - \frac{A_0(M_W^2)}{M_W^2}\right). \tag{6.14}$$

At first it might seem problematic that the subtraction of the QED correction of the Fermi model results in a UV-divergent box term, but this UV-divergence cancels exactly

the one from the subtraction of the photon contributions to the fermion self-energies and together they yield a finite contribution to Δr.

6.2. One-loop result

Adding (6.11)-(6.14), we find the combined contribution of the vertex, box and fermion self-energy corrections to Δr in Feynman-'t Hooft gauge

$$\begin{aligned}\text{Vertex} + \text{Box} - \frac{1}{2}\text{Re}\left(\Sigma_L^e(0) + \Sigma_L^\mu(0) + \Sigma_L^{\nu_e}(0) + \Sigma_L^{\nu_\mu}(0)\right) \\ = \frac{\alpha}{\pi s_W^2}\left(\Delta - \log\frac{M_W^2}{\mu^2}\right) + \frac{\alpha}{4\pi s_W^2}\left(6 + \frac{7-4s_W^2}{2s_W^2}\log\frac{M_W^2}{M_Z^2}\right),\end{aligned} \tag{6.15}$$

where Δ is defined in appendix B.2 and contains the UV-singularity. In the SM, the UV-divergent term can coincidentally be expressed in terms of the photon-Z boson mixing-energy at zero momentum transfer

$$\frac{\alpha}{\pi s_W^2}\left(\Delta - \log\frac{M_W^2}{\mu^2}\right) = \frac{2}{s_W c_W}\frac{\Sigma_T^{AZ}(0)}{M_Z^2}, \tag{6.16}$$

and thus the complete one-loop result for Δr in the SM can be written as

$$\begin{aligned}\Delta r^{(\alpha)} =& \frac{\Sigma_T^{WW}(0) - \text{Re}\left(\Sigma_T^{WW}(M_W^2)\right)}{M_W^2} + \Pi^{AA}(0) - \frac{c_W^2}{s_W^2}\text{Re}\left[\frac{\Sigma_T^{ZZ}(M_Z^2)}{M_Z^2} - \frac{\Sigma_T^{WW}(M_W^2)}{M_W^2}\right] \\ &+ 2\frac{c_W}{s_W}\frac{\Sigma_T^{AZ}(0)}{M_Z^2} + \frac{\alpha}{4\pi s_W^2}\left(6 + \frac{7-4s_W^2}{2s_W^2}\log\frac{M_W^2}{M_Z^2}\right).\end{aligned} \tag{6.17}$$

The electroweak couplings are proportional to the electric charge e and hence the one-loop results are proportional to $\alpha \propto e^2$. Therefore the one-loop results are typically written with an (α) index and referred to as order α, $\mathcal{O}(\alpha)$, results.

Already at this point, we want to demonstrate some important features of the one-loop result for Δr in the SM. The dominant contribution to this result comes from the fermion sector. This can be seen in particular, if the one-loop result is split into three parts

$$\Delta r = \Delta\alpha - \frac{c_W^2}{s_W^2}\Delta\rho + \Delta r_{\text{rem}}, \tag{6.18}$$

as is typically done. The shift of the fine structure constant $\Delta\alpha$, defined in (6.3), contains the contributions of the light fermions and is the numerically largest term with $\approx 6\%$. $\Delta\rho$ contains the fermion loop corrections to the ρ parameter, which describes the ratio between the neutral and charged weak currents, and can be written as

$$\Delta\rho = \frac{\Sigma_T^Z(0)}{M_Z^2} - \frac{\Sigma_T^W(0)}{M_W^2}\,. \tag{6.19}$$

This quantity is sensitive to the mass splitting between the isospin partners in a doublet [83], which leads to a sizable effect in particular from the heavy fermion doublet. This contribution can be written in the form

$$\Delta\rho^{\mathrm{SM}} = \frac{3\alpha}{16\pi s_W^2 c_W^2}\frac{1}{M_Z^2}F_0(m_t^2, m_b^2)\ , \tag{6.20}$$

with

$$F_0(x,y) = x + y - \frac{2xy}{x-y}\ln\frac{x}{y}\ . \tag{6.21}$$

Since

$$F_0(x,x) = 0 \quad \text{and} \quad F_0(x,0) = x\ , \tag{6.22}$$

the $\Delta\rho$ contribution vanishes for degenerate masses and is proportional to m_t^2, if the bottom mass is neglected. Due to this dependency, $\Delta\rho$ was important for predicting the mass of the top quark, in agreement with the experimental detection achieved later. The second term of (6.18), $\frac{c_W^2}{s_W^2}\Delta\rho$, accounts for about 3%. All other terms are contained in the remainder term Δr_{rem}, which is numerically smaller ($\lesssim 1\%$) but contains the full Higgs dependence and is therefore important to set bounds on the mass of the last undetected particle of the SM.

6.3. Higher order corrections

We combine our SM one-loop results with known higher order corrections to muon decay. Before we discuss the contributions included in our Δr calculation, we start by commenting on the different definitions of the mass of the Z and the W boson and show why one has to clearly distinguish between them from two-loop level onwards.

6.3.1. Mass of unstable particles

The physical mass of a particle is generally defined by the pole of its propagator. As shown in section 3.1 the propagator gets a self-energy correction factor in the denominator when higher orders are included. For a stable particle the self-energy is real and its mass is defined as the pole of the real propagator. But for an unstable particle, like the Z or the W boson, the self-energy Σ is generally complex, so that the pole of the propagator lies no longer on the real axis but in the complex plane. It has been shown in Ref. [82] that from two-loop order on, the only gauge-parameter independent way to specify the mass of an unstable particle is to define it as the real part of the complex pole. Using this definition and expanding the gauge boson propagator around the complex pole leads to a Breit-Wigner shape

$$D(q^2) = \frac{-\mathrm{i}\,\mathrm{constant}}{q^2 - \overline{M}^2 + \mathrm{i}\overline{M}\,\overline{\Gamma}} + \text{non-resonant terms} \tag{6.23}$$

with constant decay width $\overline{\Gamma}$. We call this the fixed-width description and denote the masses of the massive gauge bosons, defined by the complex pole of (6.23), by $\overline{M}_W$ and $\overline{M}_Z$.

For historical reasons, the experimental values for the gauge boson masses, denoted M_W and M_Z, are determined using a Breit-Wigner function with a running (energy-dependent) width

$$D(q^2) \propto \frac{-\mathrm{i}}{q^2 M^2 + \mathrm{i} q^2 \Gamma / M}. \tag{6.24}$$

The experimental values for the W and Z Boson mass M_W and M_Z are given in appendix A. As will be discussed below, the electroweak two-loop contributions that we incorporate into our result require the fixed width definition of the gauge boson masses, $\overline{M}_W$ and $\overline{M}_Z$.

The difference between these two descriptions is given by [84]

$$M_{W,Z} = \overline{M}_{W,Z} + \frac{\Gamma_{W,Z}^2}{2 M_{W,Z}}. \tag{6.25}$$

To obtain $\overline{M}_Z$ from the experimental input parameter M_Z, we use (6.25) with the experimental value for the Z-width also given in appendix A. For the calculation of $\overline{M}_W$ the same formula, but with the theoretical prediction for the W boson width

$$\Gamma_W = \frac{3 G_\mu M_W^3}{2\sqrt{2}\pi} \left(1 + \frac{2\alpha_s}{3\pi}\right) \tag{6.26}$$

is used. This shift between the values is of a relevant size and needs to be properly accounted for when masses, defined differently, are compared.

6.3.2. Higher order Δr contributions

Our SM one-loop calculation is combined with all known relevant higher order corrections, in order to obtain the most accurate result for Δr in the SM:

$$\begin{aligned} \Delta r^{SM} =& \Delta r^{(\alpha)} + \Delta r^{(\alpha\alpha_s)} + \Delta r^{(\alpha\alpha_s^2)} + \Delta r_{ferm}^{(\alpha^2)} + \Delta r_{bos}^{(\alpha^2)} \\ &+ \Delta r^{(G_\mu^2 \alpha_s m_t^4)} + \Delta r^{(G_\mu^3 m_t^6)} + \Delta r^{(G_\mu m_t^2 \alpha_s^3)} \,. \end{aligned} \tag{6.27}$$

The contributions entering in (6.27) are:

- The two- [6–11] and three-loop [18–21] QCD corrections, $\Delta r^{\alpha\alpha_s}$ and $\Delta r^{\alpha\alpha_s^2}$. $\alpha_s = g_s^2/4\pi$ is the strong coupling constant. The large mass of the top quark allows for a calculation of these contributions as an expansion in M_Z^2/M_t^2, which has been done in Ref. [85]. We use the two-loop $\mathcal{O}(\alpha\alpha_s)$ and three-loop $\mathcal{O}(\alpha\alpha_s^2)$ order results given in Ref. [85], consisting of the analytic functions for the first three terms in the M_Z^2/m_t^2 expansion, whereof the third term in the expansion is used

to demonstrate its smallness: The third term results in an absolute shift in M_W of about 1 MeV for order α_s and about 0.2 MeV for order α_s^2 (for $m_t = 175$ GeV) and consequently justifies this expansion.

- The fermionic $\Delta r^{\alpha^2}_{ferm}$ [12–14] and purely bosonic $\Delta r^{\alpha^2}_{bos}$ [15–17] electroweak two-loop corrections. For the combined result of these two contributions, a simple parametrization is given in Ref. [86], which approximates the exact result for $\Delta r^{\alpha^2}_{ferm}(\overline{M}_W, \overline{M}_Z, ...)+\Delta r^{\alpha^2}_{bos}(\overline{M}_W, \overline{M}_Z, ...)$ within maximal deviations of 2.7×10^{-5} for 10 GeV $\leq m_H \leq$ 1 TeV. As indicated by the argument of $\Delta r^{\alpha^2}_{ferm}$ and $\Delta r^{\alpha^2}_{bos}$, the two-loop result incorporated in the simple parametrization relies on the fixed-width description of the heavy gauge boson masses, $\overline{M}_W$ and $\overline{M}_Z$.

- The mixed QCD and electroweak three-loop contributions $\Delta r^{G_\mu^2\alpha_s m_t^4}$ and the purely electroweak three-loop contribution $\Delta r^{G_\mu^3 m_t^6}$, arising from the top quark contributions to the ρ parameter, are given in Ref. [22]. The result is obtained by expanding the contributions separately in different regions of the Higgs mass and combining these partial results into a stable prediction for the three-loop $\Delta\rho$ corrections in the full mass range of m_H. An expansion for $m_H \gg m_t$ leads to a good prediction for the $\Delta\rho$ contribution down to $m_H \approx 2m_t$, when five orders in m_t^2/m_H^2 are considered. In the region of m_H around m_t another expansion in δ, with $m_H = m_t(1+\delta)$, is performed. This provides a stable approximation for $0 \lesssim m_H \approx 2m_t$, including five orders in δ.

- The non-singlet four-loop QCD correction to the ρ parameter, $\Delta\rho^{(G_\mu m_t^2\alpha_s^3)}$, is embedded into our Δr formula by $\Delta r^{(G_\mu m_t^2\alpha_s^3)} = -c_W^2/s_W^2\ \Delta\rho^{(G_\mu m_t^2\alpha_s^3)}$. We adopted the on-shell formula from Ref. [24], where many new master integrals needed for this contribution were calculated and an earlier result [23] was confirmed.

For a consistent incorporation of the Δr^{α^2} result in the rest of our calculation, we have to use $\overline{M}_W$ and $\overline{M}_Z$ also as input parameters in our one-loop result and we do the same in all other higher order contributions. Taking the full Δr result in terms of $\overline{M}_W$ and $\overline{M}_Z$, and calculating the W boson mass iteratively using (5.13), the obtained result is also given in fixed-width definition. This result has to be transformed into M_W using (6.25) in order to compare to experimental data. This is done in our work, and the numerical results shown in section 8 always correspond to the running-width description which can be compared directly to the experimental value $M_W^{\rm exp}$.

7. Calculation of Δr in the MSSM

7.1. One-loop contributions

Since the difference between $\overline{M}_{W,Z}$ and $M_{W,Z}$ is only important from two-loop order onwards, we will, to simplify matters, not distinguish between them in this section.

Remembering the sign change in the covariant derivative of the MSSM compared to the SM, the general formula for Δr looks slightly different. Instead of (5.16), the expression

$$\begin{aligned}\Delta r =& \frac{\Sigma_T^{WW}(0) - \mathrm{Re}\left(\Sigma_T^{WW}(M_W^2)\right)}{M_W^2} + \Pi^{AA}(0) - \frac{c_W^2}{s_W^2}\,\mathrm{Re}\left[\frac{\Sigma_T^{ZZ}(M_Z^2)}{M_Z^2} - \frac{\Sigma_T^{WW}(M_W^2)}{M_W^2}\right] \\ &+ 2\frac{s_W}{c_W}\frac{\Sigma_T^{AZ}(0)}{M_Z^2} + \mathrm{Vertex} + \mathrm{Box} - \frac{1}{2}\mathrm{Re}\left(\Sigma_L^{e}(0) + \Sigma_L^{\mu}(0) + \Sigma_L^{\nu_e}(0) + \Sigma_L^{\nu_\mu}(0)\right).\end{aligned} \tag{7.1}$$

has to be used to determine Δr in the MSSM. To find the first order result, $\Delta r^{(\alpha)}$, we calculate the one-loop self-energy, vertex and box corrections and insert these into (7.1). Comparing the MSSM with the SM calculation, the number of contributing diagrams is considerably higher in the MSSM, due to the extended particle sector. Moreover the couplings, containing the sfermion, gaugino and Higgsino mixing matrices, are much more complicated. The regularization also has to be adjusted, since DR is known to break supersymmetry. Nevertheless the MSSM calculation could be performed in DR, if symmetry-restoring terms were added, but we choose instead to calculate the diagrams containing SUSY particles in CDR. In the following, details about the one-loop calculation will be presented. Instead of discussing different topology types separately, as we did in section 6.1, we will sort the MSSM contributions according to which particles occur in the loop.

7.1.1. Fermion sector

The quark and lepton sector in the MSSM is identical to the corresponding sector in the SM, therefore no new types of diagrams have to be calculated. The fermion loop contributions to the gauge boson self-energies are shown in Figure 6.1. Loop diagrams containing fermions as well as gauge bosons, will be discussed as part of the gauge boson sector.

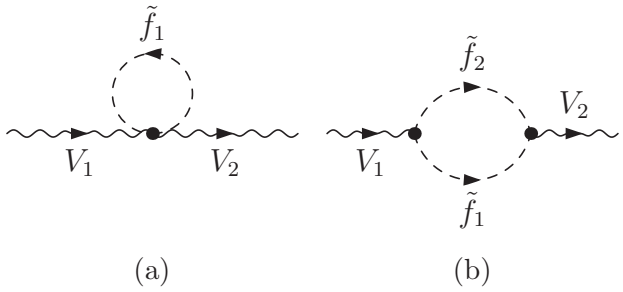

Figure 7.1.: Generic MSSM gauge boson self-energy diagrams with a sfermion loop; V_1, $V_2 = \gamma$, Z, $W^\pm$ and $\tilde{f}_1$, $\tilde{f}_2 = \tilde{\nu}$, $\tilde{l}$, $\tilde{u}$, $\tilde{d}$.

7.1.2. Gauge boson and Higgs sector

The gauge boson sector of the MSSM is the same as the SM one, whereas the Higgs sector differs significantly and consists of three physical neutral Higgs bosons h, H and A, a pair of charged Higgs bosons $H^\pm$ and the Goldstone bosons, as shown in section 2.3.2. However, the vertex, box and fermion self-energy diagrams do not get any additional contributions from the extended Higgs sector, since all Higgs-fermion couplings are proportional to the fermion mass, and the masses of the external leptons are neglected in our calculation. Therefore the MSSM gauge boson and Higgs sector contains the same fermion self-energy, vertex and box diagrams as the SM one, which are depicted in Figures 6.4, 6.5 and 6.6.

But the change in the Higgs sector affects the gauge boson self-energies, whose diagrams containing the MSSM Higgs bosons are shown in Figure 6.2. The calculation of the new diagrams is straightforward. Similar to the SM, the divergencies of the gauge boson self-energy contribution to Δr cancel the divergencies of the vertex and the vertex counter term.

7.1.3. Sfermion sector

Sfermion loops, contributing to the gauge boson self-energies are pictured in Figure 7.1 and, as in the fermion sector, their contribution to Δr is finite by itself. The fermion self-energy, vertex and box diagrams with virtual sfermions are presented in the discussion of the chargino and neutralino sector.

7.1.4. Chargino and neutralino sector

In the MSSM many loop corrections to muon decay involve charginos and neutralinos. The gauge boson self-energies contain diagrams with neutralino and chargino loops, sketched in Figure 7.2. Neutralinos and charginos contribute also to the fermion self-energies and to the vertex corrections by diagrams shown in Figures 7.3 and 7.4. The same vertex corrections exist also for the other vertex. The vertex contribution from

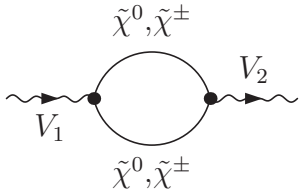

Figure 7.2.: Generic MSSM gauge boson self-energy diagram with a chargino/neutralino loop;
V_1, $V_2 = \gamma$, Z, $W^\pm$, $\tilde{\chi}^\pm = \tilde{\chi}^\pm_{1,2}$ and $\tilde{\chi}^0 = \tilde{\chi}^0_{1,2,3,4}$.

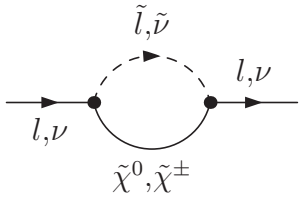

Figure 7.3.: Generic MSSM fermion self-energy diagram with a chargino/neutralino contribution. $\tilde{l}$ and $\tilde{\nu}$ are the superpartners of the lepton l and the neutrino ν; $\tilde{\chi}^\pm = \tilde{\chi}^\pm_{1,2}$ and $\tilde{\chi}^0 = \tilde{\chi}^0_{1,2,3,4}$.

the chargino and neutralino sector, together with the chargino/neutralino contributions to the vertex counter term, containing gauge boson and fermion self-energies, is finite.

There are also box diagrams in the MSSM containing neutralinos and charginos (Figure 7.5), whose calculations are more elaborate than the calculation of the self-energy and vertex diagrams.

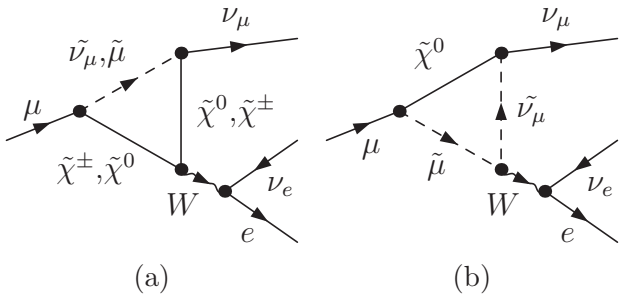

Figure 7.4.: Generic vertex diagrams in the MSSM; $\tilde{\chi}^\pm = \tilde{\chi}^\pm_{1,2}$ and $\tilde{\chi}^0 = \tilde{\chi}^0_{1,2,3,4}$.

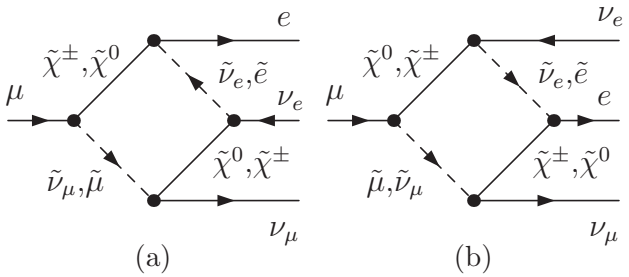

Figure 7.5.: Generic box diagram in the MSSM; $\tilde{\chi}^{\pm} = \tilde{\chi}^{\pm}_{1,2}$ and $\tilde{\chi}^{0} = \tilde{\chi}^{0}_{1,2,3,4}$.

In order to find the contribution to Δr from a particular loop diagram, the Born amplitude has to be factored out of the result. While the SM boxes directly give the structure $\mathcal{M}_{\text{Box}} = \mathcal{M}_{\text{Born}}\Delta r_{\text{Box}}$, it is not so easy to obtain the same structure for the boxes with SUSY particles in the loop. Performing the calculation of the box diagrams in Figure 7.5 in *FormCalc*, the results for the diagrams in (a) and (b) are returned in the form

$$\begin{aligned}\mathcal{M}_{\text{SUSY Box}(a)} &= (\bar{u}_e\gamma_\lambda\omega_- u_\mu)(\bar{u}_{\nu_\mu}\gamma^\lambda\omega_- v_{\nu_e})b_{(a)} \\ \mathcal{M}_{\text{SUSY Box}(b)} &= (\bar{u}_{\nu_e}\omega_- u_\mu)(\bar{u}_{\nu_\mu}\omega_+ v_e)b_{(b)}\ .\end{aligned} \tag{7.2}$$

The expressions for $b_{(a)}$ and $b_{(b)}$ are lengthy and not given here explicitly. To factor out the Born amplitude

$$\mathcal{M}_{\text{Born}} = \frac{2\pi\alpha}{s_W^2 M_W^2}\left(\bar{u}_{\nu_\mu}\gamma_\lambda\omega_- u_\mu\right)\left(\bar{u}_e\gamma^\lambda\omega_- v_{\nu_e}\right)\ ,$$

the spinor chains in (7.2) have to be transformed into the same structure as the ones appearing in $\mathcal{M}_{\text{Born}}$. In order to carry out this transformation, in a first step the Fierz identities (see for example Ref. [87]) are used and therewith the spinor structure of the diagrams in (a) can be rewritten as

$$(\bar{u}_e\gamma_\lambda\omega_- u_\mu)(\bar{u}_{\nu_\mu}\gamma^\lambda\omega_- v_{\nu_e}) = -\left(\bar{u}_{\nu_\mu}\gamma_\lambda\omega_- u_\mu\right)\left(\bar{u}_e\gamma^\lambda\omega_- v_{\nu_e}\right)\ . \tag{7.3}$$

For the spinor chain in $\mathcal{M}_{\text{SUSY Box}(b)}$ we get

$$\begin{aligned}(\bar{u}_{\nu_e}\omega_- u_\mu)(\bar{u}_{\nu_\mu}\omega_+ v_e) =& \frac{1}{2}\left(\bar{u}_{\nu_e}\gamma_\lambda\omega_+ v_e\right)\left(\bar{u}_{\nu_\mu}\gamma^\lambda\omega_- u_\mu\right) \\ =& \frac{1}{2}\left(\bar{u}_{\nu_\mu}\gamma_\lambda\omega_- u_\mu\right)\left(\bar{u}_{\nu_e}\gamma^\lambda\omega_+ v_e\right)\ .\end{aligned} \tag{7.4}$$

As desired, the spinor structure of (a) is now in the same form as the Born term, but to achieve the same for (b) the second equation has to be further rearranged. We consider

the case of massless Dirac spinors

$$u_+(p) = \begin{pmatrix} \sqrt{p^+} \\ \sqrt{p^-}e^{\mathrm{i}\phi_p} \\ 0 \\ 0 \end{pmatrix} , \quad u_-(p) = \begin{pmatrix} 0 \\ 0 \\ \sqrt{p^-}e^{-\mathrm{i}\phi_p} \\ -\sqrt{p^+} \end{pmatrix} , \quad v_\pm(p) = C\overline{u}_\pm^T(p) , \tag{7.5}$$

with the charge conjugation matrix $C = -\mathrm{i}\gamma^2\gamma^0$, $p^\pm = p^0 \pm p^3$ and

$$e^{\pm\mathrm{i}\phi_p} = \frac{p^1 \pm \mathrm{i}p^2}{\sqrt{p^+p^-}} . \tag{7.6}$$

Using the charge conjugation relations,

$$\bar{u}_\pm(p_i)\,\gamma_{\mu 1}\ldots\gamma_{\mu n}\,v_\mp(p_j) \begin{cases} \bar{u}_\mp(p_j)\,\gamma_{\mu n}\ldots\gamma_{\mu 1}\,v_\pm(p_i) & \text{for n odd} \\ -\bar{u}_\mp(p_j)\,\gamma_{\mu n}\ldots\gamma_{\mu 1}\,v_\pm(p_i) & \text{for n even} , \end{cases} \tag{7.7}$$

the definition of γ^5, and the anti-commutation relation for γ-matrices (1.18) we find $(\bar{u}_{\nu_e}\gamma_\lambda\omega_+v_e) = (\bar{u}_e\gamma_\lambda\omega_-v_{\nu_e})$. Therewith equation 7.4 reads,

$$(\bar{u}_{\nu_e}\omega_-u_\mu)(\bar{u}_{\nu_\mu}\omega_+\nu_e) = \frac{1}{2}\left(\bar{u}_{\nu_\mu}\gamma_\lambda\omega_-u_\mu\right)\left(\bar{u}_e\gamma^\lambda\omega_-v_{\nu_e}\right) . \tag{7.8}$$

By writing out the spinors and γ-matrices component-by-component, we checked and confirmed the result (7.8).

Inserting the relations (7.3) and (7.8) into the original equations of the box matrix elements (7.2), gives

$$\begin{aligned} \mathcal{M}_{\text{SUSY Box}(a)} &= -\frac{s_W^2 M_W^2}{2\pi\alpha}\, b_{(a)}\, \mathcal{M}_{\text{Born}} \\ \mathcal{M}_{\text{SUSY Box}(b)} &= -\frac{s_W^2 M_W^2}{4\pi\alpha}\, b_{(b)}\, \mathcal{M}_{\text{Born}} . \end{aligned} \tag{7.9}$$

The result for $\Delta r_{\text{SUSY Box}(a)}$ contains terms with $m_{\tilde{\nu}_e} - m_{\tilde{\nu}_\mu}$ in the denominator, but in the case of equal sneutrino masses also the numerators of the divergent terms become zero. There is thus no physical problem but zero valued denominators may cause troubles in the numerical evaluation (which we carry out in *Mathematica*). This technical issue is solved by adding a distinction of cases: If the sneutrino masses differ, the exact $\Delta r_{\text{SUSY Box}(a)}$ is evaluated, and if they are identical we set $m_{\tilde{\nu}_e} = m_{\tilde{\nu}_\mu} + \epsilon$ and expand the result for $\epsilon \to 0$. Thus we obtain a valid Δr result, for all possible input parameters, and avoid the restriction to a special set of scenarios.

There are more terms, which contain differences of SUSY particle masses in the denominator (e.g. chargino mass - sfermion mass) and could lead to divergencies for certain input parameters. We plan to further investigate this issue and cure possible numerical instabilities by adding special cases, similar to the one for equal sneutrino masses described above.

7.2. SUSY higher order corrections

The theoretical calculation of Δr in the MSSM is not as sophisticated as the calculation in the SM. To obtain the most accurate result for the W boson mass in the MSSM we combine the SM result, containing the full one- and two-loop contributions plus leading higher order corrections, with the known SUSY contributions. Therefore Δr^{MSSM} is split into

$$\Delta r^{\text{MSSM}} = \Delta r^{\text{SM}} + \Delta r^{\text{SUSY}} \,, \tag{7.10}$$

where Δr^{SM} is given by (6.27) and Δr^{SUSY} is the difference between Δr in the MSSM and the SM, i.e. it only involves the contributions from the additional SUSY particles and the extended Higgs sector. While for Δr^{SM} the full SM result including all known higher-order contributions is inserted, Δr^{SUSY} is calculated at the loop level at which the MSSM contributions are known.

The splitting in (7.10) leads to a dependence of the MSSM Δr result on the SM Higgs mass. In our calculation $m_{h_{\text{SM}}}$ is set equal to the mass of the MSSM Higgs boson that couples most SM-like. The ratio of the MSSM hZZ coupling to the SM $h_{\text{SM}}ZZ$ coupling is $\sin(\beta-\alpha)$, whereas the ratio of the MSSM HZZ coupling to the same SM coupling is $\cos(\beta-\alpha)$. As introduced in section 2.3.2 h and H denote the neutral CP-even Higgs bosons and β and α the mixing angles in the MSSM Higgs sector. So we use the identification

$$m_{h_{\text{SM}}} = \begin{cases} m_h & \text{for } |\sin(\beta-\alpha)| \geq |\cos(\beta-\alpha)| \\ m_H & \text{otherwise} \quad . \end{cases} \tag{7.11}$$

For most allowed (meaning not ruled out by theoretical or experimental constraints) parts of the MSSM parameter space, the lightest CP-even Higgs h has the most SM-like Higgs-ZZ coupling.

The SUSY part Δr^{SUSY} consists of our calculated MSSM one-loop result from which the SM one-loop result is subtracted, combined with all SUSY two-loop corrections that are known to date. The SUSY higher order corrections will be discussed in the next two sections.

It should be emphasized at this point that the approach followed in (7.10), i.e. combining the most up-to-date SM prediction with the 'new physics' contributions from supersymmetry, is well suited for extending it also to other scenarios of physics beyond the SM. This provides a good framework to compare the M_W prediction of different models in a consistent way.

7.2.1. Reducible supersymmetric two loop corrections

In the $\Delta r^{\rm SUSY}$ contribution the leading reducible $\mathcal{O}(\alpha^2)$ two-loop corrections are included, which are obtained from the resummation formula [88]

$$1+\Delta r = \frac{1}{(1-\Delta\alpha)(1+\frac{c_W^2}{s_W^2}\Delta\rho)-\Delta r_{rem}}\,, \tag{7.12}$$

which takes the terms of the type $(\Delta\alpha)^2$, $(\Delta\rho)^2$ and $\Delta\alpha\Delta\rho$ correctly into account, if $\Delta\rho$ is parametrized by G_μ. Performing the reparametrization from α to G_μ according to relation (5.9), the SM contribution to $\Delta\rho$ (6.20), parametrized by G_μ, is

$$\Delta\rho^{\rm SM} = \frac{3}{16\pi s_W^2 c_W^2}\left(\frac{2G_\mu s_W^2 M_W^2}{\sqrt{2}\pi}\right)\frac{1}{M_Z^2}F_0(m_t^2,m_b^2) = \frac{3G_\mu}{8\sqrt{2}\pi^2}F_0(m_t^2,m_b^2)\,. \tag{7.13}$$

Making use of the F_0 formula (6.21), the SUSY contributions from the stop and sbottom sector to $\Delta\rho$ can also be written in a compact form,

$$\begin{aligned}\Delta\rho^{\rm SUSY} = \frac{3G_\mu}{8\sqrt{2}\pi^2}\Big(&-\sin^2\theta_{\tilde t}\cos^2\theta_{\tilde t}F_0(m_{\tilde t_1}^2,m_{\tilde t_2}^2) - \sin^2\theta_{\tilde b}\cos^2\theta_{\tilde b}F_0(m_{\tilde b_1}^2,m_{\tilde b_2}^2)\\ &+\cos^2\theta_{\tilde t}\cos^2\theta_{\tilde b}F_0(m_{\tilde t_1}^2,m_{\tilde b_1}^2) + \cos^2\theta_{\tilde t}\sin^2\theta_{\tilde b}F_0(m_{\tilde t_1}^2,m_{\tilde b_2}^2)\\ &+\sin^2\theta_{\tilde t}\cos^2\theta_{\tilde b}F_0(m_{\tilde t_2}^2,m_{\tilde b_1}^2) + \sin^2\theta_{\tilde t}\sin^2\theta_{\tilde b}F_0(m_{\tilde t_2}^2,m_{\tilde b_2}^2)\Big)\,.\end{aligned} \tag{7.14}$$

Expanding (7.12) we find the one-loop result plus the correct two-loop terms

$$\Delta r = \Delta r^{(\alpha)} - \frac{c_W^2}{s_W^2}\Delta\alpha\Delta\rho + \frac{c_W^4}{s_W^4}\Delta\rho^2 + \Delta\alpha^2\,, \tag{7.15}$$

of which the pure SM terms are already included in Δr^{SM}. Thus, only the leading two-loop terms with SUSY contributions,

$$\Delta r_{\rm red}^{SUSY(\alpha^2)} = -\frac{c_W^2}{s_W^2}\Delta\alpha\Delta\rho^{\rm SUSY} + \frac{c_W^4}{s_W^4}\Delta\rho^{\rm SUSY\,2} + 2\frac{c_W^4}{s_W^4}\Delta\rho^{\rm SUSY}\Delta\rho^{SM}\,, \tag{7.16}$$

are additionally needed and inserted into our calculation.

7.2.2. Irreducible supersymmetric two loop contributions

The leading SUSY two-loop QCD corrections $\mathcal{O}(\alpha\alpha_s)$ to $\Delta\rho$, given in Ref. [30] and Ref. [31], as well as the dominant Yukawa-enhanced electroweak corrections $\mathcal{O}(\alpha_t^2)$, $\mathcal{O}(\alpha_t\alpha_b)$, $\mathcal{O}(\alpha_b^2)$ to $\Delta\rho$ [32,33] are incorporated in our calculation.

The two-loop $\mathcal{O}(\alpha\alpha_s)$ contributions contain gauge boson self-energy corrections from squark loops with gluon exchange and quark/squark loops with gluino exchange. The

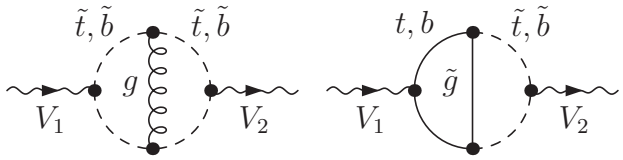

(a) (b)

Figure 7.6.: Generic $\mathcal{O}(\alpha\alpha_s)$ two-loop diagrams in the MSSM. g denotes a gluon and $\tilde{g}$ a gluino; V_1,$V_2 = \gamma$,Z,$W^\pm$.

generic diagrams are shown in Figure 7.6. While the formula for the gluino contribution is very lengthy, a compact result for the gluon contributions to $\Delta\rho$, similar to the one-loop squark contribution (7.14) was derived in Ref. [31],

$$\begin{aligned}\Delta\rho^{\text{SUSY}}_{\text{gluon}} = \frac{G_\mu \alpha_s}{4\sqrt{2}\pi^3}\Big(&- \sin^2\theta_{\tilde{t}} \cos^2\theta_{\tilde{t}} F_1(m^2_{\tilde{t}_1}, m^2_{\tilde{t}_2}) - \sin^2\theta_{\tilde{b}} \cos^2\theta_{\tilde{b}} F_1(m^2_{\tilde{b}_1}, m^2_{\tilde{b}_2}) \\ &+ \cos^2\theta_{\tilde{t}} \cos^2\theta_{\tilde{b}} F_1(m^2_{\tilde{t}_1}, m^2_{\tilde{b}_1}) + \cos^2\theta_{\tilde{t}} \sin^2\theta_{\tilde{b}} F_1(m^2_{\tilde{t}_1}, m^2_{\tilde{b}_2}) \\ &+ \sin^2\theta_{\tilde{t}} \cos^2\theta_{\tilde{b}} F_1(m^2_{\tilde{t}_2}, m^2_{\tilde{b}_1}) + \sin^2\theta_{\tilde{t}} \sin^2\theta_{\tilde{b}} F_1(m^2_{\tilde{t}_2}, m^2_{\tilde{b}_2})\Big)\,,\end{aligned} \tag{7.17}$$

where the squark masses are on-shell (pole) masses, and

$$\begin{aligned}F_1(x,y) = x + y - \frac{2xy}{x-y}\ln\frac{x}{y}\left(2 + \frac{x}{y}\ln\frac{x}{y}\right) \\ + \frac{(x+y)x^2}{(x-y)^2}\ln^2\frac{x}{y} - 2(x-y)\text{Li}_2\left(1 - \frac{x}{y}\right)\,.\end{aligned} \tag{7.18}$$

Li_2 is the dilogarithmic function, defined as

$$\text{Li}_2(x) = -\int_0^1 \frac{\mathrm{d}t}{t}\ln(1-xt)\,, \tag{7.19}$$

for $|\arg(1-x)| < \pi$. Like F_0, the function $F_1(x,y)$ vanishes for $x = y$. If one argument of the function is zero, $F_1(x,0) = x(1+\pi^2/3)$, so the F_1 functions in (7.17) increase with the heavy squark mass in the case of large mass splitting.

The SUSY $\Delta\rho$ expressions depend on the physical masses of the squarks, which are unknown and have to be calculated from the MSSM input parameters. As we have shown in section 2.3.1, SU(2) gauge invariance requires that at tree-level $M_{\tilde{t}_L} = M_{\tilde{b}_L}$, which results in a relation between the stop masses $m_{\tilde{t}_1}$, $m_{\tilde{t}_2}$, the stop mixing angle $\theta_{\tilde{t}}$, the sbottom masses $m_{\tilde{b}_1}$, $m_{\tilde{b}_2}$ and the sbottom mixing angle $\theta_{\tilde{b}}$. This means that not all four masses are independent, but one mass can be expressed in terms of the

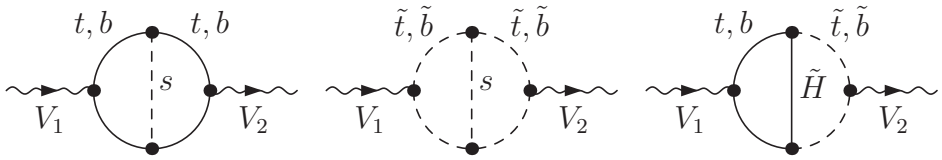

(a) (b) (c)

Figure 7.7.: Generic $\mathcal{O}(\alpha_t^2)$, $\mathcal{O}(\alpha_t\alpha_b)$, $\mathcal{O}(\alpha_b^2)$ two-loop diagrams in the MSSM. $\tilde{H}$ denotes a Higgsino and s a Higgs or Goldstone boson; V_1,$V_2 = \gamma$,Z,$W^\pm$.

other parameters. When higher order corrections are included, the masses have to be renormalized which is done in the on-shell scheme. But because of this SU(2) relation, one cannot choose independent renormalization conditions for all four masses. This implies that for the dependent mass, typically $m_{\tilde{b}_1}$, the mass parameter does not coincide with the physical mass. The functions for the one-loop and two-loop SUSY contributions, e.g. (7.14) and (7.17), require the physical (on-shell) masses as input, so an additional correction $\Delta m_{\tilde{b}_1}$ (if $m_{\tilde{b}_1}$ is chosen to be the dependent mass) has to be included. This correction term is in the following referred to as mass-shift correction.

Whereas the effect of taking the tree-level instead of the one-loop corrected squark masses is of third order for the two-loop $\Delta\rho$ contributions, for the one-loop $\Delta\rho$ the effect is of two-loop order and has to be included if other SUSY two-loop corrections are considered. This mass-shift correction is incorporated in our Δr calculation.

The $\mathcal{O}(\alpha_t^2)$, $\mathcal{O}(\alpha_t\alpha_b)$, $\mathcal{O}(\alpha_b^2)$ corrections are two-loop contributions involving quark (top and bottom) loops with Higgs exchange, squark (stop and sbottom) loops with Higgs exchange and mixed quark/squark loops with Higgsino exchange. The three type of diagrams are sketched in Figure 7.7. These diagrams have to be calculated in the gauge-less limit, in which the mass of the lightest CP-even Higgs m_h vanishes. However, it is shown in Ref. [33] that the result remains consistent if, despite this approximation, the most accurate prediction for m_h is used in the evaluation.

8. Numerical analysis

8.1. SM result

We start the numerical evaluation of our results by showing the prediction for the W boson mass in the SM. Figure 8.1(a) shows M_W, calculated iteratively using the SM one-loop result for Δr, plotted against the SM Higgs mass for three different values of the top mass: $m_t = 173$ GeV, $m_t = 173{+}1.1$ GeV (upper curve) and $m_t = 173{-}1.1$ GeV (lower curve). The most up-to-date experimental value for the W boson mass $M_W^{\rm exp} = 80.399 \pm 0.023$ GeV [3], as well as the lower bound on the SM Higgs boson mass of 114.4 GeV, from Higgs searches at LEP [47] are indicated. The most accurate theory prediction including all SM higher order corrections known at this point is plotted in the same way and can be seen in Figure 8.1(b).

The top mass is meanwhile quite accurately known and the Tevatron electroweak Working Group recently updated it to $m_t = 173.3 \pm 1.1$ GeV [89], combining different CDF and D0 measurements. With the current value for m_t, the parametric uncertainty in the prediction for the W boson mass induced by the experimental error of the top mass is significantly smaller than the experimental error of the W boson mass, $\delta M_W^{\rm exp} = 23$ MeV, as we can see in Figure 8.1. Anyhow, the dominant theoretical uncertainty still comes from the experimental error of m_t, and will remain so even with the slightly better LHC prospect of $\delta m_t \cong 1$ GeV [90,91]. A significant reduction of the parametric uncertainty will be possible with an accuracy of $\delta m_t = 0.1$ GeV, which can be achieved at the International Linear Collider (ILC) [92–94]. Uncertainties from unknown higher orders are significantly smaller and have been estimated to be around 4 MeV in the SM for light Higgs bosons, $m_{h_{\rm SM}} \lesssim 300$ GeV [25].

Comparing the two plots in Figure 8.1, we see that the corrections beyond the one-loop order cause a downward shift in the W boson mass of more than 100 MeV, corresponding to more than 4σ with respect to the experimental error. The full SM results clearly illustrates the preference for a small SM Higgs mass. It should be stressed that the incorporation of the relevant two-loop corrections is crucial for arriving at this conclusion. Notable here is that with the best theoretical prediction and the improved experimental measurements there is no overlap between the experimental 1σ band and the SM prediction.

The plots demonstrate that the total size of the contributions beyond one-loop order is large compared to the experimental error, and their incorporation is necessary for a W boson mass prediction in the SM. Next we investigate the size of the different types of loop corrections, listed and commented on in section 6.3.2. Table 8.1 shows the size of the particular Δr higher order corrections for a fixed value of W boson

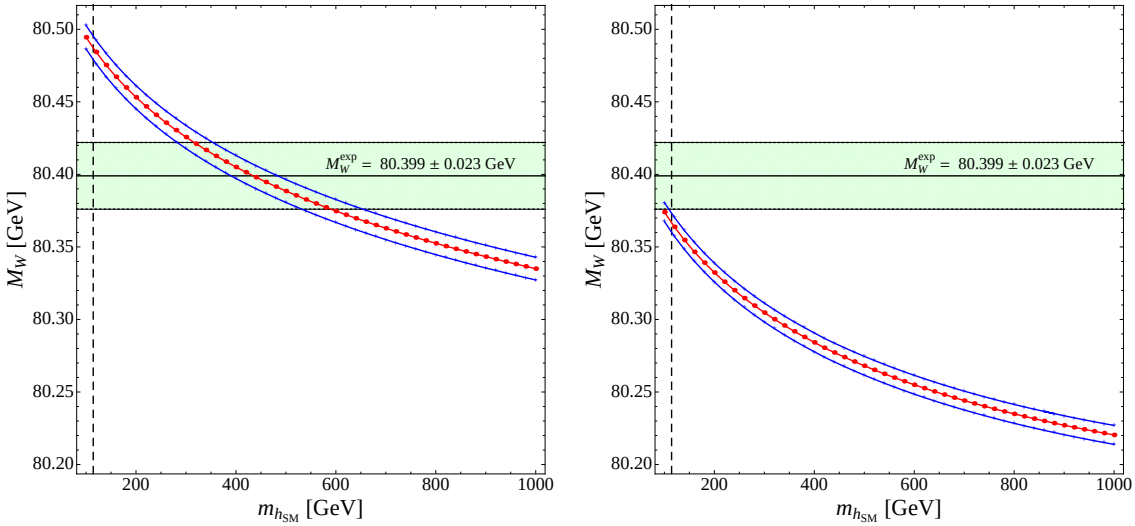

Figure 8.1.: W-boson mass prediction in the SM as a function of $m_{h_{\rm SM}}$ for $m_t = 173.3 \pm 1.1$. The left plot shows the result of the one-loop calculation. The right plot shows the result of the most accurate calculation, including all known higher order SM corrections. The current experimental value for $M_W^{\rm exp} = 80.399 \pm 0.023$ GeV [3] is indicated by a horizontal band, and the experimental lower bound on the Higgs boson mass of the SM of 114.4 GeV from Higgs searches at LEP [47] is shown as a vertical dashed line.

mass, $M_W = M_W^{exp} = 80.399$ GeV. For different values of $m_{h_{\rm SM}}$ their size relative to the SM one-loop result, $\Delta r^{(\alpha)}$, is given. The dominant contributions are the two- and three-loop QCD corrections, $\Delta r^{(\alpha\alpha_s)} + \Delta r^{(\alpha\alpha_s^2)}$, which amount to about 11%-14% of the one-loop contribution, followed by the likewise significant fermionic (plus bosonic) two-loop corrections, $\Delta r^{(\alpha^2)} = \Delta r^{(\alpha^2)}_{ferm} + \Delta r^{(\alpha^2)}_{bos}$, reaching around $8 - 10\%$ of $\Delta r^{(\alpha)}$. Both of these contributions have the same sign and are relatively larger for smaller Higgs masses. The $\Delta r^{(G_\mu^2\alpha_s m_t^4)}$ and $\Delta r^{(G_\mu^3 m_t^6)}$ corrections yield a slight reduction of the two-loop corrections and become largest for heavy Higgs. Even for $m_{h_{\rm SM}} = 1000$ GeV their effect for the W boson mass is only about 9 MeV. So the size of the three-loop $\Delta r^{(G_\mu^2\alpha_s m_t^4)} + \Delta r^{(G_\mu^3 m_t^6)}$, and also the four-loop $\Delta r^{(G_\mu m_t^2 \alpha_s^3)}$ correction to the W boson mass is smaller than the experimental error.

8.2. MSSM result

To study the W boson mass prediction in the MSSM, we discuss the one-loop and two-loop contributions separately for the sfermion sector, the Higgs sector and the chargino and neutralino sector and investigate in each case the impact of the particular SUSY

$m_{h_{\rm SM}}$ [GeV]	$\Delta r^{(\alpha^2)}$	$\Delta r^{(\alpha\alpha_s)} + \Delta r^{(\alpha\alpha_s^2)}$	$\Delta r^{(G_\mu^2\alpha_s m_t^4)} + \Delta r^{(G_\mu^3 m_t^6)}$	$\Delta r^{(G_\mu m_t^2 \alpha_s^3)}$
100	9.95	14.28	-0.48	0.42
400	9.34	12.12	-0.93	0.36
700	8.88	11.30	-1.23	0.34
1000	8.32	10.82	-1.55	0.32

Table 8.1.: Relative size of the higher order SM corrections compared to the size of the one-loop result $\Delta r^{(\alpha)}$ (in %) for $M_W = 80.399$ GeV and different values of $m_{h_{\rm SM}}$. $\Delta r^{(\alpha^2)}$ stands for $\Delta r^{(\alpha^2)}_{ferm} + \Delta r^{(\alpha^2)}_{bos}$.

parameters.

In the complex MSSM the uncertainty from unknown higher orders is a little larger than in the SM and has been estimated to be $\delta M_W = (4.7-9.9)$ MeV [29,33], depending on the SUSY mass scale.

8.2.1. Sfermion sector

First we analyze the sfermion sector and begin with the one-loop contribution where the dominant effect comes from $\Delta\rho$, which is highly sensitive to the mass spitting between the sfermions.

In the sfermion mass matrix, the partner fermion masses appear in the diagonal entries and cause a linear dependence of the squared squark masses on the squared quark masses. Since the mass splitting between top and bottom is significantly larger than the mass splitting in the first two generations, also for squarks the splitting in the third generation (stop/sbottom sector) dominates. The off-diagonal entries of the sfermion mass matrix, defining the mixing in the sfermion sector, are proportional to the partner fermion mass and therefore squark mixing is expected to be negligible in all doublets associated to light fermions. In the stop and the sbottom sector a significant splitting between the two states of one flavor is possible. Therefore we focus in our discussion on the stop and sbottom sector which gives the main sfermion contribution to Δr.

In order to examine the size and the parameter dependence of the pure one-loop sfermion contribution, we begin by showing the M_W prediction, calculated iteratively using the full Δr^{SM} combined with the one-loop SUSY contributions.

In the sfermion sector complex phases can have sizable effects. A_t, A_b and μ do not appear explicitly in the one-loop Δr result, but only in the combinations $X_t = A_t - \mu\cot\beta$ and $X_b = A_b - \mu\tan\beta$ (2.7), the off-diagonal entries of the stop and sbottom mass matrices. It has been shown in Ref. [29] that the full one-loop result is independent of the phases ϕ_{X_t} and ϕ_{X_b}, therefore the phases ϕ_μ, ϕ_{A_t} and ϕ_{A_b} enter only

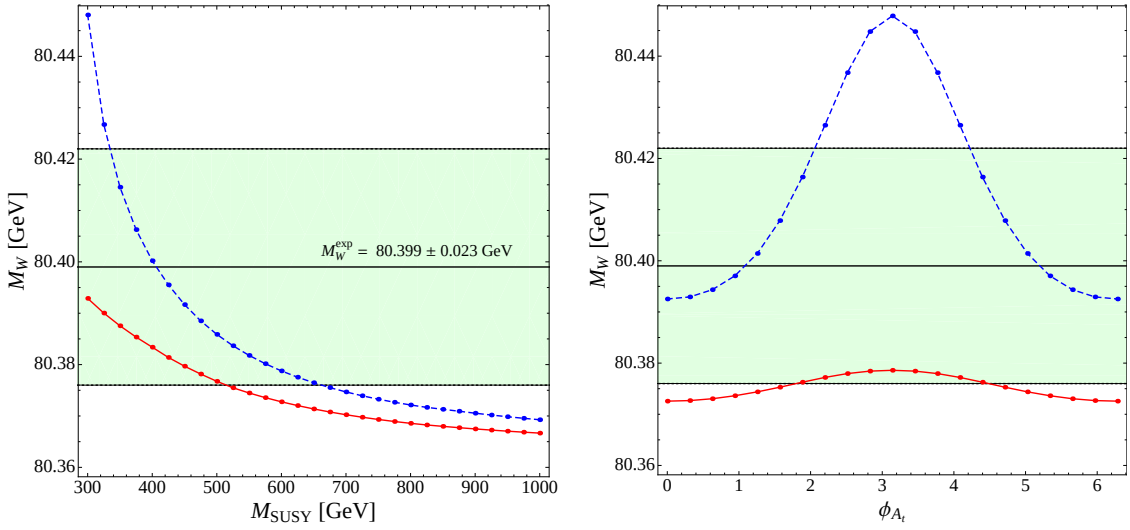

(a) (b)

Figure 8.2.: W-boson mass prediction using the full Δr^{SM} and all one-loop SUSY contributions. The left plot shows M_W as a function of $M_{\rm SUSY}$ for two values of the complex phase, $\phi_{A_t} = 0$ (red, solid line) and $\phi_{A_t} = \pi$ (blue, dashed line). The right plot shows M_W as a function ϕ_{A_t} for two values, $M_{\rm SUSY} = 300$ GeV (blue, dashed line) and $M_{\rm SUSY} = 600$ GeV (red, solid line). The current experimental value for $M_W = 80.399 \pm 0.023$ GeV is indicated. The other SUSY parameters are: $A_t = 2M_{\rm SUSY}$, $M_2 = 500$ GeV, $m_{\tilde{g}} = 500$ GeV, $\mu = 500$ GeV, $m_A = 500$ GeV, $\tan\beta = 10$.

via

$$\begin{aligned} |X_t|^2 = X_t X_t^* &= A_t A_t^* + \mu\mu^* \cot^2\beta - |A_t||\mu| \cot\beta e^{\mathrm{i}(\phi_{A_t}+\phi_\mu)} - |A_t||\mu| \cot\beta e^{-\mathrm{i}(\phi_{A_t}+\phi_\mu)} \\ &= |A_t|^2 + |\mu|^2 \cot^2\beta - 2|A_t||\mu| \cot\beta \cos(\phi_{A_t} + \phi_\mu) \,, \end{aligned} \tag{8.1}$$

and

$$\begin{aligned} |X_b|^2 = X_b X_b^* &= A_b A_b^* + \mu\mu^* \tan^2\beta - |A_b||\mu| \tan\beta e^{\mathrm{i}(\phi_{A_b}+\phi_\mu)} - |A_b||\mu| \tan\beta e^{-\mathrm{i}(\phi_{A_b}+\phi_\mu)} \\ &= |A_b|^2 + |\mu|^2 \tan^2\beta - 2|A_b||\mu| \tan\beta \cos(\phi_{A_b} + \phi_\mu) \,, \end{aligned} \tag{8.2}$$

i.e. in the combinations $(\phi_{A_b} + \phi_\mu)$ and $(\phi_{A_t} + \phi_\mu)$.

If $|A_t|^2$ and $|\mu|^2 \cot^2\beta$ are of different size, one of these terms dominates in (8.1), causing a suppression of the last term containing the phase dependence, and the same argument holds also for (8.2). Hence the impact of the complex phase is largest if all terms in (8.1) and (8.2) are of similar size. In the numerical evaluation we always set $|A_t| = |A_b|$ and $\phi_{A_t} = \phi_{A_b}$.

The one-loop effect of the sfermion phase ϕ_{A_t} on the M_W prediction is shown in Figure 8.2. In these plots $A_t = 2M_{\text{SUSY}}$, $\mu = 500$ GeV and $\tan\beta = 10$ is chosen, so the phase dependence is more significant for relatively small values of M_{SUSY}. Figure 8.2(a) shows the W boson mass prediction as a function of the common scalar mass M_{SUSY} for two different phases: The red, solid line corresponds to $\phi_{A_t} = 0$ and the blue, dashed line to $\phi_{A_t} = \pi$. Independently of the phases, we see that for small M_{SUSY} the sfermion sector gives a sizable contribution to M_W, while and for large M_{SUSY} the sfermion sector decouples and its contribution to M_W vanishes. The shift in M_W is significantly larger for $\phi_{A_t} = \pi$ than for $\phi_{A_t} = 0$. For $M_{\text{SUSY}} \lesssim 350$ MeV the difference in the W boson mass prediction between the two phases accounts for more than 25 MeV, i.e. it is larger than the experimental error. The full phase dependence can be seen in Figure 8.2(b), where the M_W prediction is plotted against ϕ_{A_t} for $M_{\text{SUSY}} = 300$ GeV (blue, dashed line) and $M_{\text{SUSY}} = 600$ GeV (red, solid line). We see once more that the phase dependence is stronger for light SUSY masses and that the two phases, shown in Figure 8.2(a) correspond to the extrema, giving the maximal ($\phi_{A_t} = \pi$) and minimal ($\phi_{A_t} = 0$) contribution to M_W. Both plots in Figure 8.2 contain also the experimental value of M_W, with the 1σ bounds. In the MSSM plots, it is important to keep in mind that the curves depend sensitively also on the other, fixed SUSY parameters, and one can not conclude that certain parameter points in the plots (e.g. in the upper plots $\phi_{A_t} = \pi$ and $M_{\text{SUSY}} = 300$ GeV) are in disagreement with experimental data because they lie outside the 1σ band. In the following we will not consider complex phases, all phases are set to zero and will not be listed as separate input parameter.

As previously mentioned, the main contribution of the sfermion sector can be associated with $\Delta\rho$ and hence depends strongly on the squark mixing. In Figure 8.3 the W boson mass prediction is shown as a function of $X_t = A_t - \mu\cot\beta$, for the two mass scales $M_{\text{SUSY}} = 300$ GeV (blue, dashed line) and $M_{\text{SUSY}} = 600$ GeV (red, solid line). Going from $X_t = 0$ to higher values of $|X_t|$ the contribution to M_W decreases first and increases again for high values of $|X_t|$. This effect is visible for both mass values but is more distinct for $M_{\text{SUSY}} = 300$ GeV, where the shift in M_W from varying X_t can be up to around 35 MeV.

For $X_t = 0$ the mixing in the stop sector is minimal, and the splitting between stops and sbottoms gives the dominant contribution to M_W. Increasing $|X_t|$, $\tilde{t}_1$ becomes lighter and $\tilde{t}_2$ heavier. Also in the sbottom sector the splitting between $\tilde{b}_1$ and $\tilde{b}_2$ increases, since we set $A_b = A_t$, but for the chosen $\tan\beta$ value the effect in the sbottom sector is less pronounced. Increasing the splitting between the squarks of one flavor enlarges the size of the F_0 functions in the first two terms of $\Delta\rho^{\text{SUSY}}$ (7.14), which enter with a negative sign and lead to a partial compensation. If the splitting is further increased, the spitting between $\tilde{t}_1$ and $\tilde{t}_2$ (and between $\tilde{b}_1$ and $\tilde{b}_2$) dominates and raises the predicted M_W value.

To investigate the SUSY two-loop effects, we start by examining the shift in M_W caused by the two-loop QCD corrections $\mathcal{O}(\alpha\alpha_s)$. Therefore we calculate M_W once, using Δr^{SM} together with only SUSY one-loop corrections. Then we add the SUSY two-loop corrections under consideration, calculate M_W and subtract the first result.

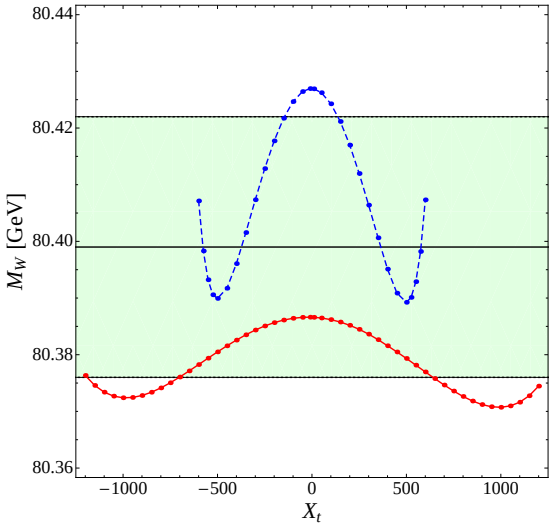

Figure 8.3.: W-boson mass prediction using the full Δr^{SM} and all one-loop SUSY contributions as a function of $X_t = A_t - \mu/\tan\beta$ for $M_{\text{SUSY}} = 300$ GeV (blue, dashed line) and $M_{\text{SUSY}} = 600$ GeV (red, solid line). The current experimental value for $M_W = 80.399 \pm 0.023$ GeV is indicated. The other SUSY parameters are: $A_t = 2M_{\text{SUSY}}$, $M_2 = 500$ GeV, $m_{\tilde{g}} = 500$ GeV, $\mu = 500$ GeV, $m_A = 500$ GeV, $\tan\beta = 10$.

In Figures 8.4 to 8.8 (explained in detail later), the shift in M_W caused by the two-loop corrections is plotted as a function of M_{SUSY}, starting with $M_{\text{SUSY}} = 225$ GeV, so that all parameter points are compatible with the lower bound on the lightest CP-even Higgs in the CP-conserving MSSM, $m_h \gtrsim 90$ GeV [95]. There are no absolute limits on the Higgs boson masses in CP-violating scenarios [95].

We investigate the effect of the gluon and gluino two-loop contributions, leaving out the mass-shift corrections in a first step. Figure 8.4 shows the contribution to M_W from two-loop corrections, containing a squark loop with an additional gluon exchange, for two values of the stop mixing, $A_t = 0$ (blue, dashed line) and $A_t = 2M_{\text{SUSY}}$ (red, solid line). The gluonic two-loop correction has the same sign as the one-loop correction and give rise to an increase of the predicted value of the W boson mass. Also the dependence on M_{SUSY} and the mixing A_t is comparable to the one-loop case, since the gluonic contribution has a similar structure (7.17) as the one-loop $\Delta\rho^{\text{SUSY}}$. The shift in M_W from the gluonic two-loop contribution can account for ≈ 5.5 MeV in the case $A_t = 0$ and ≈ 2.5 MeV in the case $A_t = 2M_{\text{SUSY}}$. If lower values for M_{SUSY} are considered, the gluonic contribution can be larger.

The gluino contributions depend sensitively on the SUSY mass scale, M_{SUSY}, the squark mixing, A_t, and the gluino mass, $m_{\tilde{g}}$. Figure 8.5 shows the shift caused by the two-loop gluino contributions as a function of M_{SUSY}. In Figure 8.5(a) the sfermion mixing $A_t = 0$ is chosen, in Figure 8.5(b) $A_t = M_{\text{SUSY}}$ and in Figure 8.5(c) $A_t = 2M_{\text{SUSY}}$. In each plot the solid lines show the contributions from a gluino with mass

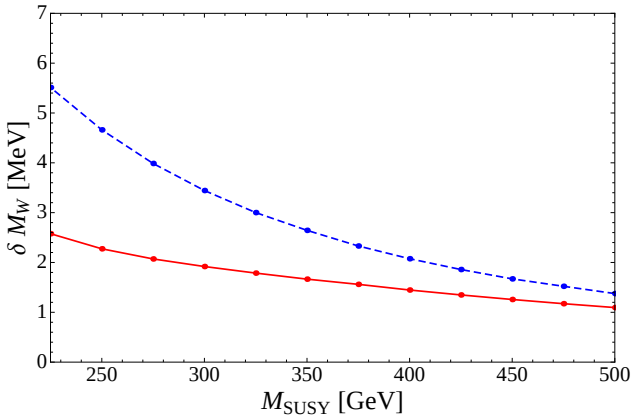

Figure 8.4.: Shift in the W-boson mass from the gluon two-loop SUSY contributions as a function of $M_{\rm SUSY}$ for two different stop mixing values $A_t = 0$ (blue, dashed line) and $A_t = 2M_{\rm SUSY}$ (red, solid line). The other SUSY parameters are: $M_2 = 500$ GeV, $m_{\tilde{g}} = 500$ GeV, $m_A = 500$ GeV, $\mu = 500$ GeV, $\tan\beta = 5$.

$m_{\tilde{g}} = 200$ GeV, the dashed ones correspond to a gluino mass of $m_{\tilde{g}} = 500$ GeV and the dotted ones to a gluino mass of $m_{\tilde{g}} = 800$ GeV.

It should be noted in this context that with the first LHC results the limits on the gluino mass have already been strengthened. The CMS collaboration found that gluinos below about 650 GeV [1, 96] are excluded in certain parts of the MSUGRA/CMSSM (minimal supergravity/constrained MSSM) [97–102] parameter space, and the ATLAS collaboration excluded $m_{\tilde{g}} < 700$ GeV at 95% confidence level for a specific scenario with equal squark and gluino masses [2]. Nevertheless, there is no absolute lower bound on the gluino mass in this mass range and it is therefore of interest to study the virtual effects also of lighter gluinos.

It can be seen in the gluino plots that the contributions decrease for high $m_{\tilde{g}}$, as a consequence of decoupling. Considering small to medium gluino masses, their contributions can be of the same size as the gluon contribution or even larger, see in particular in Figure 8.5(c). The sign of the gluino contributions changes depending on the SUSY parameters. For vanishing squark mixing, $A_t = 0$, the contributions are negative and can cause a downward shift in the W boson mass of more than 7 MeV for small $M_{\rm SUSY}$ and small $m_{\tilde{g}}$. For $A_t = M_{\rm SUSY}$ the contributions are generally smaller. For very light squarks and light gluinos the contributions are negative. Otherwise they are positive and result in a shift in M_W of about 1-2.5 MeV. Threshold effects appear for light gluinos, $m_{\tilde{g}} = 200$ GeV, and cause the kinks that can be seen in both plots, in Figure 8.5(a) and in Figure 8.5(b).

If the squark mixing is large, $A_t = 2M_{\rm SUSY}$, the gluino contributions are positive and significantly larger. Even for heavy gluinos, $m_{\tilde{g}} = 800$ GeV, the shift can be more than 6 MeV and for $m_{\tilde{g}} = 500$ GeV the shift can be up to 10 MeV. For $m_{\tilde{g}} = 200$ GeV, the gluino contribution has a high peak of about 17 MeV for $M_{\rm SUSY} = 225$ GeV and then

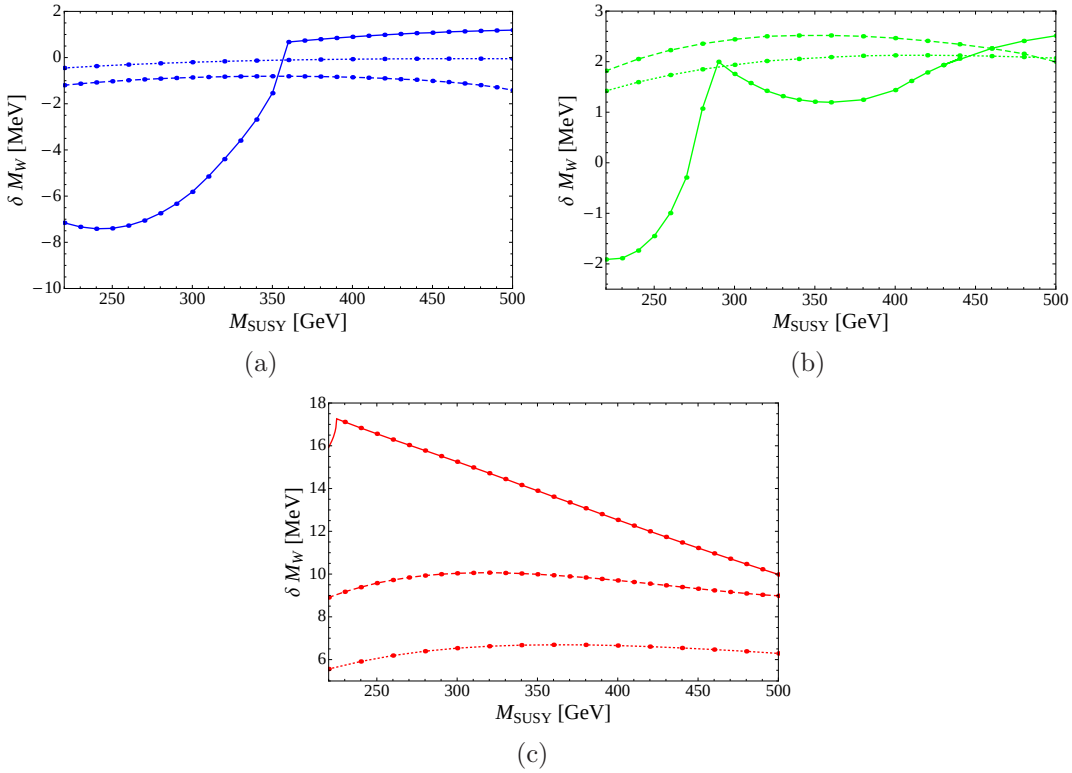

Figure 8.5.: Shift in the W-boson mass from gluino two-loop contributions as a function of M_{SUSY} for three different gluino masses, $m_{\tilde{g}} = 200$ GeV (solid lines), $m_{\tilde{g}} = 500$ GeV (dashed lines) and $m_{\tilde{g}} = 800$ GeV (dotted lines). The upper left plot (a), (blue curves) corresponds to $A_t = 0$, the upper right one (b), (green curves) to $A_t = M_{\mathrm{SUSY}}$ and the lower one (c), (red curves) to $A_t = 2M_{\mathrm{SUSY}}$. The other SUSY parameters are: $M_2 = 500$ GeV, $m_A = 500$ GeV, $\mu = 500$ GeV, $\tan\beta = 5$.

falls off almost linearly with increasing M_{SUSY}. At $M_{\mathrm{SUSY}} = 500$ GeV the shift in M_W caused by gluino contribution is still about 10 MeV.

The gluon and gluino two-loop contributions are directly related to the mass-shift correction, which has to be incorporated in order to arrive at the complete result for the $\mathcal{O}(\alpha\alpha_s)$ contributions to $\Delta\rho^{\mathrm{SUSY}}$. We will now show the impact of this additional correction. The size and the shape of the gluino contribution for $A_t = 2M_{\mathrm{SUSY}}$ and $m_{\tilde{g}} = 200$ GeV discussed above, may seem a little surprising at first sight, due to the high peak. But looking at the full contribution, together with the mass-shift correction, the high peak for small M_{SUSY} is canceled. This can be seen in Figure 8.6, where the pure gluino contribution (red, solid line) and the combined gluino plus mass-shift contribution (orange, dotted line) are plotted against M_{SUSY} for $m_{\tilde{g}} = 200$ GeV and $A_t = 2M_{\mathrm{SUSY}}$. Figure 8.7 shows only the mass-shift correction as a function of M_{SUSY} for an intermediate gluino mass of $m_{\tilde{g}} = 500$ GeV. The blue, dashed line corresponds to $A_t = 0$ and the red, solid line to $A_t = 2M_{\mathrm{SUSY}}$. The size of the mass-shift correction

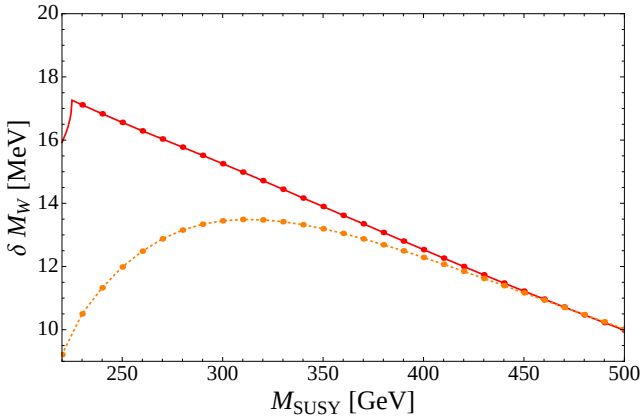

Figure 8.6.: Shift in the W-boson mass from gluino two-loop contributions as a function of M_{SUSY} for $m_{\tilde{g}} = 200$ GeV and $A_t = 2M_{\text{SUSY}}$. The red, solid line is the pure gluino contribution, while the orange, dotted curve contains the gluino contribution and the mass-shift correction. The other SUSY parameters are: $M_2 = 500$ GeV, $m_A = 500$ GeV, $\mu = 500$ GeV, $\tan\beta = 5$.

is larger than the gluonic contribution and the correction enters with the opposite sign.

We finish the discussion of the sfermion sector by looking at the combined effect of gluon, gluino and mass-shift corrections. In Figure 8.8 the effect of all $\mathcal{O}(\alpha\alpha_s)$ SUSY two-loop corrections is shown, again plotted against M_{SUSY} for three different gluino masses, $m_{\tilde{g}} = 200$ GeV (solid lines), $m_{\tilde{g}} = 500$ GeV (dashed lines) and $m_{\tilde{g}} = 800$ GeV (dotted lines). In the left plot $A_t = 0$, and in the right plot $A_t = 2M_{\text{SUSY}}$ is chosen. Depending on the squark mixing the SUSY two-loop corrections to the W boson mass can be either negative (for M_W plot with $A_t = 0$) or positive (for M_W plot with $A_t = 2M_{\text{SUSY}}$). For $A_t = 0$ the absolute size of the contribution is maximal for small M_{SUSY}. For heavy gluinos the total downward shift is larger than for light gluinos, more than -17 MeV for $m_{\tilde{g}} = 800$ GeV and about -10 MeV for $m_{\tilde{g}} = 200$ GeV. The 'kink' in the solid line of the left plot is caused by the threshold effect already observed in the gluino contribution of Figure 8.5(a). For $A_t = 2M_{\text{SUSY}}$ the characteristics of the QCD two-loop contributions are very different. For $m_{\tilde{g}} = 500$ GeV and $m_{\tilde{g}} = 800$ GeV the shift in M_W rises with M_{SUSY}. The increase is larger for small values of M_{SUSY} and reduces for high values of M_{SUSY}. For $M_{\text{SUSY}} > 500$ GeV (not shown here) the shift in M_W gets smaller. For $M_{\text{SUSY}} = 1000$ GeV (and $m_{\tilde{g}} = 500$ GeV) the combined $\mathcal{O}(\alpha\alpha_s)$ SUSY two-loop corrections result in a W boson mass shift of less than 5 MeV. As we have shown before, the gluino and mass-shift corrections behave differently for a high squark mixing and a small gluino mass. By adding the gluonic contribution to the combined gluino/mass-shift corrections shown in the orange, dotted curve in Figure 8.6, we find a maximum of the overall $\mathcal{O}(\alpha\alpha_s)$ contributions, of about 15 MeV, reached for intermediate values of M_{SUSY}, while the shift in M_W gets smaller both for decreasing and increasing M_{SUSY}. This behaviour can be understood from the shape of the gluon

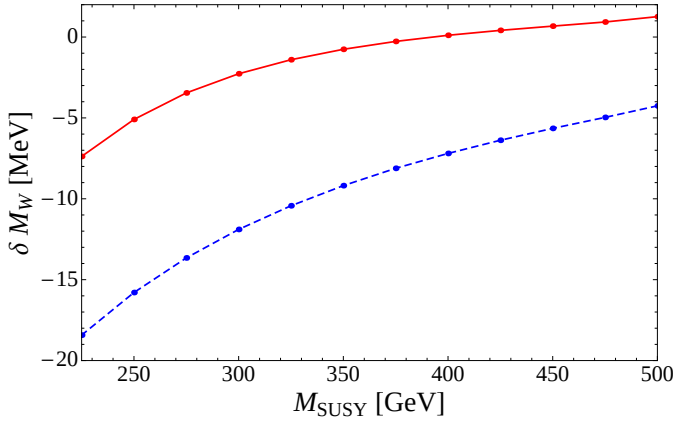

Figure 8.7.: Shift in the W-boson mass from the mass-shift correction of $\mathcal{O}(\alpha\alpha_s)$ as a function of M_{SUSY} for two different stop mixing values $A_t = 0$ (blue, dashed line) and $A_t = 2M_{\mathrm{SUSY}}$ (red, solid line). The other SUSY parameters are: $m_{\tilde{g}} = 500$ GeV, $M_2 = 500$ GeV, $m_A = 500$ GeV, $\mu = 500$ GeV, $\tan\beta = 5$.

contributions shown in Figure 8.4.

The anticipated experimental accuracy for the W boson mass at LHC is 15 MeV [103, 104] and even 7 MeV at ILC [103, 104]. So a contribution of the size of the SUSY two-loop corrections is very important for a precise calculation of the W boson mass, that can be compared to the future measurements.

8.2.2. Higgs sector

To show the impact of the MSSM Higgs sector on the one-loop SUSY contribution to Δr, the M_W prediction is shown in Figure 8.9 as a function of the relevant parameters in this sector, which are (at tree level) m_A and $\tan\beta$. For the two plots in Figure 8.9, we do not use the full Δr^{MSSM} but 'switch off' the SUSY two-loop gaugino and higgsino contributions, $\mathcal{O}(\alpha_t^2)$, $\mathcal{O}(\alpha_t\alpha_b)$ and $\mathcal{O}(\alpha_b^2)$, since these contributions also depend on m_A. So M_W is here calculated iteratively, using the full Δr^{SM}, the SUSY one-loop result and the SUSY $\mathcal{O}(\alpha\alpha_s)$ two-loop contributions. In Figure 8.9(a) the M_W prediction is plotted against m_A for three values of $\tan\beta$: The red, dotted curve corresponds to $\tan\beta = 5$, the blue, dashed curve to $\tan\beta = 10$ and the green, solid one to $\tan\beta = 25$. It shows, that the effect of the MSSM Higgs sector is largest for small m_A and can contribute to a shift of about 20 MeV to the W boson mass, which is about the size of the current experimental error.

The dependence of M_W on $\tan\beta$ is not monotonic. To show this behavior more clearly, we show the M_W prediction as a function of $\tan\beta$ in Figure 8.9(b) for $m_A = 250$ GeV, which is approximately the m_A value where the predicted M_W is the same for $\tan\beta = 25$ and $\tan\beta = 10$. Within the Higgs sector the strong $\tan\beta$ dependence can not be explained. The Higgs masses depend on $\tan\beta$, but this effect is very small for

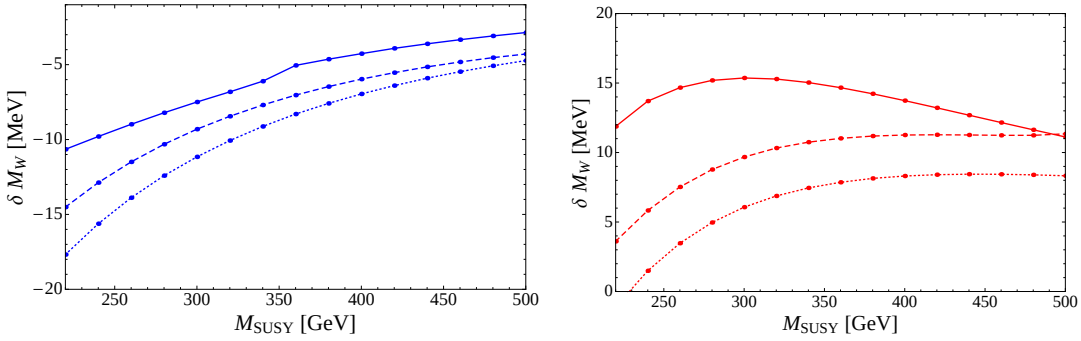

Figure 8.8.: Shift in the W-boson mass from the combined $\mathcal{O}(\alpha\alpha_s)$ SUSY two-loop corrections, containing the gluon, gluino and mass-shift correction as a function of M_{SUSY} for three different gluino masses, $m_{\tilde{g}} = 200$ GeV (solid lines), $m_{\tilde{g}} = 500$ GeV (dashed lines) and $m_{\tilde{g}} = 800$ GeV (dotted lines). The left plot (blue curves) corresponds to $A_t = 0$ and the right one (red curves) to $A_t = 2M_{\text{SUSY}}$. The other SUSY parameters are: $M_2 = 500$ GeV, $m_A = 500$ GeV, $\mu = 500$ GeV, $\tan\beta = 5$.

$\tan\beta > 10$. We checked this and found, as we expected, that for large $\tan\beta$ the shift in M_W from the change in the Higgs masses is negligible and cannot explain the $\tan\beta$ dependence in Figure 8.9(b). In the two other sectors, the chargino and neutralino sector and in the sfermion sector, $\tan\beta$ enters the calculation of M_W as well. The impact of varying $\tan\beta$ in the chargino and neutralino sector is smaller than 1 MeV and does not explain the $\tan\beta$ dependence of M_W. In the sfermion sector $\tan\beta$ also appears in the squark mass matrices. Going to higher $\tan\beta$ values means increasing the splitting between $\tilde{b}_1$ and $\tilde{b}_2$, since $X_b = A_b - \mu^* \tan\beta$ changes linearly with $\tan\beta$ (2.7) while the mixing in the stop sector $X_t = A_t - \mu^*/\tan\beta$ goes to $X_t = A_t$ for large values of $\tan\beta$. The change in the mass splittings between the stops and the sbottoms with $\tan\beta$ enters the M_W prediction via $\Delta\rho^{\text{SUSY}}$ (7.14) and gives rise to the $\tan\beta$ behavior, shown in Figure 8.9(b). For $\tan\beta > 50$ (not shown here) the mass splitting in the sbottom sector gets very large and the curve showing the M_W prediction rises very steeply.

By 'switching on' the $\mathcal{O}(\alpha_t^2)$, $\mathcal{O}(\alpha_t\alpha_b)$, $\mathcal{O}(\alpha_b^2)$ corrections the size of these two-loop effects can be seen in Figure 8.10. The lower blue, dashed curve corresponds to the blue, dashed ($\tan\beta = 10$) curve in Figure 8.9(a), so it is calculated using, besides the one-loop result, only the $\mathcal{O}(\alpha\alpha_s)$ SUSY two-loop contributions. The upper red curve is the M_W prediction, when the complete Δr^{MSSM} including the two-loop Higgsino corrections is used. The numerical effect of the $\mathcal{O}(\alpha_t^2)$,$\mathcal{O}(\alpha_t\alpha_b)$ and $\mathcal{O}(\alpha_b^2)$ SUSY two-loop contributions is rather small, in this example it only accounts for a shift of about 0.5 MeV.

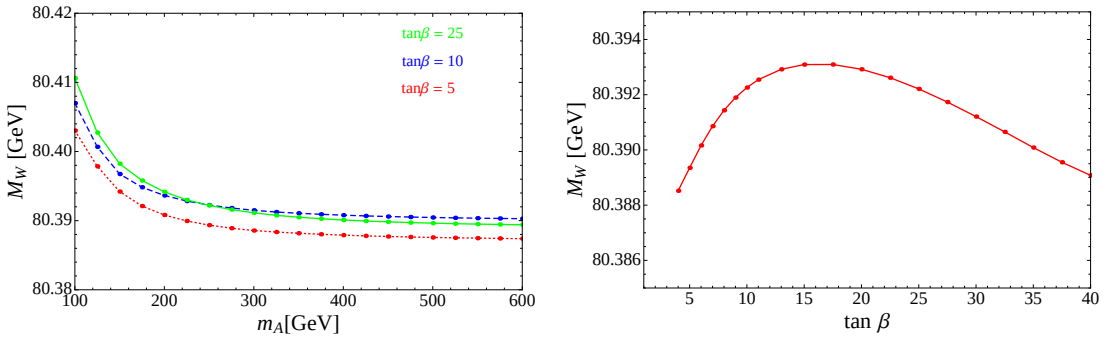

(a) (b)

Figure 8.9.: W-boson mass prediction in the MSSM as a function of m_A and $\tan\beta$. For the calculation the entire Δr^{SM} and SUSY $\mathcal{O}(\alpha\alpha_s)$ two-loop contributions are taken into account. The left plot shows M_W as a function of m_A for different values of $\tan\beta$. The right plot shows M_W as a function of $\tan\beta$ for $m_A = 250$ GeV. The other SUSY parameters are: $M_{\text{SUSY}} = 500$ GeV, $A_t = 2M_{\text{SUSY}}$, $M_2 = 500$ GeV, $m_{\tilde{g}} = 500$ GeV, $\mu = 500$ GeV.

8.2.3. Chargino and neutralino sector

The chargino and neutralino sector is governed by M_1, M_2 and μ. These three parameters can in general be complex, but the phase of M_2 can be rotated away. The effect of varying $|M_1|$ is smaller than 2 MeV and its phase is insignificant, hence we use the GUT relation [105] in our numerical evaluation and set

$$M_1 = \frac{5}{3}\frac{s_W^2}{c_W^2} M_2 \,. \tag{8.3}$$

Also the dependence of the chargino and neutralino contributions on the phase of μ is small and will not be displayed here.

In the following we investigate the impact of the parameters M_2 and $|\mu|$ on the prediction for M_W in the MSSM. Therefore the W-boson mass has been calculated, using the complete Δr^{MSSM} containing all one-loop and higher-order contributions and the results are shown in Figure 8.11. Only the one-loop diagrams containing charginos and neutralinos depend on the parameter M_2, so the effect in the W-boson mass obtained by varying M_2 arises solely from these diagrams.

Figure 8.11(a) shows the M_W prediction as a function of M_2 for three different values of $|\mu|$: $|\mu| = 800$ GeV (green line), $|\mu| = 400$ GeV (blue, dashed line) and $|\mu| = 200$ GeV (red, dotted line). M_W as a function of $|\mu|$ is shown in Figure 8.11(b), where the red line corresponds to $M_2 = 200$ GeV and the blue, dashed line to $M_2 = 600$ GeV. For both plots a small value for the SUSY mass scale, $M_{\text{SUSY}} = 250$ GeV, is chosen, since the effect of the chargino and neutralino contributions is more pronounced for small sfermion masses.

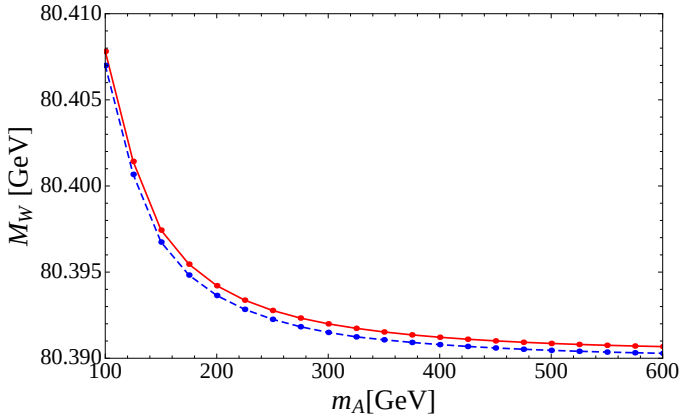

Figure 8.10.: W-boson mass prediction as function of m_A. The entire Δr^{SM} and SUSY $\mathcal{O}(\alpha\alpha_s)$ two-loop contributions are taken into account for the blue, dashed curve, while for the red, solid curve the entire Δr^{MSSM} is taken into account. The other SUSY parameters are: $M_{\rm SUSY} = 500$ GeV, $A_t = 2M_{\rm SUSY}$, $M_2 = 500$ GeV, $m_{\tilde{g}} = 500$ GeV, $\mu = 500$ GeV, $\tan\beta = 10$.

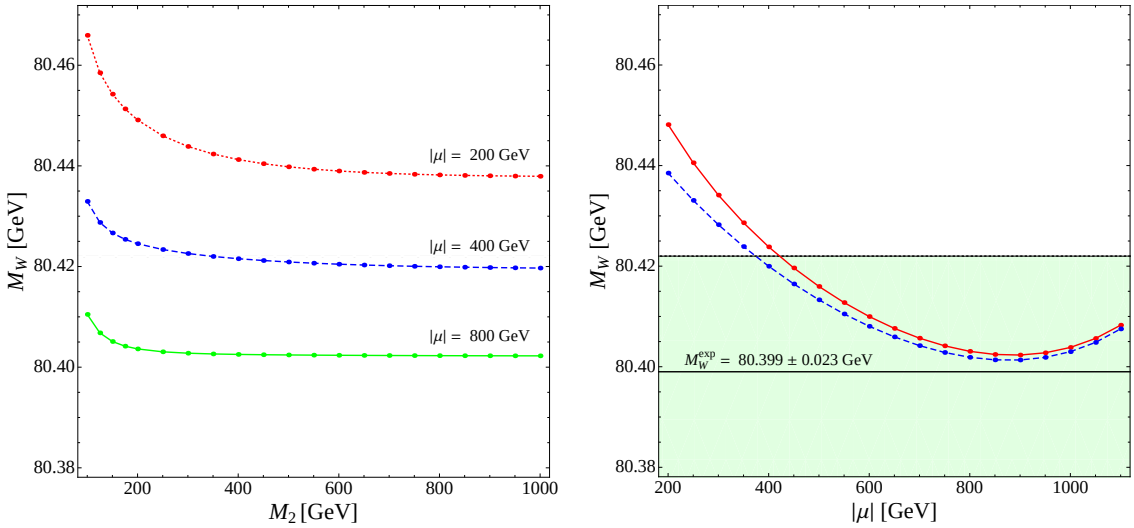

(a) (b)

Figure 8.11.: W-boson mass prediction as function of M_2 and $|\mu|$. For the calculation the entire Δr^{SM} and all SUSY one- and two-loop contributions are taken into account. The left plot shows M_W against M_2 for three different values of $|\mu|$. The right plots shows M_W against $|\mu|$ for $M_2 = 200$ GeV (red, solid line) and $M_2 = 600$ GeV (blue, dashed line). The other SUSY parameters are: $M_{\rm SUSY} = 250$ GeV, $\tan\beta = 10$, $A_t = 2M_{\rm SUSY}$, $m_{\tilde{g}} = 500$ GeV, $m_A = 500$ GeV.

For small M_2 the contribution arising from the chargino and neutralino sector can be relevant. The impact is larger for small values of $|\mu|$. With $|\mu| = 800$ GeV this contribution can shift M_W by up to 8 MeV, and with $|\mu| = 200$ GeV even by up to 28 MeV, clearly an effect that should not be neglected.

In contrast to the shift of M_W from varying M_2, the large impact on M_W from choosing different $|\mu|$ values is not solely due to the chargino and neutralino contributions. The strong $|\mu|$ dependence comes both from the chargino-neutralino one-loop contributions and from sfermion one- and two-loop contributions. As one can clearly see in Figure 8.11(a), the effect on M_W from different $|\mu|$ remains considerable also for large M_2, where the chargino and neutralino contribution vanishes. Varying $|\mu|$ from 200 GeV to 900 GeV yields a downward shift of more than 45 MeV for $M_2 = 200$ GeV, and about 37 MeV for $M_2 = 600$ GeV. For very high values of $|\mu|$ the splitting in the sbottom sector gets large, and the sfermion contribution pushes the M_W prediction up again. Increasing the value of $\tan\beta$ the minimum in the plot of Figure 8.11(b) moves to the left, and accordingly it moves to the right when $\tan\beta$ is decreased, which becomes clear by looking at the formula for the off-diagonal sfermion matrix elements (2.7).

The purpose of the plots in Figure 8.11 is to demonstrate the size of the contributions from the chargino and neutralino sector. The other parameters are chosen at a low scale to illustrate that these contributions can be sizable. The fact that the MSSM prediction for M_W shown in Figure 8.11 turns out to be outside of the experimental 1σ band for small $|\mu|$ is specific to the chosen set of SUSY parameters and should not be interpreted as a general conclusion on the allowed range of $|\mu|$.

We furthermore analyze the difference between the M_W calculation using the complete Δr contribution of the chargino and neutralino sector and the M_W calculation using an approximation where only the chargino and neutralino contribution to $\Delta\rho$ is taken into account, as often done. $\Delta\rho$ (6.19) contains only the W and Z boson self-energies at zero momentum transfer. In order to investigate the impact of this approximation, we calculate the W boson mass prediction using all other SM and SUSY one-loop and higher order contributions, combined with only the $\Delta\rho$, instead of the full Δr, contribution from the chargino and neutralino sector. The result is shown in the lower (blue, solid) curve of Figure 8.12. The same input values as before are used with $|\mu| = 200$ GeV. The red, dotted curve is our result using the full Δr chargino neutralino contribution and corresponds to the red, dotted curve in Figure 8.11(a). The difference between the full Δr chargino and neutralino contribution and the approximation via $\Delta\rho$ is small for large M_2 but goes up to 10 MeV for $M_2 = 100$ GeV.

8.3. Total result

In this section we show our final result for the M_W prediction in the MSSM, including all higher order contributions of SM- and SUSY-type, and compare it to the SM prediction.

Figure 8.13 shows the W boson mass prediction in the MSSM and the SM. The MSSM prediction is calculated with the complete Δr^{MSSM}, and for the SM prediction Δr^{SM}

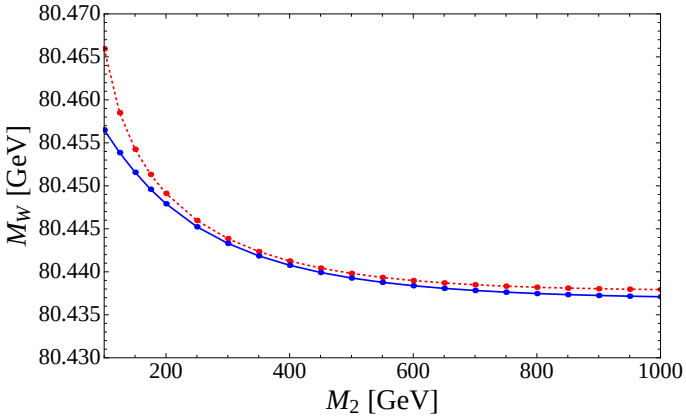

Figure 8.12.: W-boson mass prediction as function of M_2. For the calculation the entire Δr^{SM}, the one-loop contributions of all SUSY sectors, besides the chargino/neutralino one, and all SUSY two-loop contributions to Δr are taken into account. For the red, dotted curve the complete Δr contribution from the chargino and neutralino sector is used. For the blue, solid curve the contribution from the chargino neutralino sector is instead approximated by $\Delta\rho$. The other SUSY parameters are: $\mu = 200$ GeV, $M_{\text{SUSY}} = 250$ GeV, $\tan\beta = 10$, $A_t = 2M_{\text{SUSY}}$, $m_{\tilde{g}} = 500$ GeV, $m_A = 500$ GeV.

has been used. For the left plot $M_{\text{SUSY}} = 300$ GeV is chosen and for the right plot a higher mass scale of $M_{\text{SUSY}} = 600$ GeV. In both plots the red lines (cross markers) show the prediction for $\tan\beta = 5$ and the blue lines (point markers) for $\tan\beta = 10$. Further the solid lines indicate the MSSM prediction and the dashed ones the SM prediction. Also the SM prediction depends on the SUSY parameters m_A, $\tan\beta$ and slightly on m_{SUSY}, due to the fact that the SM Higgs mass is set to the mass of the MSSM Higgs which couples most SM-like. We calculate the Higgs masses in *FeynHiggs* including one- and two-loop corrections, therefore they also depend on M_{SUSY}. The lower bound on a SM-like Higgs of 114.4 GeV [47] is not explicitly imposed here. For our parameters, the CP-even Higgs h is lighter than 114.4 GeV for $m_A < 170$ GeV, if $M_{\text{SUSY}} = 300$ GeV is chosen, and $m_A < 120$ GeV, if $M_{\text{SUSY}} = 600$ GeV is chosen. However, as mentioned before, this limit is not valid in the MSSM but Higgs masses down to $m_h \gtrsim 90$ GeV are allowed in the CP-conserving MSSM and the Higgs can be even lighter in the CP-violating case.

Generally we see that the MSSM prediction is higher than the SM prediction and lies, for this set of parameters, within the 1σ interval of the experimental value $M_W^{\text{exp}} = 80.399 \pm 0.023$ GeV. For small values of m_A both curves rise, indicating that the 20 MeV effect in the W boson mass we showed in Figure 8.9(a) is not a pure SUSY effect, but the shift in the SM M_W prediction (for the corresponding Higgs masses) is of a similar size. The difference between the SM prediction and the MSSM prediction is larger for smaller values of M_{SUSY}, since the sfermion contributions get larger in this mass

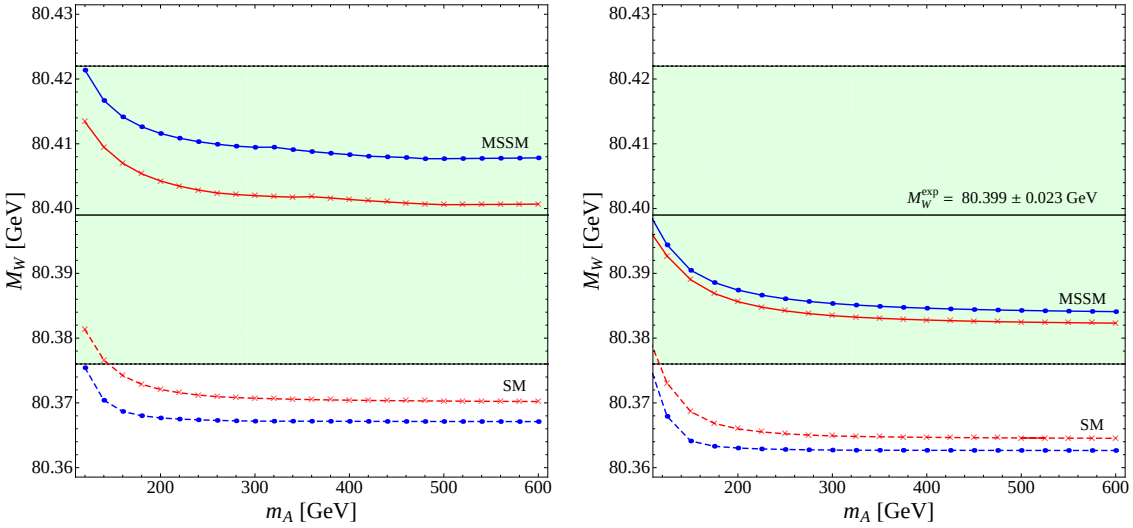

(a) (b)

Figure 8.13.: W-boson mass prediction in the MSSM and the SM as a function of m_A for $\tan\beta = 5$ (red curves, cross markers) and $\tan\beta = 10$ (blue curves, point markers). For the SM prediction $m_{h_{\mathrm{SM}}}$ is chosen as the mass of the MSSM Higgs that couples SM-like. The MSSM predictions are shown as solid lines, the SM prediction as a dashed line. In the left plot $M_{\mathrm{SUSY}} = 300$ GeV is chosen and in the right plot $M_{\mathrm{SUSY}} = 600$ GeV. The experimental value $M_W^{\mathrm{exp}} = 80.399 \pm 0.023$ GeV is indicated. The other SUSY parameters are: $A_t = 2M_{\mathrm{SUSY}}$, $M_2 = 500$ GeV, $m_{\tilde{g}} = 500$ GeV, $\mu = 500$ GeV.

range, as already shown in the previous section. The small 'kinks' in the MSSM M_W prediction for $M_{\mathrm{SUSY}} = 300$ GeV are caused by a threshold effect.

Finally, we analyze the general behaviour of the W boson mass in the MSSM compared to the SM by performing a random scan over the MSSM parameter space. We scan over M_{SUSY}, A_t, μ, $\tan\beta$, $m_{\tilde{g}}$, m_A and M_2 in the following ranges:

$$\begin{aligned} M_{\mathrm{SUSY}} &= 100...2000 \text{ GeV} \\ A_t &= -2M_{\mathrm{SUSY}}...2M_{\mathrm{SUSY}} \\ \mu &= -2000...2000 \text{ GeV} \\ \tan\beta &= 1.1...60 \\ m_{\tilde{g}} &= 200...1000 \text{ GeV} \\ m_A &= 90...1000 \text{ GeV} \\ M_2 &= 100...2000 \text{ GeV} \end{aligned} \tag{8.4}$$

We check the limit on the light MSSM Higgs mass $m_h \gtrsim 90$ GeV, and if it is fulfilled

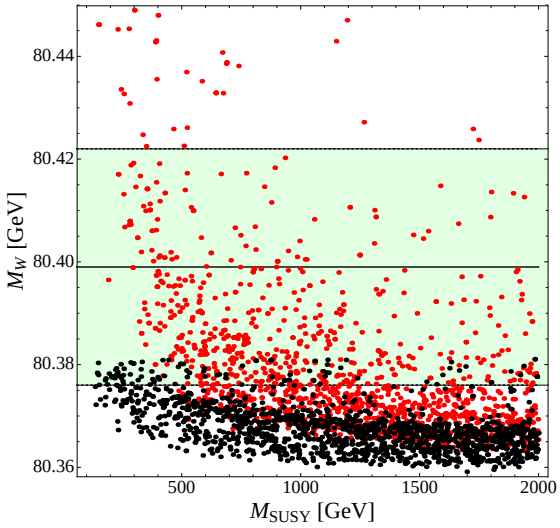

Figure 8.14.: W-boson mass prediction in the MSSM (red points) and the SM (black points) as function of M_{SUSY}. A random scan over the SUSY parameter space is performed within the ranges given in the text. For the SM prediction the SM Higgs mass is set to the value of the lightest CP-even Higgs mass.

the W boson mass prediction in the MSSM and the SM is calculated. The result can be seen in Figure 8.14 where the M_W prediction in the MSSM is plotted in red and the M_W prediction in the SM on top in black. For the SM prediction we take the mass for the lightest CP-even Higgs as input value for the Higgs mass, therefore it also depends on the SUSY parameters. It should be mentioned that for the SM points, the limit $m_{h_{\mathrm{SM}}} > 114.4$ GeV is not imposed. The SM points in Figure 8.14 with $M_W > 80.37$ GeV correspond to parameters involving Higgs masses below this limit.

The prediction for the W boson mass in the MSSM is generally higher than the prediction within the SM and hence favoured by the current experimental value of M_W. The difference between the M_W prediction in the MSSM and the SM can amount to more than 2σ, showing that M_W is highly sensitive to quantum effects of SUSY particles.

9. Summary, conclusions and outlook

In this thesis we computed the one-loop result in the SM and the MSSM with complex parameters. With the exception of one diagram, which required a specific treatment, we calculated the SM diagrams using Dimensional Regularization and the SUSY diagrams with Constrained Differential Renormalization. The renormalization was done in the on-shell scheme.

We combined our one-loop results with all available higher order corrections. Since the calculation of the W boson mass in the SM is more advanced than in the MSSM we organized our result such that the sophisticated SM result can be used also for the MSSM prediction. Therefore the MSSM result is split into a SM part, containing the state-of-the-art SM prediction with all loop corrections, and a SUSY part, consisting of our one-loop result and the known leading two-loop corrections. In this way the MSSM result recovers the full SM result in the decoupling limit, where the lightest MSSM Higgs becomes SM-like and all other SUSY particles are very heavy. Thus we obtained the most accurate theoretical prediction of the W boson mass in the SM and the MSSM.

The one-loop calculation has been performed in *Mathematica* (using *FeynArts* and *FormCalc*) and we transcribed also all higher order contributions into *Mathematica* form. With our stand-alone computer program one of the most important precision observables, $\Delta r^{\rm SUSY}$, can be calculated, which is needed whenever a theoretical prediction is parametrized in terms of G_μ. *Mathematica* provides the flexibility which allows us to analyze the functions also at the analytical level and if threshold effects or numerical instabilities appear in a future scan, an analytic treatment of special cases can easily be added, as we did already for the case of degenerate sneutrino masses.

We have shown that in the SM case the higher order corrections lower the M_W prediction significantly. With the up-to-date experimental value and a state-of-the-art theoretical prediction, the theoretical calculation shows more than 1σ deviation from the measured value in the entire range of allowed Higgs masses.

We have analyzed the impact of the different SUSY sectors and the size of higher order corrections. If the parameters are chosen such that the masses of the SUSY particles are heavy, their contributions to M_W are small as expected from the decoupling properties of supersymmetric theories. On the other hand the SUSY contributions can get substantial at lower mass scales. The one-loop contributions are dominated by the squark sector, but also the other SUSY sectors can give sizable effects. For light sleptons the contribution from the chargino and neutralino sector can account for up to 28 MeV,

a value that is larger than the current experimental error of 23 MeV. A comparison of the full contribution to Δr with the $\Delta\rho$ approximation shows differences for small SUSY masses and demonstrates that this approximation may not be sufficiently accurate for predicting M_W in this parameter range.

We studied the numerical impact of SUSY two-loop contributions in detail. In contrast to the SM higher order corrections, the SUSY two-loop contributions can enter with both signs. For a large squark mixing they are positive and can account for up to 15 MeV, a significant effect which enhances the sensitivity in the search for squarks through their virtual effects.

We compared the W boson mass prediction in the MSSM and the SM and found that the SUSY contributions raise the predicted M_W value, resulting in a MSSM value lying above the SM result. The parameter region in which the predictions from the two models overlap corresponds to the decoupling limit of the MSSM, i.e. heavy superpartner masses, while the Higgs mass is bounded from below by the exclusion limit from LEP $m_h > 114.4$ GeV and from above by the upper limit on the light CP-even Higgs in the MSSM of about 130 GeV. We demonstrated the feature that the MSSM gives rise to a prediction for M_W that tends to be higher than the prediction within the SM by a random scan over the MSSM parameter space. The current experimental value of M_W therefore favours a non-zero SUSY contribution.

The very precise theoretical calculations allow to set limits on the SM and MSSM parameters. The impact of the indirect theoretical constraints will be further enhanced when the experimental measurements are improved in the next years at LHC and even further at a future linear collider, such as the ILC.

A comparable calculation, as the one we did for the MSSM is desirable also for other models beyond the SM and would help to distinguish between them and to find out which models are preferred by the experimental results. Predicting their effect on electroweak precision observables can help identify the nature of new physics at the experiments.

As a first step in this direction we already started to extend our calculation of the W boson mass also to the NMSSM as well as a model with a fourth fermion generation. The theoretical framework set up in this thesis allows to easily extend the analysis also to further models of new physics.

A. Input parameters

For the numerical evaluation we used an up-to-date set of input values, given in Table A.1.

Parameter	Exp. value	Reference
M_W	80.399 ± 0.023 GeV	[3]
M_Z	91.1875 ± 0.0021 GeV	[43, 44]
Γ_Z	2.4952 ± 0.0023 GeV	[3]
G_μ	$(1.1663788 \pm 0.0000007) \times 10^{-5}\text{GeV}^{-2}$	[69]
α	1/137.035999679	[3]
$\alpha_s(M_Z)$	0.1184 ± 0.0007	[106]
m_t	173.3 ± 1.1 GeV	[89]
m_b	4.67 GeV	[3]
m_c	1.286 GeV	*FeynHiggs* default value
m_s	95 MeV	*FeynHiggs* default value
m_u	3 MeV	*FeynHiggs* default value
m_d	6 MeV	*FeynHiggs* default value
m_e	0.510998902 MeV	*FeynHiggs* default value
m_μ	105.658357 MeV	*FeynHiggs* default value
m_τ	1777.03 MeV	*FeynHiggs* default value

Table A.1.: Experimental values for the relevant SM parameters needed in our calculation.

The value for G_μ includes the extra shift from a non-vanishing electron mass $\Delta q(m_e)$ that has recently been calculated in [68].

B. One-loop integrals

B.1. Rules for the calculation in D dimensions

The metric tensor in D dimensions,

$$g^{\mu\nu} \quad \text{with} \quad \mu,\nu = 0,1,...,D-1\ , \tag{B.1}$$

is defined by

$$g^{\mu\nu}g_{\mu\nu} = \delta^{\mu}_{\mu} = D\ . \tag{B.2}$$

The Dirac matrices are defined by

$$\{\gamma^{\mu},\gamma^{\nu}\} = 2g^{\mu\nu} \quad \text{with} \quad \text{Tr}\ 1 = 4\ , \tag{B.3}$$

and some useful relations for the calculation in D dimensions are:

$$\begin{aligned} &\gamma^{\mu}\gamma_{\mu} = \frac{1}{2}\{\gamma^{\mu},\gamma_{\mu}\} = D \\ &\gamma^{\mu}\gamma_{\nu}\gamma_{\mu} = 2g_{\mu\nu}\gamma^{\mu} - \gamma^{\mu}\gamma_{\mu}\gamma_{\nu} = (2-D)\gamma_{\nu}\ . \end{aligned} \tag{B.4}$$

B.2. Standard one-loop integrals

The general rank M tensor integral for a one-loop diagram with N legs with momenta p'_i and

$$p_1 = p'_1\ \ ,\ \ p_2 = p'_2 + p'_1\ \ ,\ \ ...\ \ ,\ \ p_{N-1} = p'_{N-1} + p'_{N-2} \tag{B.5}$$

is defined as

$$\begin{aligned} &T^{N}_{\mu_1...\mu_M}(p_1,...p_{N-1},m_0,...m_{N-1}) \\ &= \frac{(2\pi\mu)^{4-D}}{i\pi^2}\int d^Dq\,\frac{q_{\mu_1}...q_{\mu_M}}{[q^2-m_0^2][(q+p_1)^2-m_1^2]...[(q+p_{N-1})^2-m_{N-1}^2]} \end{aligned} \tag{B.6}$$

where m_i $(i = 1...N)$ are the masses of the particles in the loop. μ is an arbitrary energy scale needed to keep the argument of logarithms, occurring in the results, dimensionless.

By convention the T^1 (Tadpole) integral is called A, T^2 (Self-energy) is called B, T^3 (vertex) is called C and so forth. The tensor integrals can be reduced into functions of the scalar integrals A_0, B_0, C_0, D_0 without Lorentz indices in the numerator. The basic steps of the calculation of these scalar functions are described in the following.

Using Wick rotation and carrying out the D dimensional integration in polar coordinates one finds (for $D < 2n$ and $M > 0$)

$$\int d^D q \, \frac{1}{(q^2 - M)^n} = i(-1)^n \pi^{\frac{D}{2}} \frac{\Gamma(n - \frac{D}{2})}{\Gamma(n)} \, M^{\frac{D}{2}-n} \, , \tag{B.7}$$

where Γ is the Gamma function, which is defined for complex numbers with a positive real part by

$$\Gamma(z) = \int_0^\infty t^{z-1} e^{-t} dt \, . \tag{B.8}$$

For positive integers this is equivalent to

$$\Gamma(n) = (n-1)! \, , \tag{B.9}$$

and expansion for small $|z|$ gives

$$\Gamma(z) \approx \frac{1}{z} - \gamma_E + O(z) \, , \tag{B.10}$$

where γ_E is the Euler constant. With this auxiliary integral and the Feynman parameters

$$\prod_{i=1}^{N} \frac{1}{A_i} = \Gamma(N) \, (\prod_{i=1}^{N} \int_0^1 \mathrm{d}\alpha_i) \, \delta(1 - \sum_{i=1}^{N} \alpha_i) (\sum_{i=1}^{N} \alpha_i A_i)^{-N} \tag{B.11}$$

the calculation of the scalar integrals can be carried out. Expanding the results around $D \to 4$ gives the one-point function

$$A_0(m_0) = m_0^2 \left(\Delta - \ln \frac{m_0^2}{\mu^2} + 1 \right) + \mathcal{O}(D-4) \, , \tag{B.12}$$

where Δ is given by

$$\Delta = \frac{2}{4-D} - \gamma_E + \ln 4\pi \tag{B.13}$$

and contains the UV-divergency. The two-point function is

$$B_0(p_1, m_0, m_1) = \Delta - \int_0^1 \mathrm{d}x \ln \left(\frac{x^2 p_1^1 - x(p_1^2 - m_1^2 + m_0^2) + m_0^2}{\mu^2} \right) + \mathcal{O}(D-4) \, , \tag{B.14}$$

and the UV-convergent three point function is

$$C_0(p_1,p_2,m_0,m_1,m_2) = -\int_0^1 \mathrm{d}x \int_0^{1-x} \mathrm{d}y \\ (x^2p_1^2 + y^2p_2^2 + 2xyp_1p_2 - x(p_1^2 - m_1^2 + m_0^2) - y(p_2^2 - m_2^2 + m_0^2) + m_0^2)^{-1} \ . \tag{B.15}$$

So the UV-divergent parts are

$$\begin{aligned} (D-4)A_0(m_0) &= -2m_0^2 + \mathcal{O}(D-4) \\ (D-4)B_0(m_0) &= -2 + \mathcal{O}(D-4) \\ (D-4)C_0(m_0) &= \mathcal{O}(D-4) \ . \end{aligned} \tag{B.16}$$

To express the tensor integrals in terms of the scalar functions, they are first decomposed into covariant expressions by constructing $T^N_{\mu_1\ldots\mu_M}$ from all symmetric tensor structures of rank M that can be formed out of p_1^μ, ... , p_{N-1}^μ and $g^{\mu\nu}$. For B^μ and $B^{\mu\nu}$ this gives

$$\begin{aligned} B^\mu &= p_1^\mu B_1 \\ B^{\mu\nu} &= g^{\mu\nu}B_{00} + p_1^\mu p_1^\nu B_{11} \ , \end{aligned} \tag{B.17}$$

and B_1, B_{00} and B_{11} can then be expressed through scalar integrals. The reduction formulas are obtained by contracting the decomposition (right side of (B.17)) and the integral expression (B.6) with the external momentum p_1^μ and the metric $g^{\mu\nu}$. Contracting the first formula of (B.17) with p_1^μ yields

$$\begin{aligned} p_1^2 B_1(p_1,m_0,m_1) &= \frac{(2\pi\mu)^{4-D}}{i\pi^2}\int d^Dq \, \frac{p_1 q}{[q^2-m_0^2][(q+p_1)^2-m_1^2]} \\ &= \frac{(2\pi\mu)^{4-D}}{i\pi^2}\int d^Dq \, \frac{\frac{1}{2}[(q+p_1)^2-m_1^2] - \frac{1}{2}[q^2-m_0^2] - \frac{1}{2}(p_1^2-m_1^2+m_0^2)}{[q^2-m_0^2][(q+p_1)^2-m_1^2]} \\ &= \frac{1}{2}A_0(m_0) - \frac{1}{2}A_0(m_1) - \frac{1}{2}(p_1^2-m_1^2+m_0^2)B_0(p_1,m_0,m_1) \ , \end{aligned} \tag{B.18}$$

so

$$B_1(p_1,m_0,m_1) = \frac{1}{2p_1^2}\left(A_0(m_0) - A_0(m_1) - (p_1^2-m_1^2+m_0^2)B_0(p_1,m_0,m_1)\right) \ . \tag{B.19}$$

Similarly one finds also B_{00} and B_{11}, and higher order scalar and tensor integrals can be calculated.

Bibliography

[1] The CMS Collaboration, V. Khachatryan *et al.*, *Search for Supersymmetry in pp Collisions at 7 TeV in Events with Jets and Missing Transverse Energy*, arXiv:1101.1628.

[2] The ATLAS Collaboration, *Search for supersymmetry using final states with one lepton, jets, and missing transverse momentum with the ATLAS detector in sqrts = 7 TeV pp*, arXiv:1102.2357.

[3] K. Nakamura and the Particle Data Group, *Review of Particle Physics*, Journal of Physics G: Nuclear and Particle Physics **37(7A)** (2010).

[4] A. Sirlin, *Radiative Corrections in the SU(2)-L x U(1) Theory: A Simple Renormalization Framework*, Phys.Rev. **D22** (1980) 971.

[5] W. Marciano and A. Sirlin, *Radiative Corrections to Neutrino Induced Neutral Current Phenomena in the SU(2)-L x U(1) Theory*, Phys.Rev. **D22** (1980) 2695.

[6] A. Djouadi and C. Verzegnassi, *Virtual Very Heavy Top Effects in LEP / SLC Precision Measurements*, Phys. Lett. **B195** (1987) 265.

[7] A. Djouadi, *O(alpha alpha-s) Vacuum Polarization Functions of the Standard Model Gauge Bosons*, Nuovo Cim. **A100** (1988) 357.

[8] B. Kniehl, *Two Loop Corrections to the Vacuum Polarizations in Perturbative QCD*, Nucl. Phys. **B347** (1990) 86.

[9] F. Halzen and B. Kniehl, Δ *r beyond one loop*, Nucl. Phys. **B353** (1991) 567.

[10] B. Kniehl and A. Sirlin, *Dispersion relations for vacuum polarization functions in electroweak physics*, Nucl. Phys. **B371** (1992) 141.

[11] B. Kniehl and A. Sirlin, *On the effect of the $t\bar{t}$ threshold on electroweak parameters*, Phys. Rev. **D47** (1993) 883.

[12] A. Freitas, W. Hollik, W. Walter, and G. Weiglein, *Complete fermionic two-loop results for the M(W)-M(Z) interdependence*, Phys. Lett. **B495** (2000) 338, hep-ph/0007091.

[13] A. Freitas, W. Hollik, W. Walter, and G. Weiglein, *Electroweak two-loop corrections to the M(W) - M(Z) mass correlation in the standard model*, Nucl. Phys. **B632** (2002) 189, hep-ph/0202131.

[14] M. Awramik and M. Czakon, *Complete two loop electroweak contributions to the muon lifetime in the standard model*, Phys. Lett. **B568** (2003) 48, hep-ph/0305248.

[15] M. Awramik and M. Czakon, *Complete two loop bosonic contributions to the muon lifetime in the standard model*, Phys. Rev. Lett. **89** (2002) 241801, hep-ph/0208113.

[16] A. Onishchenko and O. Veretin, *Two-loop bosonic electroweak corrections to the muon lifetime and M(Z) M(W) interdependence*, Phys. Lett. **B551** (2003) 111, hep-ph/0209010.

[17] M. Awramik, M. Czakon, A. Onishchenko, and O. Veretin, *Bosonic corrections to Delta(r) at the two loop level*, Phys. Rev. **D68** (2003) 053004, hep-ph/0209084.

[18] L. Avdeev, J. Fleischer, S. Mikhailov, and O. Tarasov, *0 (alpha alpha-s**2) correction to the electroweak rho parameter*, Phys.Lett. **B336** (1994) 560, hep-ph/9406363.

[19] K. G. Chetyrkin, J. H. Kuhn, and M. Steinhauser, *Corrections of order* $\mathcal{O}(G_F M_t^2 \alpha_s^2)$ *to the* ρ *parameter*, Phys. Lett. **B351** (1995) 331, hep-ph/9502291.

[20] K. G. Chetyrkin, J. Kuhn, and M. Steinhauser, *QCD corrections from top quark to relations between electroweak parameters to order alpha-s**2*, Phys. Rev. Lett. **75** (1995) 3394, hep-ph/9504413.

[21] K. Chetyrkin, J. Kuhn, and M. Steinhauser, *Three loop polarization function and O (alpha-s**2) corrections to the production of heavy quarks*, Nucl.Phys. **B482** (1996) 213, hep-ph/9606230.

[22] M. Faisst, J. H. Kuhn, T. Seidensticker, and O. Veretin, *Three loop top quark contributions to the rho parameter*, Nucl. Phys. **B665** (2003) 649, hep-ph/0302275.

[23] K. Chetyrkin, M. Faisst, J. H. Kuhn, P. Maierhofer, and C. Sturm, *Four-Loop QCD Corrections to the Rho Parameter*, Phys.Rev.Lett. **97** (2006) 102003, hep-ph/0605201.

[24] R. Boughezal and M. Czakon, *Single scale tadpoles and O(G(F m(t)**2 alpha(s)**3)) corrections to the rho parameter*, Nucl.Phys. **B755** (2006) 221, hep-ph/0606232.

[25] M. Awramik, M. Czakon, A. Freitas, and G. Weiglein, *Precise prediction for the W boson mass in the standard model*, Phys.Rev. **D69** (2004) 053006, hep-ph/0311148.

[26] P. H. Chankowski, A. Dabelstein, W. Hollik, W. Mosle, S. Pokorski, *et al.*, *Delta(r) in the MSSM*, Nucl.Phys.Proc.Suppl. **37B** (1994) 232.

[27] D. Garcia and J. Sola, *Full one loop supersymmetric quantum effects on M(W)*, Mod.Phys.Lett. **A9** (1994) 211.

[28] D. M. Pierce, J. A. Bagger, K. T. Matchev, and R. Zhang, *Precision corrections in the minimal supersymmetric standard model*, Nucl.Phys. **B491** (1997) 3, `hep-ph/9606211`.

[29] S. Heinemeyer, W. Hollik, D. Stockinger, A. M. Weber, and G. Weiglein, *Precise prediction for M(W) in the MSSM*, JHEP **08** (2006) 052, `hep-ph/0604147`.

[30] A. Djouadi, P. Gambino, S. Heinemeyer, W. Hollik, C. Junger, and G. Weiglein, *Supersymmetric contributions to electroweak precision observables: QCD corrections*, Phys.Rev.Lett. **78** (1997) 3626, `hep-ph/9612363`.

[31] A. Djouadi, P. Gambino, S. Heinemeyer, W. Hollik, C. Junger, and G. Weiglein, *Leading QCD corrections to scalar quark contributions to electroweak precision observables*, Phys.Rev. **D57** (1998) 4179, `hep-ph/9710438`.

[32] S. Heinemeyer and G. Weiglein, *Leading electroweak two loop corrections to precision observables in the MSSM*, JHEP **0210** (2002) 072, `hep-ph/0209305`.

[33] J. Haestier, S. Heinemeyer, D. Stockinger, and G. Weiglein, *Electroweak precision observables: Two-loop Yukawa corrections of supersymmetric particles*, JHEP **0512** (2005) 027, `hep-ph/0508139`.

[34] J. Cao and J. M. Yang, *Anomaly of Zb anti-b coupling revisited in MSSM and NMSSM*, JHEP **0812** (2008) 006, `arXiv:0810.0751`.

[35] F. Domingo and T. Lenz, *W mass and Leptonic Z-decays in the NMSSM*, `arXiv:1101.4758`.

[36] S. Glashow, *Partial Symmetries of Weak Interactions*, Nucl.Phys. **22** (1961) 579.

[37] S. Weinberg, *A Model of Leptons*, Phys.Rev.Lett. **19** (1967) 1264.

[38] A. Salam, *Weak and Electromagnetic Interactions*, in Svartholm: Elementary Particle Theory, Proceedings Of The Nobel Symposium Held 1968 At Lerum, Stockholm 1968, 367.

[39] R. K. Ellis, W. Stirling, and B. Webber, *QCD and collider physics*, vol. 8, Camb.Monogr.Part.Phys.Nucl.Phys.Cosmol., (1996).

[40] W. Pauli, *The Connection Between Spin and Statistics*, Phys. Rev. **58** (1940) 716.

[41] A. Denner, *Techniques for calculation of electroweak radiative corrections at the one loop level and results for W physics at LEP-200*, Fortsch.Phys. **41** (1993) 307, arXiv:0709.1075.

[42] M. Bohm, A. Denner, and H. Joos, *Gauge theories of the strong and electroweak interaction*, Vieweg +Teubner, (2001).

[43] The LEP Electroweak Working Group, SLD Electroweak and Heavy Flavour Groups, ALEPH Collaboration, DELPHI Collaboration, L3 Collaboration, OPAL Collaboration, SLD Collaboration, *Precision Electroweak Measurements on the Z Resonance*, Phys. Rept. **427** (2006) 257, hep-ex/0509008.

[44] See: http://lepewwg.web.cern.ch/LEPEWWG/.

[45] R. Feynman, *Space-time approach to nonrelativistic quantum mechanics*, Rev.Mod.Phys. **20** (1948) 367.

[46] R. P. Feynman and A. R. Hibbs, *Quantum Mechanics and Path Integrals*, McGraw-Hill, New York, (1965).

[47] The LEP Working Group for Higgs boson searches, ALEPH Collaboration, DELPHI Collaboration, L3 Collaboration, OPAL Collaboration, R. Barate *et al.*, *Search for the standard model Higgs boson at LEP*, Phys.Lett. **B565** (2003) 61, hep-ex/0306033.

[48] S. Heinemeyer, W. Hollik, and G. Weiglein, *FeynHiggs: A Program for the calculation of the masses of the neutral CP even Higgs bosons in the MSSM*, Comput.Phys.Commun. **124** (2000) 76, hep-ph/9812320.

[49] M. Frank, T. Hahn, S. Heinemeyer, W. Hollik, H. Rzehak, and G. Weiglein, *The Higgs Boson Masses and Mixings of the Complex MSSM in the Feynman-Diagrammatic Approach*, JHEP **0702** (2007) 047, hep-ph/0611326.

[50] G. 't Hooft and M. Veltman, *Regularization and Renormalization of Gauge Fields*, Nucl.Phys. **B44** (1972) 189.

[51] M. Chanowitz, M. Furman, and I. Hinchliffe, *The axial current in dimensional regularization*, Nuclear Physics B **159(1-2)** (1979) 225.

[52] D. M. Capper, D. R. T. Jones, and P. Van Nieuwenhuizen, *Regularization by dimensional reduction of supersymmetric and non-supersymmetric gauge theories*, Nuclear Physics B **167(3)** (1980) 479.

[53] W. Siegel, *Supersymmetric dimensional regularization via dimensional reduction*, Physics Letters B **84(2)** (1979) 193.

[54] D. Stockinger, *Regularization by dimensional reduction: consistency, quantum action principle, and supersymmetry*, JHEP **0503** (2005) 076, hep-ph/0503129.

[55] D. Stockinger, *Regularization of supersymmetric theories: Recent improvements*, hep-ph/0506258.

[56] F. del Aguila, A. Culatti, R. Munoz-Tapia, and M. Perez-Victoria, *Constraining differential renormalization in Abelian gauge theories*, Phys.Lett. **B419** (1998) 263, hep-th/9709067.

[57] T. Hahn and M. Perez-Victoria, *Automatized one loop calculations in four-dimensions and D-dimensions*, Comput.Phys.Commun. **118** (1999) 153, hep-ph/9807565.

[58] G. 't Hooft, *Renormalization of Massless Yang-Mills Fields*, Nucl.Phys. **B33** (1971) 173.

[59] T. Hahn, *Generating Feynman diagrams and amplitudes with FeynArts 3*, Comput.Phys.Commun. **140** (2001) 418, hep-ph/0012260.

[60] J. Vermaseren, *New features of FORM*, math-ph/0010025.

[61] C. Jacobi, Crelle **30** (1846) 51.

[62] R. Behrends, R. Finkelstein, and A. Sirlin, *Radiative corrections to decay processes*, Phys.Rev. **101** (1956) 866.

[63] S. Berman, *Radiative corrections to muon and neutron decay*, Phys.Rev. **112** (1958) 267.

[64] T. Kinoshita and A. Sirlin, *Radiative corrections to Fermi interactions*, Phys.Rev. **113** (1959) 1652.

[65] T. van Ritbergen and R. G. Stuart, *Complete two loop quantum electrodynamic contributions to the muon lifetime in the Fermi model*, Phys.Rev.Lett. **82** (1999) 488, hep-ph/9808283.

[66] T. van Ritbergen and R. G. Stuart, *On the precise determination of the Fermi coupling constant from the muon lifetime*, Nucl.Phys. **B564** (2000) 343, hep-ph/9904240.

[67] M. Steinhauser and T. Seidensticker, *Second order corrections to the muon lifetime and the semileptonic B decay*, Phys.Lett. **B467** (1999) 271, hep-ph/9909436.

[68] A. Pak and A. Czarnecki, *Mass Effects in Muon and Semileptonic $b \to c$ Decays*, Phys. Rev. Lett. **100(24)** (2008) 241807.

[69] The MuLan Collaboration, D. Webber *et al.*, *Measurement of the Positive Muon Lifetime and Determination of the Fermi Constant to Part-per-Million Precision*, arXiv:1010.0991.

[70] M. Steinhauser, *Leptonic contribution to the effective electromagnetic coupling constant up to three loops*, Phys.Lett. **B429** (1998) 158, hep-ph/9803313.

[71] N. Cabibbo and R. Gatto, *Electron-Positron Colliding Beam Experiments*, Phys. Rev. **124(5)** (1961) 1577.

[72] M. Davier, A. Hoecker, B. Malaescu, and Z. Zhang, *Reevaluation of the Hadronic Contributions to the Muon g-2 and to alpha(MZ)*, Eur.Phys.J.C71 (2010), arXiv:1010.4180.

[73] The KLOE Collaboration, F. Ambrosino *et al.*, *Measurement of sigma(e+ e- → pi+ pi-) from threshold to 0.85 GeV^2 using Initial State Radiation with the KLOE detector*, arXiv:1006.5313.

[74] The BABAR Collaboration, B. Aubert *et al.*, *Study of e+ e- → pi+ pi- pi0 process using initial state radiation with BABAR*, Phys.Rev. **D70** (2004) 072004, hep-ex/0408078.

[75] The BABAR Collaboration, B. Aubert *et al.*, *The e+ e- → pi+ pi- pi+ pi-, K+ K- pi+ pi-, and K+ K- K+ K- cross sections at center-of-mass energies 0.5-GeV to 4.5-GeV measured with initial-state radiation*, Phys.Rev. **D71** (2005) 052001, hep-ex/0502025.

[76] The BABAR Collaboration, B. Aubert *et al.*, *The e+ e- → 3(pi+ pi-), 2(pi+ pi- pi0) and K+ K- 2(pi+ pi-) cross sections at center-of-mass energies from production threshold to 4.5-GeV measured with initial-state radiation*, Phys.Rev. **D73** (2006) 052003, hep-ex/0602006.

[77] V. Druzhinin, *Study of e+e- annihilation at low energies*, arXiv:0710.3455.

[78] The BABAR Collaboration, B. Aubert *et al.*, *The e+ e- → 2(pi+ pi-) pi0, 2(pi+ pi-) eta, K+ K- pi+ pi- pi0 and K+ K- pi+ pi- eta Cross Sections Measured with Initial-State Radiation*, Phys.Rev. **D76** (2007) 092005, arXiv:0708.2461.

[79] The BABAR Collaboration, B. Aubert *et al.*, *Measurements of e+ e- → K+ K- eta, K+ K- pi0 and K0(s) K+- pi-+ cross- sections using initial state radiation events*, Phys.Rev. **D77** (2008) 092002, arXiv:0710.4451.

[80] The BABAR Collaboration, B. Aubert *et al.*, *The e+ e- → K+ K- pi+ pi-, K+ K- pi0 pi0 and K+ K- K+ K- cross-sections measured with initial-state radiation*, Phys.Rev. **D76** (2007) 012008, arXiv:0704.0630.

[81] The BABAR Collaboration, B. Aubert *et al.*, *Precise measurement of the e+ e- → pi+ pi- (gamma) cross section with the Initial State Radiation method at BABAR*, Phys.Rev.Lett. **103** (2009) 231801, arXiv:0908.3589.

[82] A. Freitas, W. Hollik, W. Walter, and G. Weiglein, *Electroweak two-loop corrections to the M(W) - M(Z) mass correlation in the standard model*, Nucl. Phys. **B632** (2002) 189, `hep-ph/0202131`.

[83] M. Veltman, *Limit on Mass Differences in the Weinberg Model*, Nucl.Phys. **B123** (1977) 89.

[84] D. Y. Bardin, A. Leike, T. Riemann, and M. Sachwitz, *Energy dependent width effects in e^+e^- annihilation near the Z pole*, Phys. Lett. **B206** (1988) 539.

[85] K. G. Chetyrkin, J. H. Kuhn, and M. Steinhauser, *QCD corrections from top quark to relations between electroweak parameters to order alpha-s**2*, Phys. Rev. Lett. **75** (1995) 3394, `hep-ph/9504413`.

[86] M. Awramik, M. Czakon, and A. Freitas, *Electroweak two-loop corrections to the effective weak mixing angle*, JHEP **11** (2006) 048, `hep-ph/0608099`.

[87] L. Okun, *Leptons and quarks*, Elsevier Science Pub Co, (1985), ISBN 0444869247.

[88] M. Consoli, W. Hollik, and F. Jegerlehner, *The Effect of the Top Quark on the M(W)-M(Z) Interdependence and Possible Decoupling of Heavy Fermions from Low-Energy Physics*, Phys.Lett. **B227** (1989) 167.

[89] The CDF and D0 Collaboration, *Combination of CDF and D0 Results on the Mass of the Top Quark using up to 5.6 fb^{-1} of data*, `arXiv:1007.3178`.

[90] M. Beneke, I. Efthymiopoulos, M. L. Mangano, J. Womersley, A. Ahmadov, *et al.*, *Top quark physics*, `hep-ph/0003033`.

[91] A. Quadt, *Top quark physics at hadron colliders*, Eur.Phys.J. **C48** (2006) 835.

[92] The ECFA/DESY LC Physics Collaboration, J. Aguilar-Saavedra *et al.*, *TESLA: The Superconducting electron positron linear collider with an integrated x-ray laser laboratory. Technical design report. Part 3. Physics at an e+ e- linear collider*, `hep-ph/0106315`.

[93] The American Linear Collider Working Group Collaboration, T. Abe *et al.*, *Linear collider physics resource book for Snowmass 2001. Part 1. Introduction*, `hep-ex/0106055`.

[94] A. Hoang, M. Beneke, K. Melnikov, T. Nagano, A. Ota, *et al.*, *Top - anti-top pair production close to threshold: Synopsis of recent NNLO results*, Eur.Phys.J.direct **C2** (2000) 1, `hep-ph/0001286`.

[95] The ALEPH Collaboration, DELPHI Collaboration, L3 Collaboration, LEP Working Group for Higgs Boson Searches, OPAL Collaboration, S. Schael *et al.*, *Search for neutral MSSM Higgs bosons at LEP*, Eur.Phys.J. **C47** (2006) 547, hep-ex/0602042.

[96] A. Strumia, *The fine-tuning price of the early LHC*, arXiv:1101.2195.

[97] A. H. Chamseddine, R. L. Arnowitt, and P. Nath, *Locally Supersymmetric Grand Unification*, Phys.Rev.Lett. **49** (1982) 970.

[98] R. Barbieri, S. Ferrara, and C. A. Savoy, *Gauge Models with Spontaneously Broken Local Supersymmetry*, Phys.Lett. **B119** (1982) 343.

[99] L. E. Ibanez, *Locally Supersymmetric SU(5) Grand Unification*, Phys.Lett. **B118** (1982) 73.

[100] L. J. Hall, J. D. Lykken, and S. Weinberg, *Supergravity as the Messenger of Supersymmetry Breaking*, Phys.Rev. **D27** (1983) 2359.

[101] N. Ohta, *Grand Unified Theories Based on Local Supersymmetry*, Prog. Theor. Phys. **70** (1983) 542.

[102] G. L. Kane, C. F. Kolda, L. Roszkowski, and J. D. Wells, *Study of constrained minimal supersymmetry*, Phys.Rev. **D49** (1994) 6173, hep-ph/9312272.

[103] J. Erler, S. Heinemeyer, W. Hollik, G. Weiglein, and P. Zerwas, *Physics impact of GigaZ*, Phys.Lett. **B486** (2000) 125, hep-ph/0005024.

[104] U. Baur, R. Clare, J. Erler, S. Heinemeyer, D. Wackeroth, *et al.*, *Theoretical and experimental status of the indirect Higgs boson mass determination in the standard model*, hep-ph/0111314.

[105] J. F. Gunion, H. E. Haber, G. L. Kane, and S. Dawson, *The Higgs Hunter's Guide* , Addison-Wesley, (1990), ISBN 0201509350.

[106] S. Bethke, *The 2009 World Average of alpha(s)*, Eur.Phys.J. **C64** (2009) 689, arXiv:0908.1135.

Acknowledgements

First and foremost I would like to thank my supervisor Prof. Georg Weiglein for giving me this interesting and challenging project, for patiently answering my questions and explaining me things in an understandable way and finally for reading the manuscript.

Special thanks goes to Prof. Arnulf Quadt for supporting me the last years and giving me the opportunity to work in the field of SUSY phenomenology by enabling an external diploma thesis.

I want to thank Oscar Stål not only for his great help with my thesis but also for good collaboration in the last years, for helpful advises and suggestions and many interesting discussions.

I thank Ayres Freitas for clarifying discussions on the electroweak two-loop corrections in the SM and I want to thank Sven Heinemeyer for assistance with FeynHiggs and interesting input.

I would like to thank Prof. Gudrid Moortgat-Pick for an excellent lecture in the last year and teaching me many basics needed for this thesis.

Furthermore I thank many people of the DESY theory group for a productive and pleasant time here and for very many helpful discussions and advises. Especially I would like to thank Andreas Goudelis, Aoife Bharucha, Julia Harz, Tigran Kalaydzhyan and Kai Schmitz.

My very special thanks go to Tomas Kasemets for his patience and support, for help with my thesis and especially for making the last month, despite a lot of work, very special and enjoyable.

Und zum Schluss möchte ich meinen Eltern, Sophie, Leo und Johanna danken, die immer für mich da sind, mich unterstützen, ermutigen und aufmuntern. Danke für alles!